Optical and magnetic behaviour of metal doped-CdS nanostructures

A THESIS

Submitted to the

FACULTY OF SCIENCE

THAPAR UNIVERSITY, PATIALA

for the degree of

Doctor of Philosophy

By

KAMALDEEP KAUR

Regn. No. 901112004

School of Physics & Materials Science

Thapar University

Patiala - 147 004

INDIA

JULY 2016

DECLARATION

It is certified that the thesis is entirely my own and that the ideas and references cited herein have been duly acknowledged.

Kamaldeep Kaur

(Kamaldeep Kaur)

Attestation by supervisor

(Dr. N. K. Verma)

Visiting Professor

School of Physics and Materials Science,

Thapar University,

Patiala – 147 004

Punjab, INDIA

CERTIFICATE

This is to certify that the thesis entitled, "Optical and magnetic behaviour of metal doped-CdS nanostructures", submitted by Mrs. Kamaldeep Kaur in the fulfillment of the requirement for the award of the degree of Doctor of Philosophy in the School of Physics and Materials Science, Thapar University, Patiala, is a record of candidate's own work carried out by her under my supervision and guidance. The matter presented in this thesis has not been submitted in part or full for the award of any degree in any other University or Institute.

Attestation by supervisor

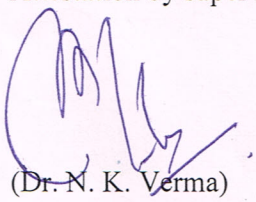

(Dr. N. K. Verma)

Visiting Professor

School of Physics and Materials Science,

Thapar University,

Patiala – 147 004

Punjab, INDIA

ACKNOWLEDGEMENT

I humbly prostrate myself before the Almighty for HIS grace and abundant blessings which enabled me to complete my work successfully and to my full satisfaction.

First and foremost, I would like to express my sincere gratitude to my supervisor Dr. N. K. Verma for his precious advices, continuous guidance and motivation. I also extend my gratitude to Mrs. (Dr.) Rama Verma for her motherly affection and care.

I am obliged to Professor Prakash Gopalan, Director, Thapar University, for providing infrastructure to carry out research work in a friendly environment. I am highly obliged to Dr. Manoj Kumar, Head of School of Physics and Materials Science, Thapar University, Patiala.

My sincere thanks to Prof. O.P. Pandey (Dean Research and Sponsored Projects) for the various encouraging lectures during course work classes.

I express my deep gratitude to Dr. Kulvir Singh and Dr. Bhaskar Chandra Mohanty. I would like to thank the doctoral committee members comprising Dr. B.N Chudasama, Dr. D.P. Singh and Dr. Bonamali Paul, for their encouragement, constructive comments, and guidance throughout this period. I am thankful to the faculty of School of Physics and Materials Science, Thapar University, Patiala for their timely guidance and encouragement.

I also acknowledge the wholehearted support of the technical and secretarial staff of the Department.

I acknowledge University Grants Commission, Delhi for their financial support as a 'UGC SRF Fellow' under MANF scheme.

I am also thankful to all Staff of SPMS, Thapar University, Patiala for their helping nature throughout my research work.

I would like to thank my seniors Dr. Zinki Jindal, Dr. Sanjeev Kumar, Dr. Manveen Kaur, Dr. Lavanya Khanna, Dr. Jaspal Singh, Dr. Gurmeet Singh for their guidance, suggestions and inspiration. My colleagues Dr. Sunil Kumar, Gitanjali Dhir have always been a source of motivation, support, laughter and fight throughout this journey.

I am thankful to my friends Imanpreet Kaur, Parveer Kaur, Kuljeet Singh, Shivani Jindal, Nupur Aggarwal for their help and good time which we have spent together.

I dedicate this thesis to my loving parents S. Bhupinder Singh, Smt Baljit Kaur and mother in law Smt. Paramjeet Kaur to whom I owe my life and if it wasn't for their constant support, unconditional love and encouragement, I would not have been what I am today.

I especially thank my husband Er. Arshdeep Singh, my brother, Dilpreet Singh and my sister in law Mrs. Sukhjit Kaur for their co-operation and encouragement.

Above all, I am obliged to Almighty God for giving me strength to complete this project smoothly and successfully.

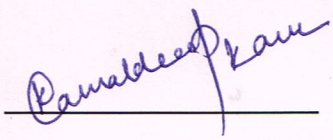

(Kamaldeep Kaur)

DEDICATED

TO MY LOVING

FAMILY

CONTENTS

Chapter 2 Syntheses and Characterizations

LIST OF FIGURES

LIST OF TABLES

List of Publications

I. SCI Journal (Accepted)

1. **Kamaldeep Kaur**, Gurmeet Singh Lotey and N. K. Verma, "Structural, optical and magnetic properties of cobalt-doped CdS dilute magnetic semiconducting nanorods." Materials Chemistry and Physics 143.1 (2013): 41-46.

2. **Kamaldeep Kaur**, G S Lotey, N. K. Verma, "Ferromagnetism in Gd-doped CdS dilute magnetic semiconducting nanorods." Journal of Materials Science: Materials in Electronics 25.1 (2014): 311-316.

3. **Kamaldeep Kaur**, N. K. Verma, "Optical and magnetic properties of Fe-doped CdS dilute magnetic semiconducting nanorods." Journal of Materials Science: Materials in Electronics 25.6 (2014): 2605-2610.

4. **Kamaldeep Kaur,** N. K. Verma, "Ferromagnetic behavior of $Cd_{1-x}Ni_xS$ nanorods: a novel study." Journal of Materials Science: Materials in Electronics 26.11 (2015): 8285-8291.

5. **Kamaldeep Kaur**, N. K. Verma, "Hydrothermally Synthesized CdS Nanoparticles: Effect of Fe Doping on Optical and Magnetic Properties." Journal of Superconductivity and Novel Magnetism 28.11 (2015): 3317-3322.

II. SCI Journal (Communicated)

1. **Kamaldeep Kaur,** N. K. Verma, "Ferromagnetic behavior of Ni-doped CdS nanoparticles." Journal of Superconductivity and Novel Magnetism, June, 2016.

III. Publications in addition to Ph.D. work

1 **Kamaldeep Kaur**, G S Lotey, N. K. Verma, "Structural, magnetic, dielectric and magnetodielectric properties of Gd-doped CdS nanorods." Materials Science in Semiconductor Processing 19 (2014): 6-10.

2. Nupur Aggarwal, **Kamaldeep Kaur**, Ajay vasishth, N.K. Verma," Magnetic behavior of Gadolinium doped ZnO nanoparticles" Journal of Materials Science: Materials in Electronics, June, 2016. (Communicated)

IV. Non-SCI Journal

1. **Kamaldeep Kaur**, N. K. Verma, Structural and optical properties of Co-doped CdS nanostructures, AIP proceedings, 1536, 141-142, 2013.

2. **Kamaldeep Kaur**, N K Verma, "Study on structural, optical properties of solvothermally synthesized Ni doped CdS nanorods." Proceedings of the International Conference On Condensed Matter Physics 2014 (ICCMP 2014). Vol. 1661. No. 1. AIP Publishing, 2015.

3. NK Verma, Imanpreet Kaur, **Kamaldeep Kaur**, Gurmeet Singh Lotey, "Enhanced Efficiency of Au-Deposited $BiFeO_3$ Nanoparticles Based Dye-Sensitized Solar Cells." Advanced Materials Research. Vol. 856. Trans Tech Publications, 2014.

V. Papers in Conferences/Proceedings

1. **Kamaldeep Kaur**, N. K. Verma, Structural and magnetic properties of CdS nanorods, Excel India Publishers, 2166-2170, (2013).

2. **Kamaldeep Kaur,** N.K. Verma, “Optical behaviour of Transition metal doped CdS nanostructures” at International conference, NANOSCITECH 2014, held at Punjab University, Chandigarh, India on 13-15 February, 2014.
3. Nupur Aggarwal, Ajay vasishth, **Kamaldeep kaur**, N.K. Verma," Study of magnetism in Tb doped ZnO nanoparticles", in 2nd conference on Microscopy in material science & 2nd AMST held at Thapar University, Patiala, India on 25-27 Feb, 2016.
4. Nupur Aggarwal, Ajay Vasishth, **Kamaldeep Kaur,** N.K. Verma," Study of magnetism in Gd doped ZnO nanoparticles ", presented in 3rd International Conference on “Nanotechnology for Better Living" (NBL -2016) held at NIT, Srinagar, India on 25th to 29th may, 2016, ISBN: 978-981-09-7519-7, Vol. 03, No. 01, p. 200.

ABSTRACT

Spintronics represents the field of electronics, in which the spin of electron is utilized along with its charge. Dilute magnetic semiconductors (DMS) materials are promising for future spintronic device applications. A lot of research has been devoted to generate magnetism in semiconductor materials via doping of transition metals, known as DMS materials. However, the origin of magnetism remains controversial till date. There are various mechanisms (or theories) which have been proposed in order to explain the origin of magnetism in these DMS materials such as Ruderman-Kittel-Kasuya-Yosida (RKKY), double exchange interactions, superexchange interactions, and bound magnetic polaron (BMP). Also, from the application point of view, low T_C further hinders their practical utility, and thus, many efforts have been made to find ferromagnetic DMS having T_C higher than room temperature. This has motivated us to carry out investigations in order to achieve and understand the origin of observed magnetism in DMS materials.

In present thesis work, the structural, optical and magnetic properties of transition and rare earth metal-doped CdS nanostructures, nanoparticles and nanorods, synthesized using chemical synthesis route, have been examined. The properties have been studied using various techniques viz. transmission electron microscope (TEM), High resolution (HRTEM), X-ray diffraction (XRD), energy dispersive spectroscopy (EDS), UV-Visible spectroscopy (UV-Vis.), photoluminescence spectroscopy (PL) and vibrating sample magnetometer (VSM).

PREFACE

This thesis presents the synthesis and characterization of transition and rare earth metal doped CdS nanostructures by chemical synthesis route. The structural, optical, morphological and magnetic properties of the synthesized nanostructures have been observed using various characterization techniques. The possible origin of magnetism has been discussed in detail. The chapter-wise description of the thesis has been given below:

Chapter 1 gives an introduction to the need and importance of DMS materials. A brief of various mechanisms or theories discussing the origin of magnetism in DMS materials have been included in this chapter. The literature review has been given along with motivation to carry out this work. CdS emerges as a potential candidate as a DMS material.

Chapter 2 provides information regarding the materials and their properties used in the present work. It describes the synthesis procedure adopted for Co, Ni, Fe and Gd-doped CdS nanostructures (nanoparticles and nanorods). Also, it includes various characterization techniques employed for the study of doped CdS nanostructures as DMS material. The introduction, theory, instrumentation, working and applications of each characterization technique have been described in detail.

Chapter 3 presents results and their discussions for Co, Ni, Fe and Gd-doped CdS nanostructures (nanoparticles and nanorods). The synthesized nanostructures have been characterized through XRD, TEM, EDS, UV-visible, PL spectroscopy and VSM. The origin of magnetism has been discussed in detail. The magnetic analysis leads to the conclusion that there are different reasons for observed ferromagnetism in doped CdS nanostructures depending on the type of dopant used.

Chapter 4 includes conclusion of the research work undertaken along with achievements and future scope of the work.

Chapter 1

Introduction

Chapter 1

Introduction

This chapter gives an introduction to the need and importance of nanotechnology and DMS materials. A brief of various mechanisms or theories discussing the origin of magnetism in DMS materials have been included in this chapter. The literature review has been given along with motivation to carry out this work. CdS appears as a potential candidate for DMS materials.

1.1 Nanotechnology

'Nanotechnology' is the relatively new area of science and technology that conducted at the nanoscale which lies between 1 to 100 nm [1]. The prefix nano is a Greek word means dwarf that depicts that nanotechnology is a field which deals with the miniatures having size 1 billionth of a meter. It deals with the things which exhibit novel physical and chemical properties due to their unique size. Nanomaterials are not new and moreover they were not first created by man but there are many examples of nanomaterials from nature such as butterfly's wings are multilayer nanoscale patterns, and peacock feathers. Nanomaterials are considered as the most promising materials for the future generation devices. Figure 1.1 helps us in order to view the size range of various materials common in our daily life. Richard Feynman in 1959 at the American Physical Society gave a modern origin of nanotechnology by delivering a talk "There is plenty of room at the bottom". This idea generated great interest of the research community to give a physical image to his vision that would make a new world with changed technologies around us [2]. The conversion from the bulk to nanoparticles can transform the physical properties for betterment. The word nanotechnology was first introduced by Norio Taniguchi in 1974 [3].

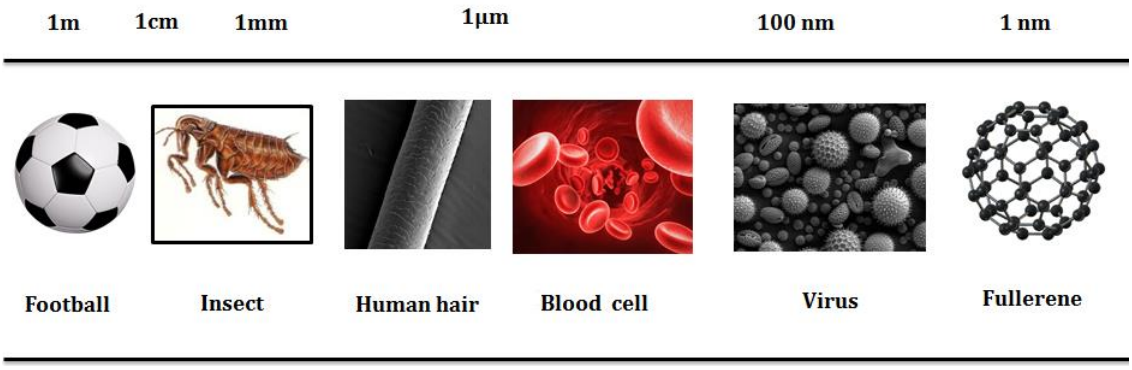

Figure 1.1 Common objects from daily life with their dimensions [4].

In 1981 at IBM Zurich Research Laboratory Scanning Tunneling Microscope was invented by Binning and Rohrer and for this invention they got the Noble Prize in 1986. Afterwards various new instruments were discovered such as scanning electron microscope (SEM), transmission electron microscope (TEM) and atomic force microscope (SPM) [5].

The main parameters those make the nanomaterials different from the others is the quantum confinement effects and higher surface to volume ratio as shown in Figure 1.2.

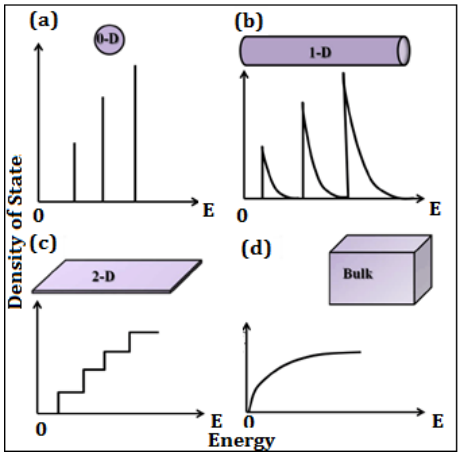

Figure 1.2 Density of states vs. Energy plots of (a) 0-D (b) 1-D (c) 2-D (d) Bulk structures [6].

Due to quantum confinement effects nanomaterials may be of zero dimensions (0-D), one dimensional (1-D), and of two dimensional (2-D). In 0-D nanostructures, all the three dimensions lie in the nanoscale, examples include, nanoparticles, quantum dots. In 1-D nanostructures, two of the three dimensions lie in the nanoscale, examples include, nanowires, nanotubes, DNA. In 2-D nanostructures, one of the three dimensions lies in the nanoscale, examples include: interfaces, membranes, thin films, multi-layers. The discreteness in density of states depends upon the dimensionality of the nanostructures. Moreover, it can also be concluded that at nanoscale various properties of the material mainly depends upon the dimensions of the material.

1.2 Moore's law

On December 16, 1947 at Bell laboratories first transistor was developed by William Shockley, John Bardeen and Walter Brattain [7]. This invention was a milestone for solid-state electronics in the 20th century. Later in 1956 Nobel Prize was awarded for this invention. In 1965 Gordon Moore, predicted that the number of transistors would be doubled on an IC chip in every 18 months resulting from the miniaturization of electronic devices [8]. However, now a days Moore’s law has reached its physical limit and we are moving towards the atomic scale dimensions. So, it would not be possible to continue Moore's law in future technology. Therefore, the research has been directed to synthesize materials, which can be fabricated as per the existing fabrication line [9, 10].

1.3 Spintronics

Earlier only charge of the electron was considered for the memory storage devices, the spin of the electron was ignored, whose consideration had emerged as spintronics. In such kind of materials the spin of the electron carries information. This new category of the memory devices

can combine both semi conductivity and magnetism in one device. This technology offers the combination of standard microelectronics and spin dependent properties which causes due to the interaction of the spin of the carrier and magnetic parameters of the material [11, 12].

Upon the addition of the spin degree of freedom to semiconductor substantially add more ability and performance to electronic products. There are various advantages of these new devices such as nonvolatility, decreased electric power consumption, increased data processing speed, and increased integration densities [13]. In 1988 the invention of giant magneto resistive effect (GMR) is responsible for the new era of electronics i.e spintronics [14]. Moreover the theoretical model proposed by Datta-Das field effect transistor in 1990 also enhances the interest of the researchers in developing the new materials those comprises of the properties of magnetic material and a semiconductor [15-17].

1.4 Dilute magnetic semiconductor

In new category of semiconducting materials in which random replacement of the parent atoms by magnetic atoms are known as semimagnetic semiconductors (SMSC) or Dilute magnetic semiconductors (DMS) as shown in Figure 1.3 [16,18,19].

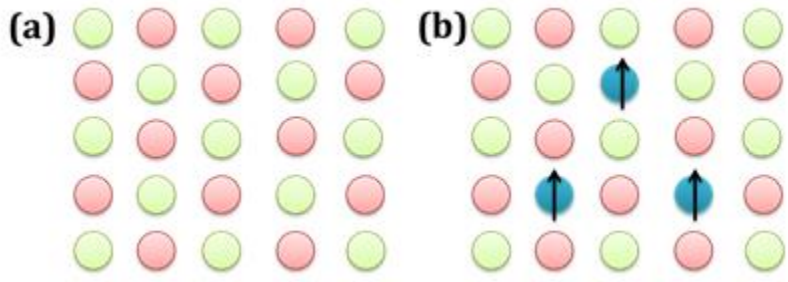

Figure 1.3 (a) Non - magnetic host semiconductor material (b) DMS material; magnetic dopant atoms are shown by blue dots.

By varying the concentration of the magnetic ions the magneto optical and magnetic properties of the material can be modified. Following criteria are a great help in the selection of materials for semiconductor spintronics. First, the ferromagnetism is retained at room temperature. Second, it would much advantageous if there be some existing technology base in other applications [20].

DMS materials can have applications in light emitting diodes, spintronics devices, band-gap lasers, magnetic resonance imaging (MRI), engineering devices, field detectors, and solar cells [21]. In the last few years, scientific community has shown intense interest in the doping of magnetic ions into the II-VI and III-V semiconductors.

1.5 Mechanisms (or theories) explaining the magnetism in DMS materials

Till date the origin of magnetism remains controversial in DMS materials. The various mechanisms (or theories) were proposed to enlighten the origin of magnetism in these DMS materials and are summarized below.

1.5.1 RKKY Interactions

RKKY exchange interactions were proposed by Ruderman and Kittel and later explained by Kasuya and Yosida [22].These are the long range indirect exchange interactions between the magnetic dopant and delocalized conduction band electrons of the host material. It is defined by Hamiltonian H_{ex} as:

$$H_{ex} = \sum_{ij} J \frac{2K_F\delta \cos(2K_F\delta) - \sin(2K_F\delta)}{(2K_F\delta)^4} \overrightarrow{s_i}\,\overrightarrow{s_j}$$

Where $\delta(r_{ab})$is the distance between the interacting magnetic ions a and b, (K_F) is Fermi wave vector of electron gas and J is the interaction parameter, $\underset{S_i}{\rightarrow}$and $\underset{S_i}{\rightarrow}$spins of electrons at sites i and j, respectively [23]. In case of metals these types of interactions are seen, as there is no direct overlapping of electronic orbitals of adjoining magnetic ions. The localized ion spin behave as an effective field to polarize the spin of conduction band and further decays oscillatory as shown in Figure 1.4 [23].

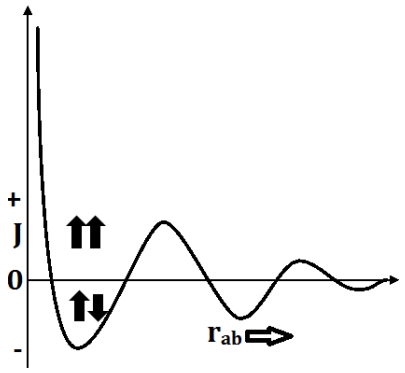

Figure 1.4 RKKY Exchange parameters (J) as a function of inter atomic distance of magnetic atoms.

Depending upon separation of between magnetic ions, the oscillations may have ferromagnetic or anti ferromagnetic exchange couplings. When there are large number of localized electrons in the host material then these exchange interaction becomes dominant [23].

1.5.2 Double exchange interactions

In 1951, Clarence Zener gives an idea about Double exchange interactions [24]. These types of interactions occur in ions having different oxidation states. Due to the difference in the oxidation states, the shifting of electron takes place from one ion to another. In case of DMS materials the doped magnetic ions (Transition metal(TM) or Rare earth (RE) metal) interact through the p-

orbital of host semiconductor. The overall energy of the system decreases which in turn give rise to ferromagnetic behaviour [25].

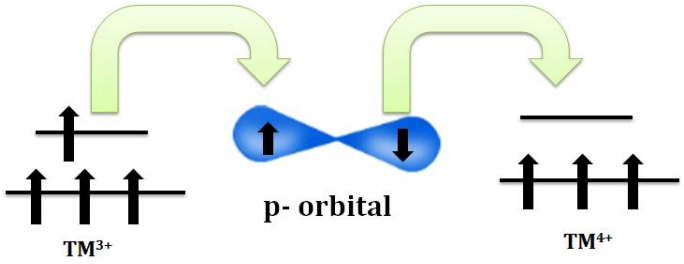

Figure 1.5 The schematic representation of double exchange interactions in DMS materials.

1.5.3 Superexchange interactions

Superexchange interactions were discovered by Hendrik Kramers in 1934 [26], while observing that in MnO, Mn atoms are interacting despite nonmagnetic oxygen atoms are between them. In this case the interacting electrons of the dopant do not move from one to another. Antiferromagnetic behavior of DMS materials is mainly due to the super exchange interactions [27].

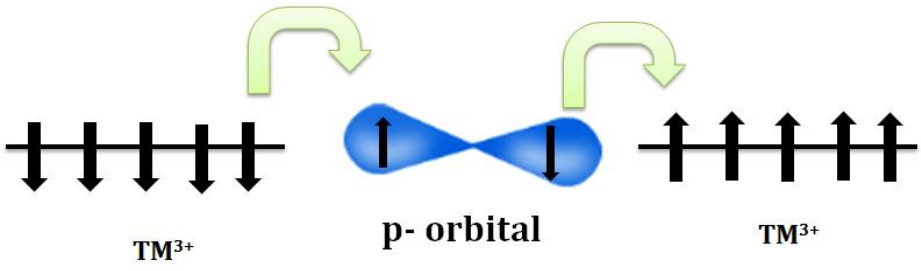

Figure 1.6 The schematic representation of Superexchange interactions in DMS materials.

1.5.4 Bound magnetic polaron (BMP)

During the interaction of electron and hole in the vicinity of the dopant ion in the host material, a magnetization cloud has been formed which is known as BMP. In case there is a large number of BMPs, then they start overlapping with each other and give rise to long-range ferromagnetism. BMP model for the magnetism in oxide based DMS materials was purposed by coey et al. which is shown in Figure 1.7 [28].

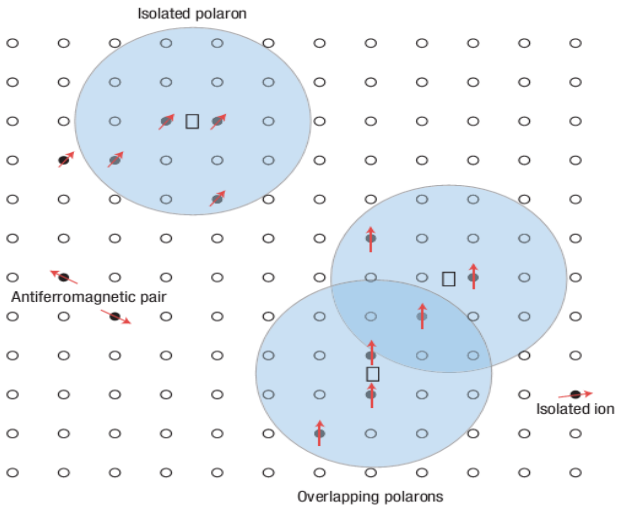

Figure 1.7 Schematic representation of BMP mechanism in DMS materials [23].

In model the cation ions of the host oxide are depicted by small circles, also the oxygen vacancy is shown by square. Magnetic dopant ions are shown by black solid circles with red arrows. In the host semiconductor there were vacancies in which the charge carriers i.e. electrons and holes gets trapped. The interaction of dopant magnetic ions via trapped charge carriers, results an effective magnetic field.

1.6 Literature Review

On reviewing literature, following technical applications emerge:

Category of materials called Concentrated Magnetic Semiconductors and Semimetals were first introduced in 1960s, reporting both the ferromagnetic and semiconducting properties of $CrBr_3$having Curie temperature (T_C) of 37 K which was found to be very low [29]. Later on, there were studies on some other metals such as $CdCr_2S_4$ (T_C = 84.5 K), $YTiO_3$ (T_C = 29 K), EuO (T_C = 79 K), $CdCr_2Se_4$ (T_C = 130 K), Fe_3O_4, EuX (X = Se, Te ,O, S), CrO_2 (T_C = 400 K), $SeCuO_3$ (T_C = 26 K), $BiMnO_3$ (T_C = 105 K), $HgCr_2Se_4$ (T_C = 106 K). Semimetals–double perovskites $A_2BB'O_6$:Sr_2CrReO_6 (T_C = 635K), Sr_2FeMoO_6 (T_C = 420 K), Sr_2FeMoO_6 (T_C = 416 K), Sr_2CrReO_6 (T_C = 620 K); Semimetals: CrAs, MnSb, MnAs, CrSb and Heusler alloys X_2YZ (X, Y are transition metals; Z is III–V group elements).

In beginning of 1970s, Eu-based chalcogenide materials exhibiting ferromagnetism with T_C = 50K or less were of major interest. These systems were strongly insulating but poor in semi-conducting transport properties [18].

In 1980s, major efforts were made in magnetically doped II–VI quaternary and ternary semiconductors alloys such as: (CdT)Te, (CdT)Se (T = Fe^{2+}, Mn^{2+},$Co^{2+,}$), PbSnMnTe, $Cd_{1-x}Mn_xTe$, (T_C< 10 K); anti-ferromagnets, paramagnets and spin glasses but most of these materials had spin glass or related disordered magnetic behavior and also had very low curie temperature i.e. 5K.

Semimagnetic semiconductors were introduced in 1990s, which were as: $A^{IV}B^{VI}$ and $A^{II}B^{VI}$ hosts(A^{IV} = Sn, Pb; A^{II} = Cd, Zn, Hg; B^{VI} = Se, S, Te) such as II-VI (ZnMnSe, ZnCrTe, ZnCrSe,

CdMnTe, CdMnSe), IV-VI (PbMnTe, (Pb, SnMn)Te, VI (GeMn, SiMnC), Oxides (ZnO, TiO_2, SnO_2, Cu_2O), ($CdGeMnP_2$, $ZnGeMnP_2$, ZnSnMnAs)[30, 31].

In 2000, Dietl gave the theoretical prediction of such materials those possess the features of DMS. Mn-doped GaN and ZnO exhibit the room temperature ferromagnetism. After this examination various reports were published on different materials those shows room temperature ferromagnetism such as; III-VI compounds (In, Mn)As, (Ga,Mn)As, (Ga,Mn)P, (Ga,Mn)N. But the doping of Mn into the host semiconductor was not thermodynamically stable [30].There are also reports on the doping with other transition metal ions in III-nitride materials, such as Mn-doped AIN [32], Cr-doped GaN [33], Cr-doped AIN [33, 34], Co-doped GaN [35], Fe-implanted p type GaN epilayer [36], Gd-doped GaN films [37], and Vanadium (V) doped GaN [35]. Moreover, for the III–V DMSs, the ferromagnetism with T_C often above room temperature has been found in several other DMSs, including $Ge_{1-x}Mn_x$ [38], $Cd_{1-x}Mn_xGeP_2$ [39], $Ti_{1-x}Co_xO_2$ [40], and $Zn_{1-x}Co_xO$ [41].

From the class of III-V semiconductors, GaAs is one of the promising semiconductor that widely used in electronic equipment's like cellular phones, compact disks (semiconductor lasers) etc. One of the major difficulties in case of III-V semiconductors is the less solubility of the order of 10^{18} cm^{-3} or less of transition metals in the host semiconductors.On the completion of 1990s thin films were grown by the newly developed techniques such as metal-organic chemical vapour deposition (MOCVD), molecular beam epitaxy (MBE), chemical vapour deposition (CVD), radio frequency sputtering (rf-sputter) which makes it possible the addition of magnetic materials beyond solubility limit. The drawbacks of these techniques are that they are very costly, time consuming, and require high purity precursors as well as high vacuum system [42].

In 1978 Scientist Robert R. Galazka coined the term DMS for the first time [43]. They reported the growth of II-VI alloys. The group studied the magneto-optical features of the different II-VI alloys, also reported very low Curie temperature. Due to the unique magnetic and optical properties of transition and rare earth metal-doped II-VI semiconductors such as CdS [44], ZnS [45], CdSe [46], CdTe [47], ZnSe [48], ZnO [49] are of much interest for the researchers now a days.

Among these II-VI semiconductors CdS could be a most promising candidate as DMS material. CdS is direct band gap semiconductors i.e. (2.4eV). CdS is the very attractive material due to its unique optoelectronic properties; due to these various features it has a variety of the applications like light emitting diodes, nonlinear optical devices, electrically driven lasers etc.Furthermore, CdS becomes the most promising materials which can behave as a diluted magnetic semiconductor. Today, the research in this field has gained great renewed interest as it made possible to integrate electrical, optical, and magnetic properties in a particular material. It has been found that the electronic as well as the magnetic properties of such DMSs nanostructures are affected greatly by reducing its dimensions. The understanding of change in the magnetic behaviour at reduced dimensions is essential for device miniaturization.

First report on magnetic property of undoped CdS has been reported in 1955. With the help of Gouy method magnetic susceptibility of CdS and ZnS at various temperatures from 77K to 300K has been measured. No temperature dependent Para-magnetism was found in the cadmium sulfide. It has observed that CdS is diamagnetic in nature whose specific diamagnetic susceptibility is -0.268×10^{-5} [50].

Krkitman et al. (1966) worked on spherical shaped CdS single crystals those consists of impurity in the form of manganese which ranges from 0.026 to 5.0% mole fraction. The magnetic-susceptibility measurements have indicated the importance of next-nearest-neighbour and higher interactions. The result analysis shows the existence of isotropic antiferromagnetic exchange interactions between next nearest- neighbour and also in pairs of Mn^{2+} ions [51].

Barraclough et al. (1974) reported the synthesis of magnetic semiconducting spinel $Cd_{1-x}Fe_xCr_2S_4$ ($0 \leqq x \leqq 1$) by chemical vapour transport with $CrCl_3$. It has been found that the electrical resistivity at room temperature varies by seven orders of magnitude from semi-insulating $CdCr_2S_4$ to semi-metallic $FeCr_2S_4$. Resistivity Anomalies occurred at Curie temperature in case of the crystals with $x \geqq 0.46$.Due to the substitution of Cr with Fe there is rise in Curie temperature with some microstructural anomalies [52].

Homan et al. (1979) reported the pressure quenched magnetic moment measurements of CdS polycrystalline samples. The samples possess the diamagnetic behaviour ($\chi > -5x10^5$ cgs units) that transforms to positive magnetic behaviour ($\chi > 3x10^{-4}$)cgs units at higher magnetic field. This type of magnetic effects was observed at both room temperatures and liquid N_2temperatures at atmospheric pressure [53].

In 1980s, Mac Crone reported the pressure dependent high positive magnetism in polycrystalline CdS material. Between 3 and 12 kOe of field the magnetism reaches at 40G [54].

Homan reported positive magnetization in “pressure quenched” CdS. During quenching, the pressure release rates is approximately 106 bar s^{-1}.The samples were quenched at room

temperature. With the help of vibrating sample magnetometer (VSM) a linear M-H curve is measured [55].

Cote et al. report (1983) describes the magnetism in pressure-quenched CdS and Cl-doped CdS. Cl-doped CdS samples were synthesised by precipitation method with the help of acid doping. There is a huge variation in electrical and magnetic properties on doping CdS with 0.75 ± 0.1 wt. % Cl [56].

Gunnarsson et al. (1981) reported the effective Coulomb interaction U in between 3d Mn electrons in II-VI semiconductors along with the effect of host on renormalization of U. It has been found that screening effect is more efficient in case of CdTe as compared to CdS and ZnO [57].

Spasojevic et al. (1992) reported the synthesis of Mn-doped CdS ($Cd_{1-x}Mn_xS$; with x = 0.05, 0.10, 0.20, 0.35, 0.43) dilute semimagnetic polycrystalline samples. The high temperature susceptibility of $Cd_{1-x}Mn_xS$ was found according to the Curie-Weiss law. From this law, exchange integral of Mn^{2+}-Mn^{2+} interactions were obtained. He also studied the role of super exchange interaction in $Cd_{1-x}Mn_xS$ [58].

Twardowski et al. (1994) reported the doping of Fe in CdS host lattice $Cd_{1-x}Fe_xS$. The magnetic susceptibility of $Cd_{1-x}Fe_xS$ was calculated and the Curie-Weiss behaviour was found to be observed above 100 K. He, too, provided the value of the nearest neighbour exchange coupling constant JNN = −20 K [59].

Dahl et al. (1995) reported the nearest neighbour d-d exchange interaction constant J for Co in CdS (Cd_{1-x} Co_xS) using Faraday rotation (FR) experiment using magnetic field of nearly 60 T [60].

Levy et al. (1996) reported the synthesis of diluted magnetic semiconductor $Cd_{1-y}Mn_yS$ (y = 0.0 to 0.3) nanoparticles by reverse micelles method with particle size in the range of 1.9 to 3.5 nm. The non-linear variation for $Cd_{0.9}Mn_{0.1}S$ particles, in band gap and composition, was observed to due to the quantum size effect. With the help of EPR measurements, the distribution of Mn ions was analysed [61].

Feltin et al. (1999) reported, the magnetic properties of $Cd_{1-y}Mn_yS$ nanocrystals having average size of 4 nm at different concentrations of y. Magnetic properties for the nanocrystals were found to get enhanced as compared to those of bulk material. In case of bulk phase, isolated Mn^{2+} ions in the tetrahedral coordination with higher y composition were responsible for the photoluminescence and the EPR hyperfine structure. The fluorescence due to isolated Mn^{2+} ions was observed at large composition in the nanoparticles [62].

Pan et al. (2008) reported the doping of carbon in CdS. Using (g) first-principles calculations, ferromagnetism was predicted due to the substitution of carbon. Hole is responsible for double exchange interactions causing ferromagnetism. The Monte Carlo simulation provided transition temperature of 270 K at 5.55% of carbon concentration [63].

Madhu et al. (2008) reported the synthesis of undoped GaN and CdS nanoparticles of size 10-25 nm. From the magnetic measurements, it was found that the synthesised nanoparticles exhibited the ferromagnetic behaviour of the order of 10^{-3} emu/gm. The observed magnetization was

similar to that of nonmagnetic oxides. The diamagnetic behaviour was observed in the agglomerated nanoparticles of GaN and CdS [64].

Bogle et al. (2008) reported the synthesis of Co-doped CdS nanoparticles by high energy electron irradiation technique. The successful incorporation of dopant was verified with the help of optical and photoluminescence studies. Magnetism was observed in the samples though its weak and moreover it decreases at higher concentration of cobalt. To analyse this anomalous magnetic behaviour first principle density functional calculations were executed. This study confirmed that the presence of defects have a fascinating effect on the Co-CdS semiconductors [65].

Chandramohan et al. (2010) presented the synthesis of Co-doped CdS thin films with ion implantation method at 573 K and studied their structural and optical properties. After structural investigation it was observed that upon doping, no secondary phase was observed. The values of d-spacing were found to be reduced. However, Raman scattering confirmed the higher crystalline quality of the thin films [66].

Hu et al. (2011) reported the synthesis of Co doped CdS diluted magnetic semiconductor nanocrystals having size of 3-4 nm. First-principle calculations confirmed the ferromagnetism in Co-doped CdS nanocrystals not only because of the Co doping but also due to Cd vacancies. The experimental and the theoretical explanations were found to be in agreement with each other [67].

Li et al. (2011) studied the electronic and magnetic behaviour of Cu-doped CdS diluted magnetic semiconductors using FLAPW method. Half -metallic character with magnetic moment of 1.0

μB per supercell was observed. There exists a Cu(3d)–S(3p)–Cd–S(3p)–Cu(3d) coupling chain, which gives rise to the ferromagnetism. Curie temperature was predicted as 400 K. This study reveals that Cu-doped CdS supercell is the promising candidate for applications in electronics and spintronics [68].

Srivastava et al. (2011) reported the synthesis of magic-sized undoped and Cr-doped CdS dilute magnetic quantum dots by lyothermal method. Quantum confinement effects were observed in the synthesised quantum dots. Ferromagnetic behaviour due to interaction of Cr ions in the CdS matrix was explained with the help of BMP model [69].

Murali et al. (2012) reported the synthesis of undoped and Fe-doped CdS (2–5 at %) nanocrystals by chemical co-precipitation method having average crystallite size, 1.2–2 nm. Mercaptoethonal was used as a capping agent. From XRD pattern, undoped CdS nanocrystals were bi-phasic but on the other hand Fe-doped nanocrystals were of hexagonal phase. It has been observed that undoped nanocrystals exhibit diamagnetic character whereas upon Fe doping the ferromagnetic behaviour arises due to the Fe-Fe super exchange interactions. Electron paramagnetic resonance (EPR) study confirms the incorporation of Fe into CdS host lattice [70].

Ren et al. (2012) reported the magnetic and electronic properties of Pd-doped CdS using first principles study. This theory confirms that the sample becomes spin–polarized upon Pd-doping and behaves as a dilute magnetic semiconductor. Hybridized chain formation is responsible for the long-range FM coupling [71].

Kumar (2012) reported on co-doped Ni- and Cu-CdS nanoparticles synthesized using wet chemical synthesis method having size about 5 nm; superconducting quantum interference device (SQUID) confirms their ferromagnetic behaviour [72].

Murali (2013) reported the synthesis of undoped and Mn-doped CdS nanowires through chemical vapor deposition method and used Au as a catalyst. Structural analysis reveals the wurtzite phase of the synthesized nanowires. They observed quenching of the red band emission upon Mn doping, which is due to the defect formation. Ferromagnetic behaviour was exhibited by synthesized nanowires [73].

Giribabu (2014) reported the co-doping of cobalt and manganese into CdS host lattice by the surfactant assisted simple chemical co-precipitation method. From XRD they confirmed that there was no secondary phase formation and TEM reveals the particle size to be 4-5 nm. EPR hyperfine splitting confirms the presence of Mn on the surface of the nanocrystals but not fully substituted into the lattice. On the basis of Bound magnetic polaron (BMP) theory the interactions between the Mn ions were explained [74].

From above discussion, it is clear that with the doping of transition metals and rare earth metals in CdS nanostructures, ferromagnetism is induced in CdS nanostructures. From maximum of the reports on transition metals-doped and rare earth metal doped CdS nanostructures are focused on optical studies and structural studies, whereas very less efforts have been done on magnetic studies. In this work, we have tried to unite both studies, optical as well as magnetic along with the structural one, so as to exploit CdS as a potential DMS material [75, 76].

The dopants selected are transition metals with partially filled d-states as well as f-states of rare earth elements. Combination of both of the properties, semiconducting and magnetic, DMS material leads to magneto-resistance, magneto-optical effect, spin manipulation and quantum hall effect. DMS are very promising materials for future device applications which find technological importance and help to understand basic fundamentals. The transition metal doped CdS semiconductor nanoparticles are found to be one of the promising candidates for spintronic applications.

The low T_C of DMS material poses serious challenges, and several efforts were made to achieve T_C higher than room temperature. Spintronics calls for DMS materials with high T_C to understand their magnetic behaviour, which is due their complex mechanism. This motivated us to carry out investigations in order to achieve and understand the observed magnetism in DMS materials.

1.7 CdS nanostructures as potential DMS material

II-VI DMS materials are particularly interesting as their doping with magnetic ions turn them into compounds exhibiting diverse magnetic properties at room temperature. CdS is an important candidate this group with excellent physical properties having direct band gap of 2.4 eV (bulk). CdS is a wide-band gap II–VI semiconducting material with high mobility, electronic transport, and, in addition, it displays good magnetic, optical, and magneto-optical properties. This necessitates the possibility of integrating multifunctions such as electrical, optical, and magnetic in CdS nanomaterials. CdS being of immense use in optoelectronics has been studied at length in devices such as light emitting diodes, solar cells, photocatalysis, biological sensors,

photodegradation of water pollutants [77]. A variety of nanostructures such as quantum dots, nanoparticles, nanorods, nanowires, tetrapods branched shaped have been synthesized [78].

The CdS is equally important as a dilute magnetic semiconductor when it is doped with transition metal and rare earth impurities [79]. Transition and rare earth metals, respectively, having partially filled d states and f states, act as magnetic impurities bearing large magnetic moments. It is important to combine electrical, optical and magnetic properties into a single material.

1.7.1 CdS Crystal Structures

Cadmium sulfide is toxic yellow solid having two crystal forms such as hexagonal (Greenockite) wurtzite with space group $P6_3mc - C_6V^4$ and the zinc blende structure (Hawleyite) with space group $F\bar{4}3m - Id^2$- the former being more stable than the latter. The wurtzite structure consists of hexagonal closed packed (hcp) structure: ABABAB…… and the zinc blende that of closed packed (ccp) structure: ABCABC…. [80]. In case of both of these structures, the cadmium and sulphur atom has four coordination numbers as shown in Figure 1.8 [81]. The several properties of CdS have been tabulated in Table 1.1.

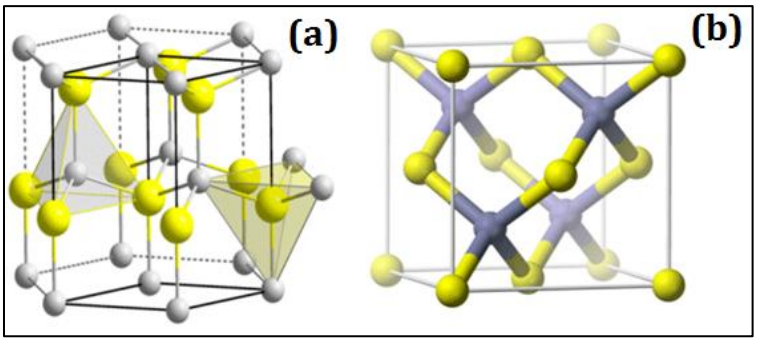

Figure1.8 (a) Wurtzite crystal structure and (b) Zinc blende crystal structure of CdS.

Table 1.1 Properties of CdS [82].

Properties	Types or values
Phase stable at 300 K	Wurtzite (Hexagonal)
Solubility in water	Insoluble
Lattice parameters at 300 K	Zinc blende (a = 0.582 nm), Wurtzite (a = 0.4135 nm, c = 0.6749 nm)
Solubility	Soluble in acid
Molar mass	144.47 g mol^{-1}
Refractive index (n_D)	2.529
Melting point	1700 ℃
Density of wurtzite phase	4.82 g cm^{-3}
Toxicity	Low

1.8 Objectives of the thesis

In this thesis, the synthesis of undoped and transition metal (Fe, Ni, Co, Gd)-doped CdS nanostructures, viz., nanoparticles and nanorods were carried out by various chemical routes. Various techniques such as XRD, TEM, EDS, UV-visible, PL spectroscopy, and VSM were employed for their characterization. The effect of doping on structural, optical and magnetic properties was investigated as well as the possible origin of magnetism was discussed in detail.

References

[1] Hosokawa M, Nogi K, Naito, Yokoyama, "Nanoparticle technology handbook", Elsevier, UK (2010).

[2] R.P. Feynman, There's plenty of room at the bottom, Miniaturization, H. D. Gilbert, ed., Reinhold Publishing, New 1961 pp. 282-296.

[3] Whatmore RW. Ferroelectrics, microsystems and nanotechnology. Ferroelectrics. 1999 Mar 1;225(1):179-92.

[4] Shah, M. A., and Tokeer Ahmad. Principles of Nanoscience and Nanotechnology. Alpha Science Internat (2010).

[5] Binnig G, Rohrer H, Gerber C, Weibel E. Tunneling through a controllable vacuum gap. Applied Physics Letters. 1982 Jan 15;40(2):178-80.

[6] http://www.edn.com/Home/PrintView?contentItemId=4391796

[7] Brinkman WF, Haggan DE, Troutman WW. A history of the invention of the transistor and where it will lead us. IEEE Journal of Solid-State Circuits. 1997 Dec;32(12):1858-65.

[8] Schaller RR. Moore's law: past, present and future. IEEE spectrum. 1997 Jun;34(6):52-59.

[9] Sarma SD. A new class of device based on electron spin, rather than on charge, may yield the next generation of microelectronics. American Scientist. 2001 Nov;89(6):516.

[10] Wolf SA, Awschalom DD, Buhrman RA, Daughton JM, Von Molnar S, Roukes ML, Chtchelkanova AY, Treger DM. Spintronics: a spin-based electronics vision for the future. Science. 2001 Nov 16;294(5546):1488-95.

[11] Žutić I, Fabian J, Sarma SD. Spintronics: Fundamentals and applications. Reviews of modern physics. 2004 Apr 23;76(2):323.

[12] Awschalom DD, Flatté ME. Challenges for semiconductor spintronics. Nature Physics. 2007 Mar 1;3(3):153-9.

[13] Bahar RI, Hammerstrom D, Harlow J, Joyner WH, Lau C, Marculescu D, Orailoglu A, Pedram M. Architectures for silicon nanoelectronics and beyond. IEEE Computer. 2007 Jan 1;40(1):25-33.

[14] Fert A. The present and the future of spintronics. Thin Solid Films. 2008 Nov 3;517(1):2-5.

[15] Datta S, Das B. Electronic analog of the electro-optic modulator. Applied Physics Letters. 1990 Feb 12;56(7):665-7.

[16] Singh N, Goolaup S, Adeyeye AO. Fabrication of large area nanomagnets. Nanotechnology. 2004 Oct 1;15(11):1539.

[17] Jeon HC, Jeong YS, Kang TW, Kim TW, Chung KJ, Jhe W, Song SA. (In1–xMnx) As Diluted Magnetic Semiconductor Quantum Dots with Above Room Temperature Ferromagnetic Transition. Advanced Materials. 2002 Dec 3;14(23):1725-8.

[18] Furdyna JK. Diluted magnetic semiconductors. Journal of Applied Physics. 1988 Aug 15;64(4):R29-64.

[19] Takeyama S, Adachi S, Takagi Y, Aguekian VF. Exciton localization by magnetic polarons and alloy fluctuations in the diluted magnetic semiconductor $Cd_{1-x}Mn_xTe$. Physical Review B. 1995 Feb 15;51(8):4858.

[20] Pearton SJ, Abernathy CR, Norton DP, Hebard AF, Park YD, Boatner LA, Budai JD. Advances in wide bandgap materials for semiconductor spintronics. Materials Science and Engineering: R: Reports. 2003 Feb 28;40(4):137-68.

[21] Bhargava RN. Doped nanocrystalline materials—physics and applications. Journal of luminescence. 1996 Oct 31;70(1):85-94.

[22] Ruderman MA, Kittel C. Indirect exchange coupling of nuclear magnetic moments by conduction electrons. Physical Review. 1954 Oct 1;96(1):99.

[23] Singh R. Unexpected magnetism in nanomaterials. Journal of Magnetism and Magnetic Materials. 2013 Nov 30;346:58-73.

[24] Zener C. Interaction between the d-shells in the transition metals. III. Calculation of the Weiss factors in Fe, Co, and Ni. Physical Review. 1951 Jul 15;83(2):299.

[25] Sato K, Katayama-Yoshida H. Material design for transparent ferromagnets with ZnO-based magnetic semiconductors. Japanese Journal of Applied Physics. 2000 Jun;39(6B):L555.

[26] Kramers HA. L'interaction entre les atomes magnétogènes dans un cristal paramagnétique. Physica. 1934 Dec 31;1(1):182-92.

[27] Anderson PW. Antiferromagnetism. Theory of superexchange interaction. Physical Review. 1950 Jul 15;79(2):350..

[28] Coey JM, Venkatesan M, Fitzgerald CB. Donor impurity band exchange in dilute ferromagnetic oxides. Nature materials. 2005 Feb 1;4(2):173-9.

[29] Ivanov VA. Diluted magnetic semiconductors and spintronics. Bulletin of the Russian Academy of Sciences: Physics. 2007 Nov 1;71(11):1610-2.

[30] Dietl T, Ohno H. Ferromagnetic III–V and II–VI Semiconductors. MRS bulletin. 2003 Oct 1;28(10):714-9.

[31] Ivanov VA, Ugolkova EA, Pashkova ON, Sanygin VP, Padalko AG. Ferromagnetism in dilute magnetic semiconductors and new materials for spintronics. Journal of Magnetism and Magnetic Materials. 2006 May 31;300(1):e32-6.

[32] Frazier R, Thaler G, Overberg M, Gila B, Abernathy CR, Pearton SJ. Indication of hysteresis in AlMnN. Applied physics letters. 2003 Sep 1;83(9):1758-60.

[33] Liu HX, Wu SY, Singh RK, Gu L, Smith DJ, Newman N, Dilley NR, Montes L, Simmonds MB. Observation of ferromagnetism above 900K in Cr–GaN and Cr–AlN. Applied Physics Letters. 2004 Nov 1;85(18):4076-8.

[34] Park SE, Lee HJ, Cho YC, Jeong SY, Cho CR, Cho S. Room-temperature ferromagnetism in Cr-doped GaN single crystals. Applied physics letters. 2002 Jun 3;80(22):4187-9.

[35] Lee JS, Lim JD, Khim ZG, Park YD, Pearton SJ, Chu SN. Magnetic and structural properties of Co, Cr, V ion-implanted GaN. Journal of applied physics. 2003 Apr 15;93(8):4512-6.

[36] Shon Y, Kwon YH, Park YS, Yuldashev SU, Lee SJ, Park CS, Chung KJ, Yoon SJ, Kim HJ, Lee WC, Fu DJ. Ferromagnetic behavior of p-type GaN epilayer implanted with Fe+ ions. Journal of applied physics. 2004 Jan 15;95(2):761-3.

[37] Davies RP, Abernathy CR, Pearton SJ, Norton DP, Ivill MP, Ren F. Review of recent advances in transition and lanthanide metal–doped GaN and ZnO. Chemical Engineering Communications. 2009 May 7;196(9):1030-53.

[38] Cho S, Choi S, Hong SC, Kim Y, Ketterson JB, Kim BJ, Kim YC, Jung JH. Ferromagnetism in mn-doped ge. Physical Review B. 2002 Jul 16;66(3):033303.

[39] Kleinman L, Bylander DM. Efficacious form for model pseudopotentials. Physical Review Letters. 1982 May 17;48(20):1425.

[40] Matsumoto Y, Murakami M, Shono T, Hasegawa T, Fukumura T, Kawasaki M, Ahmet P, Chikyow T, Koshihara SY, Koinuma H. Room-temperature ferromagnetism in transparent transition metal-doped titanium dioxide. Science. 2001 Feb 2;291(5505):854-6.

[41] Lee HJ, Jeong SY, Cho CR, Park CH. Study of diluted magnetic semiconductor: Co-doped ZnO. Applied Physics Letters. 2002 Nov 18;81(21):4020-2.

[42] Ohno H. Making nonmagnetic semiconductors ferromagnetic. science. 1998 Aug 14;281(5379):951-6.

[43] R. R. Galazka, Proc. 14th Int. Conf. on Physics of Semiconductors, Inst. Phys. Conf. Ser. 43, edited by B.L.H. Wilson (Institute of Physics, Bristol, 1978) p. 133.

[44] Kaur K, Lotey GS, Verma NK. Structural, optical and magnetic properties of cobalt-doped CdS dilute magnetic semiconducting nanorods. Materials Chemistry and Physics. 2013 Dec 16;143(1):41-6..

[45] Lotey GS, Jindal Z, Singhi V, Verma NK. Structural and photoluminescence properties of Eu-doped ZnS nanoparticles. Materials Science in Semiconductor Processing. 2013 Dec 31;16(6):2044-50.

[46] Singh J, Kumar S, Verma NK. Effect of Ni-doping concentration on structural, optical and magnetic properties of CdSe nanorods. Materials Science in Semiconductor Processing. 2014 Oct 31;26:1-6.

[47] Majid A, Tanveer M, Rana UA, Khan SU, Kousar S. Facile Synthesis of Mn-Doped CdTe Nanoparticles: Structural and Magnetic Properties. Journal of Superconductivity and Novel Magnetism. 2016:1-5.

[48] Norman TJ, Magana D, Wilson T, Burns C, Zhang JZ, Cao D, Bridges F. Optical and surface structural properties of Mn2+-doped ZnSe nanoparticles. The Journal of Physical Chemistry B. 2003 Jul 3;107(26):6309-17.

[49] Shatnawi M, Alsmadi AM, Bsoul I, Salameh B, Alna'washi GA, Al-Dweri F, El Akkad F. Magnetic and optical properties of Co-doped ZnO nanocrystalline particles. Journal of Alloys and Compounds. 2016 Jan 15;655:244-52.

[50] Larach S, Turkevich J. Magnetic properties of zinc sulfide and cadmium sulfide phosphors. Physical Review. 1955 May 15;98(4):1015.

[51] Kreitman MM, Milford FJ, Kenan RP, Daunt JG. Magnetic Susceptibility of Mn 2+ in CdS and Effects of Antiferromagnetic Exchange. Physical Review. 1966 Apr 15;144(2):367.

[52] Barraclough KG, Lugscheider W, Meyer A, Schäfer H, Treitinger L. Preparation, electrical and magnetic properties of $Cd_{1-x}Fe_xCr_2S_4$ single crystals. physica status solidi (a). 1974 Apr 16;22(2):401-9.

[53] Homan CG, Kendall DP, MacCrone RK. Magnetic moment of pressure quenched cadmium sulfide. Solid State Communications. 1979 Nov 1;32(7):521-4.

[54] MacCrone RK, Homan CG. Paramagnetic properties in pressure quenched CdS. Solid State Communications. 1980 Aug 31;35(8):615-8.

[55] Homan C, MacCrone RK. Anomalous paramagnetism in pressure quenched CdS. Journal of Non-Crystalline Solids. 1980 Jul 31;40(1):369-75.

[56] Cote PJ, Homan CG, Moffatt WC, Block S, Piermarini GP, MacCrone RK. Magnetic behavior of pressure-quenched CdS containing Cl. Physical Review B. 1983 Nov 1;28(9):5041.

[57] O. Gunnarsson, A. V. Postnikov, and O. K. Andersennd Zno, Density-functional calculation of effective Coulomb interactions in nonmetallic systems: Application to Mn in CdTe, CdS, and ZnO, Physical Review. 1981 Nov 15;8(40):10407-11.

[58] Spasojevic V, Rodic D, Szytula A, Bajorek A. High-temperature susceptibility of semimagnetic-semiconductor Cd1− xMnxS. Journal of magnetism and magnetic materials. 1992 Aug 1;114(1-2):70-4.

[59] Twardowski A, Chen YF, Chou WC, Demianiuk M. The dd exchange interaction in the diluted magnetic semiconductor $Cd_{1-x}Fe_xS$. Solid state communications. 1994 May 31;90(8):493-6.

[60] Dahl M, Heiman D, Foner S, Vu TQ, Kershaw R, Dwight K, Wold A. Observation of the nearest-neighbor magnetization step in CdS: Co by Faraday rotation in magnetic fields to 60 T. Physical Review B. 1995 Jun 15;51(24):17561.

[61] Levy L, Hochepied JF, Pileni MP. Control of the size and composition of three dimensionally diluted magnetic semiconductor clusters. The Journal Of Physical Chemistry. 1996 Nov 21;100(47):18322-6.

[62] Feltin N, Levy L, Ingert D, Pileni MP. Magnetic Properties of 4-nm $Cd_{1-y}Mn_yS$ Nanoparticles Differing by Their Compositions, y. The Journal of Physical Chemistry B. 1999 Jan 7;103(1):4-10.

[63] Pan H, Feng YP, Wu QY, Huang ZG, Lin J. Magnetic properties of carbon doped CdS: a first-principles and Monte Carlo study. Physical Review B. 2008 Mar 13;77(12):125211.

[64] Madhu C, Sundaresan A, Rao CN. Room-temperature ferromagnetism in undoped GaN and CdS semiconductor nanoparticles. Physical Review B. 2008 May 29;77(20):201306.

[65] Bogle KA, Ghosh S, Dhole SD, Bhoraskar VN, Fu LF, Chi MF, Browning ND, Kundaliya D, Das GP, Ogale SB. Co: CdS Diluted Magnetic Semiconductor Nanoparticles: Radiation Synthesis, Dopant− Defect Complex Formation, and Unexpected Magnetism. Chemistry of Materials. 2007 Dec 19;20(2):440-6.

[66] Chandramohan S, Kanjilal A, Sarangi SN, Majumder S, Sathyamoorthy R, Hong CH, Som T. Effect of substrate temperature on implantation doping of Co in CdS nanocrystalline thin films. Nanoscale. 2010;2(7):1155-9.

[67] Hu T, Zhang M, Wang S, Shi Q, Cui G, Sun S. CdS: Co diluted magnetic semiconductor nanocrystals: synthesis and ferromagnetism study. CrystEngComm. 2011;13(19):5646-9..

[68] Li P, Zhang CW, Lian J, Gao S, Wang X. First-principles study on electronic and magnetic properties of Cu-doped CdS. Solid State Communications. 2011 Nov 30;151(22):1712-5.

[69] Srivastava P, Kumar P, Singh K. Room temperature ferromagnetism in magic-sized Cr-doped CdS diluted magnetic semiconducting quantum dots. Journal of Nanoparticle Research. 2011 Oct 1;13(10):5077-85.

[70] Murali G, Reddy DA, PoornaPrakash B, Vijayalakshmi RP, Reddy BK, Venugopal R. Room temperature magnetism of Fe doped CdS nanocrystals. Physica B: Condensed Matter. 2012 Jun 15;407(12):2084-8.

[71] Ren M, Zhang C, Li P, Song Z, Liu X. The origin of ferromagnetism in Pd-doped CdS. Journal of Magnetism and Magnetic Materials. 2012 Jul 31;324(13):2039-42.

[72] Kumar S, Kumar S, Jain S, Verma NK. Magnetic and structural characterization of transition metal co-doped CdS nanoparticles. Applied Nanoscience. 2012 Jun 1;2(2):127-31.

[73] Murali G, Reddy DA, Giribabu G, Vijayalakshmi RP, Venugopal R. Room temperature ferromagnetism in Mn doped CdS nanowires. Journal of Alloys and Compounds. 2013 Dec 25;581:849-55.

[74] Giribabu G, Murali G, Vijayalakshmi RP. Structural, magnetic and optical properties of cobalt and manganese codoped CdS nanoparticles. Materials Letters. 2014 Feb 15;117:298-301.

[75] Kaur K, Verma NK. Hydrothermally Synthesized CdS Nanoparticles: Effect of Fe Doping on Optical and Magnetic Properties. Journal of Superconductivity and Novel Magnetism. 2015 Nov 1;28(11):3317-22.

[76] Garg I, Sharma H, Kapila N, Dharamvir K, Jindal VK. Transition metal induced magnetism in smaller fullerenes (C n for n≤ 36). Nanoscale. 2011;3(1):217-24.

[77] Elavarthi P, Kumar AA, Murali G, Reddy DA, Gunasekhar KR. Room temperature ferromagnetism and white light emissive CdS: Cr nanoparticles synthesized by chemical co-precipitation method. Journal of Alloys and Compounds. 2016 Jan 25;656:510-7.

[78] Kamran MA, Zou B, Majid A, Alharbi T, Saeed MA, Abdullah A. Synthesis and Photoluminescence of Single-Crystalline Fe (III)-Doped CdS Nanobelts. Journal of Nanoscience and Nanotechnology. 2016 Apr 1;16(4):4086-93.

[79] Kurian P, Vijayan C, Sathiyamoorthy K, Sandeep CS, Philip R. Excitonic transitions and off-resonant optical limiting in CdS quantum dots stabilized in a synthetic glue matrix. Nanoscale Research Letters. 2007 Oct 25;2(11):561.

[80] http://link.springer.com/chapter/10.1007/10681719_546#page-1

[81] https://en.wikipedia.org/wiki/Cadmium_sulfide

[82] http://www.semiconductors.co.uk/propiivi5410.html

Chapter 2

Syntheses and Characterizations

Chapter 2

Syntheses and Characterizations

There is a significant development in the field of nanostructured materials, their syntheses and characterizations due to shape and size dependent properties. In the present chapter, a unified approach has been presented for the synthesis of CdS nanostructures using solvothermal/hydrothermal route. Also, the characterization techniques employed have been discussed briefly, which include x-ray diffraction (XRD), photoluminescence (PL), UV-visible absorption spectroscopy, energy dispersive spectroscopy (EDS), transmission electron microscopy (TEM), vibrating sample magnetometer (VSM).

2.1 Synthesis of CdS nanostructures

The synthesis of various nanostructures with well-defined size and morphology is the most important part of the whole procedure. Various techniques are used for the synthesis of nanomaterials, which depend on the material chosen and the size and shape involved. Following points are to be considered during the synthesis processes such as [1]:

a) Range of applicability for different class of materials
b) Reproducibility of the average size and shape of the nanostructures
c) Control over the average particle size and range of sizes obtainable
d) Homogeneity of the phase formed.

Various synthesis techniques have been used for the synthesis of the CdS nanostructures. Among those techniques, some are: solvothermal method [2], laser ablation method [3], hydrothermal

method [4], photochemical method [5], one pot synthesis method [6], mesoporous copolymer template method [7] etc.

For synthesis, we must choose a technique, which involves less toxic precursors, cheap and highly controllable. In the present work, the hydrothermal technique has been used for the synthesis of CdS nanoparticles. A hydrothermal technique is ‘‘a chemical reaction inside closed system in the presence of a solvent (aqueous solvent) at some temperature, which must be greater than the boiling point of the solvent’’ [8].

2.1.1 Synthesis of CdS nanoparticles:

The apparatus for synthesis consists of a steel pressure vessel generally called autoclave shown in Figure 2.1

Figure 2.1 Pictorial view of Autoclave.

Hydrothermal process has some significant advantages over the other chemical methods. By varying the simple conditions like temperature, pressure, time, concentration, we can easily control the particle size and morphology of the nanostructures. Moreover, nanoparticles can be directly synthesized in one step [1, 9].

During synthesis of CdS nanoparticles by hydrothermal process shown in Figure 2.2 cadmium chloride $CdCl_2$was taken as a source of cadmium, thiourea NH_2CSNH_2 as a source of sulphur, and de-ionized (DI) water as the solvent. Appropriate amount of $CdCl_2$and thiourea was dissolved in DI water. For doping of transition (Fe, Ni, Co) and rare metals (Gd) into the CdS lattice, respectively, iron chloride, nickel chloride, cobalt chloride, gadolinium chloride were taken as source of dopant.

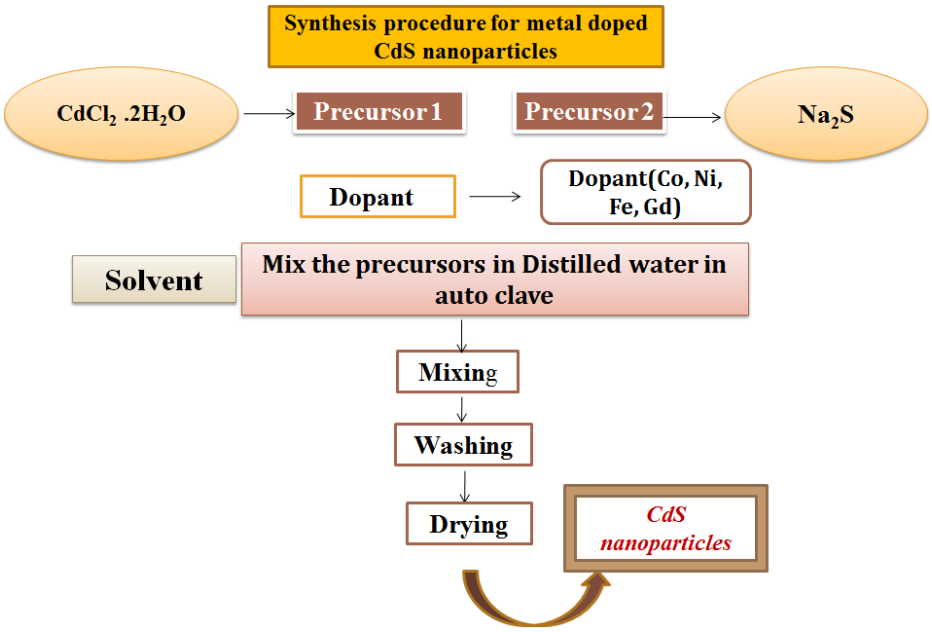

Figure 2.2 Schematic of hydrothermal/solvothermal synthesis of CdS nanostructures.

The stoichiometric amount of precursors has been added into an autoclave. Further the autoclave is sealed and kept inside a furnace at appropriate temperature for a certain required time. After completion of the reaction, the autoclave is allowed to cool. Then the precipitates of CdS nanostructures are taken out. To remove impurities, the precipitates need washing using water and ethanol and then dried to get nanoparticles.

2.1.2 Reaction mechanism

The formation of nanoparticles can be understood by nucleation and growth process [10]. During the hydrolysis of thiocarbamide in an alkaline medium, S^{-2}ions are formed:

$$NH_2CSNH_2 + 2OH^- \rightarrow S^{-2} + NH_2CN + 2H_2O$$

Cd (II) ions react with S^{-2}ions to form CdS molecules, which are further nucleated and grown to make CdS nanoparticles.

$$Cd^{2+} + S^{2-} \rightarrow CdS$$

$$n(CdS) \rightarrow (CdS)_n \rightarrow Nucleation/Growth \rightarrow CdS_{nanoparticles}$$

2.1.3 Synthesis of CdS nanorods

During synthesis of CdS nanorods, using solvothermal technique, various parameters such as temperature, time, and concentration plays very important role. The Schematic of the synthesis of nanorods is similar to that for nanoparticles (Figure 2.2) with the only difference are that in this case ethylenediamine is used as a solvent.

2.1.4 Reaction Mechanism

The solvent coordination molecular template (SCMT) mechanism is used to explain the formation of CdS nanorods [11]. For synthesis of nanorods, ethylenediamine is used both as a solvent as well as a chelating agent. The reaction process for the formation of CdS nanorods is shown in Figure 2.3. First the formation of layered structure of CdS·0.5en takes place. These layers are connected by en molecules via coordination bonds between two neighboring Cd^{2+} ions. Finally the en molecules come out of it leading to the formation of nanorods,

During first step, Cd^{2+}ions react with en molecules to give bidentate ligand $[Cd(en)_2]^{2+}$.

$$Cd^{2+} + 2en \leftrightarrow [Cd(en)_2]^{2+}$$

Finally, the CdS nanocrystals start nucleating and grow according to the following reaction:

$$[Cd(en)_2]^{2+} + S^{2-} \rightarrow CdS \cdot 0.5en \rightarrow CdS + en$$

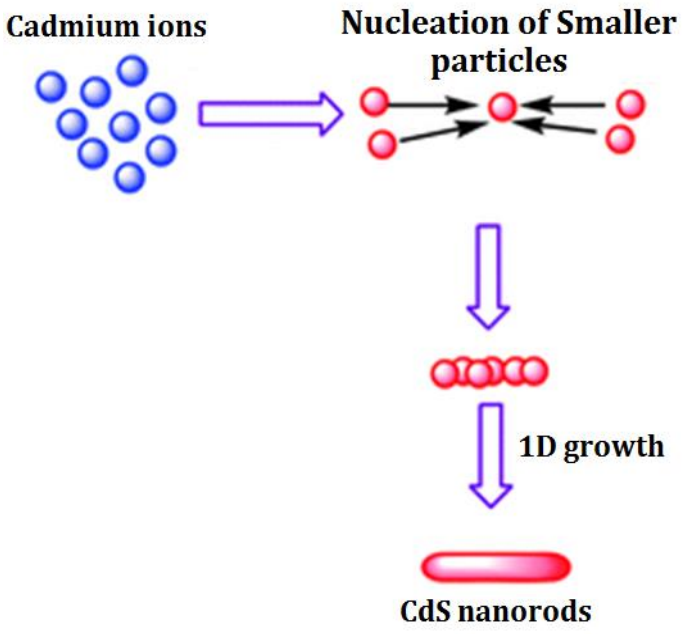

Figure 2.3 Schematic representation of formation of CdS nanorods [12].

2.1.5 Doping in CdS nanostructures

In the present work, doping has been done of transition metals (Fe, Ni, Co) and rare earth metal (Gd) into CdS nanostructures. Addition of dopant into CdS plays vital role in making CdS as a significant DMS material. The various precursors used in the synthesis of metal doped CdS nanostructures are listed below:

- Cadmium precursors- Cadmium acetate ($Cd(ac)_2.2H_2O$), Cadmium chloride($Cdcl_2.H_2O$)
- Sulphur precursors- Sodium sulphide (Na_2S), Thiourea (CSN_2H_4)

- Transition metals precursors- Ferrous chloride tetra-hydrate ($FeCl_2.4H_2O$), nickel chloride hexa-hydrate ($NiCl_2.6H_2O$) and cobaltous chloride hexa-hydrate ($CoCl_2.6H_2O$)
- Rare earth metal- Gadolinium (III) nitrate hexa-hydrate (Gd (NO_3).$6H_2O$)

Following compositions were synthesized using the above procedure:

- *Fe, Co, Ni, Gd-doped CdS nanorods*
    - $Cd_{1-x}Fe_xS$(x = 0.00, 0.03, 0.05, 0.10, 0.15)
    - $Cd_{1-x}Co_xS$ (x = 0.00, 0.05, 0.10 and 0.15)
    - $Cd_{1-x}Ni_xS$ (x = 0.00, 0.03, 0.05, 0.10)
    - $Cd_{1-x}Gd_xS$ (x = 0.00, 0.01, 0.03, 0.05, 0.10, 0.15)
- *Fe, Co, Ni, Gd-doped CdS nanoparticles*
    - $Cd_{1-x}Fe_xS$ (x = 0.00, 0.03, 0.05 and 0.10)
    - $Cd_{1-x}Co_xS$ (x = 0.00, 0.03,0.05, 0.10)
    - $Cd_{1-x}Ni_xS$ (x = 0.00, 0.03, 0.05 ,0.10)
    - $Cd_{1-x}Gd_xS$ (x = 0.00, 0.03, 0.05, 0.10)

2.2 Characterization techniques

2.2.1 X-ray diffraction (XRD)

2.2.1.1 Introduction

In 1895 Roentgen revolutionized the scientific community with the discovery of X-rays, and in this regard he was honoured with the noble prize in 1901.X-rays are electromagnetic waves having wavelength in the range of 0.01 to 0.1 nm [13]. The interatomic distance in the crystals is comparable to the wavelength of the X-rays, so when these materials are exposed to the X-rays, a diffraction pattern is formed due to constructive interference. X-rays are scattered by the constituents of the solids comprising atoms, molecules or ions and provide information about the structure of the solids including phase identification, grain size, bond angles crystallinity, crystal defects and strain. X-ray diffraction can be used for the qualitative and quantitative investigation of the various crystals. Every solid produces a distinct X-ray pattern, which is characteristic of its crystalline structure [14].

2.2.1.2 Bragg's Law

The Bragg's law condition can be expressed as (Figure 2.4):

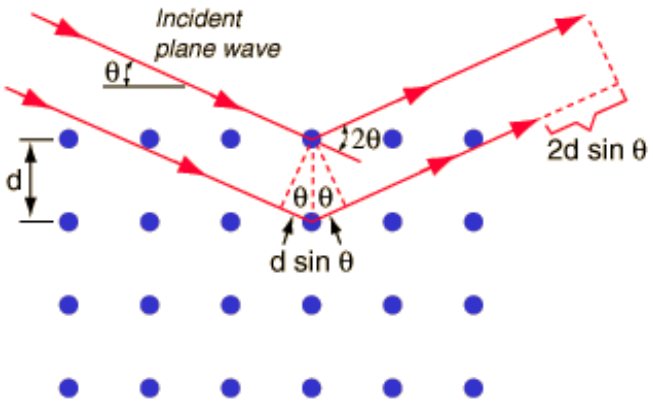

Figure 2.4 Bragg's law of diffraction [15].

The Bragg's law condition can be expressed as:

$$2dsin\,\theta = n\lambda$$

Where, n (an integer) is the order of reflection; λ, wavelength of the incident X-rays; d, interplanar spacing of the crystal; θ, is the glancing angle.

2.2.1.3 Instrumentation and working of XRD

Figure 2.5 shows the photograph of X-ray diffractometer installed at Thapar University, Patiala. To produce X-rays, the electrons from the cathode-ray tube filament are accelerated towards the target by applying a very high voltage of the order of 15-60 kV.

Various target materials are used for producing X-rays such as Cu, Fe, Mo, Cr. However, the most commonly used for single-crystal diffraction is Cu with $K_\alpha$radiation having wavelength = 1.5418Å.Characteristic X-ray spectra consist of various K_α and K_β radiation, which are produced when electrons from the inner shell of the target material are removed with the help of an electron beam of adequate amount of energy. The intensity of the reflected X-rays is recorded [16].

The various types of detectors used to detect X-rays are scintillation detector, gas proportional counter, Ge solid state detector, linear CCD, image plate detector, CCD-camera, photographic film.

Figure 2.5 Pictorial view of x-ray diffractometer.

2.2.1.4 Sample preparation

In case of x-ray powder diffraction structural analysis, sample preparation plays a vital role. For the powdered samples, there is a need to grind well with the help of an agate mortar and pestle. Moreover, the sample should be well mixed as only its thin surface layer is required for analysis. However, polishing of the powdered sample is not required. The sample is then poured on to a sample holder made of plastic, aluminum or glass and compressed with a glass plate to attain a flat surface to ensure no reduction in the intensity of low angle peaks [17].

2.2.1.5 Applications of XRD

XRD is most commonly used for phase analysis of crystalline materials. The analysis of XRD diffraction patterns is done using standard JCPDS (Joint Committee on Powder Diffraction Standards) data base. There are different JCPDS cards for different materials. Following information can be obtained:

- Determination of unit cell dimensions
- X-ray density

- Porosity
- Particle size

In the present thesis, recording of XRD patterns of the synthesized samples has been done using PANalytical X'Pert PRO X-ray diffractometer with CuK$_\alpha$ (λ = 1 .5418 Å) radiation operated at 45 kV and 40 mA as well as Shi-madzu, LabX XRD-6000, diffractometer with CuK$_\alpha$ (=1.5418 Å) operated at 40 kV and 30 mA.

2.2.2 UV-visible spectroscopy (UV-vis)

2.2.2.1 Introduction

UV–visible spectroscopy pertains to absorption spectra when visible (400 to 800 nm.) and ultraviolet (190 to 400 nm) light sources are used. Using UV-vis set up, precise wavelength of the light source used and the intensity of light absorbed by the sample are measured. On absorbing UV or visible light, the molecules cause excitation of atoms from ground state to excited state.

2.2.2.2 Beer-Lambert law

In case of UV-visible spectroscopy a light beam of intensity(I_o) passes through a solution whose concentration(c) in a sample holder known as cuvette (Figure 2.6) (path length, b), then some of the amount of light the amount of light is absorbed and rest of the part is transmitted(I_t) [18].

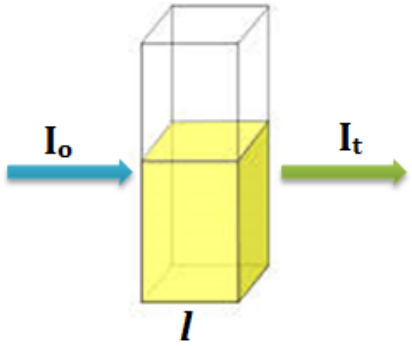

Figure 2.6 Illustration of Beer-Lambert law.

Transmittance is the defined as the ratio light intensity entering the sample (I_o) to that leaving the sample (I_t) at a particular wavelength. The percent transmittance (%T) can be expressed as:

$$\%T = \left(\frac{I_o}{I_t}\right) \times 100$$

Beer- Lambert law, for an ideal solution, there is a linear relationship between concentration and absorbance at fixed path length and wavelength:

$$A = \varepsilon cl$$

Where A = absorbance, l = length of cuvette, ε = molar absorptivity.

2.2.2.3 Instrumental and working of UV-visible spectroscopy

A schematic diagram of a UV-visible spectrometer is given in Figure 2.7 and a pictorial view is shown in figure 2.8. A UV-visible spectrometer is made up of five basic parts: *light source* which may be deuterium lamp (190-400 nm), a *monochromatic* which selects the single wavelength from a wide range of wavelengths of the incident light. For each wavelength the intensity of light passing through both the reference (Io) and the sample cuvette (I) is measured. The *sample holder* cuvette is used.

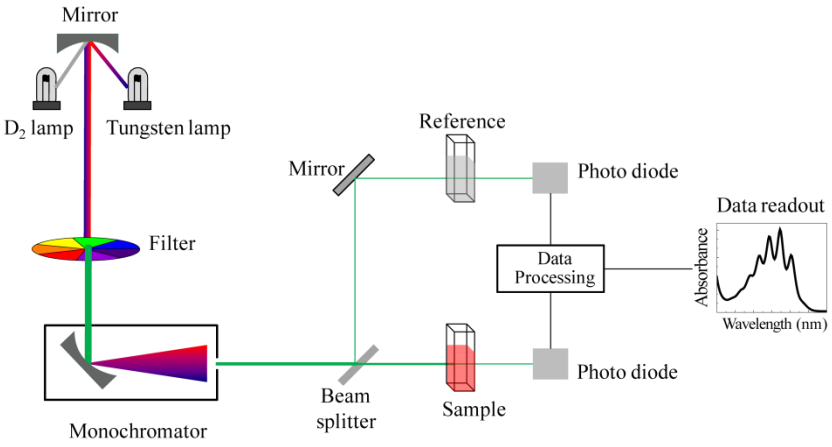

Figure 2.7 Illustration of essential components in a UV-vis spectrophotometer.

The sample holder for the sample and reference solution needs to be transparent to the radiation so that it will pass through them. Cuvettes for the spectroscopy are generally made up of quartz or fused silica. To detect the intensity of the radiation passing through the sample a *detector* (a photo- or photomultiplier tube) is used and it also converts light signals to electrical signals. The *Signal processor* plots the absorbance against wavelength [19, 20].

Figure 2.8 Pictorial view of UV-visible spectrophotometer.

2.2.2.4 Sample preparation

For UV-Visible spectroscopy, the powdered sample, i.e., the synthesized nanoparticles are dispersed in a solvent, which dissolves them completely. Moreover, the solvent should not react with the sample. Finally, the solution is kept for ultra sonication for a few hours.

2.2.2.5 Information from UV-Visible

- Band gap measurement
- To detect the impurities
- Structure clarification of organic compounds
- Quantitative/Qualitative analysis
- Dissociation constants of bases and acids
- Molecular weight determination [21]

2.2.3 Transmission electron microscopy (TEM)

2.2.3.1 Introduction

In the present thesis, TEM images of the synthesized samples have been recorded using Hitachi (H-7500) transmission electron microscope. SAED and HRTEM images were recorded using TEM (JEOL 2100F) operated at 200 keV.

Ernst Ruska in 1931 fabricated the first transmission electron microscope. For this he was awarded 1986 Nobel Prize for Physics. Transmission electron microscopy is a microscopy technique in which a beam of electrons (energy 100keV to 3MeV) is transmitted through a

specimen(of size less than 200nm), interacting with the specimen. The de-Broglie wavelength of the electron beam lies in the range 6.13-2.24pm so that it can be able to get image of smaller features of the specimen. TEM is therefore a very powerful tool for material characterization that can provide microstructural, crystal structure information [22].

2.2.3.2 Interactions of electron beam with specimen

In case of TEM, the specimen is taken so thin that an electron beam can easily penetrate through it. Various types of interactions happen between electrons and the specimen, which help in categorizing whether the electrons are unscattered, elastically scattered, or inelastically scattered ones (Figure 2.9).

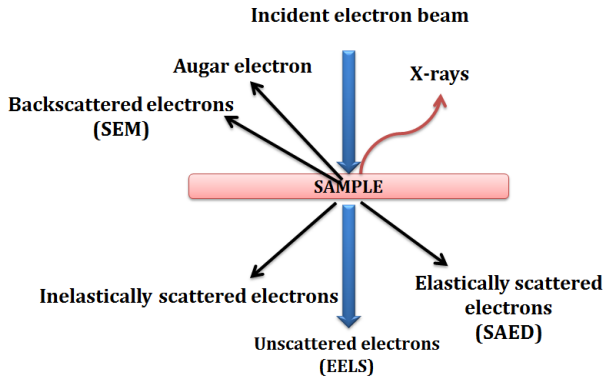

Figure 2.9 Illustration of various types of interactions between electrons and sample.

Unscattered electrons: The electrons, which get transmitted through the specimen without any interaction are called unscattered electrons; their transmitted flux is inversely proportional to the thickness of the specimen. These electrons through a thicker sample appear darker while through a thinner one, lighter.

Elastically scattered electrons: The electrons, which do not lose any energy while interacting with the sample are called elastically scattered electrons.

Inelastically scattered electrons: The electrons those on interaction with the sample lose energy [23].

2.2.3.3 Instrumentation and working

The working principle of a TEM and an optical microscope is same with the difference that the former uses electrons as a source and the latter, light.

TEM consist of four main components: electron gun, vacuum system and electromagnetic lenses along with electrostatic plates (Figure 2.10).

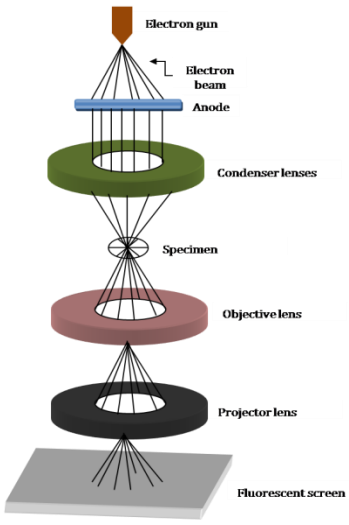

Figure 2.10 Working of TEM.

Electron gun, generally a tungsten filament and located at the top of the instrument, produces a monochromatic beam of electrons [23]. A set of two condenser lenses focus them into a coherent beam. On hitting the specimen, a part of the beam gets transmitted, which further being focused by an objective lens and then projected onto a phosphor fluorescent screen by a projector lens, produces an image. Pictorial view of TEM is shown in Figure 2.11.

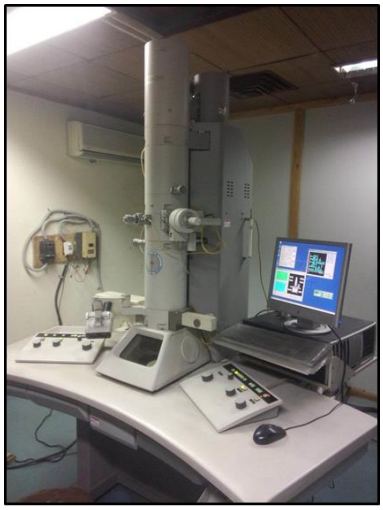

Figure 2.11 Pictorial view of TEM [24].

2.2.3.4 Sample preparation

Sample preparation demands an utmost attention as ultra-thin samples are required for TEM; it is quite easy in case the sample is of nanomaterials, otherwise proper grinding and dispersion in the solvent is called for. After ultra sonication, the solution is put on a carbon-coated grid. Finally, the grid is placed in a sample holder to view the images.

2.2.3.5Applications of TEM

TEM in different modes gives following information about the sample:

- Its morphology and topography
- Its crystallography and composition
- Its molecular information in high resolution (HRTEM) mode
- Its crystalline nature in selected area electron diffraction (SAED) mode
- Its defects and flaws

2.2.4 Energy dispersive spectroscopy (EDS)

2.2.4.1 Introduction

The Energy Dispersive X-ray analysis is the surface analytical techniques used to identify the elemental composition of materials. It is a versatile accessory of scanning electron microscope (SEM), which uses x-rays [25]. It can detect all elements from 4 (Be) to 92 (U).

2.2.4.2 Interaction volume

When a sample is bombarded by an SEM electron beam, various interactions takes place under 1-6µm depth (Figure 2.12); the electrons being scattered elastically or inelastically from the surface atoms.

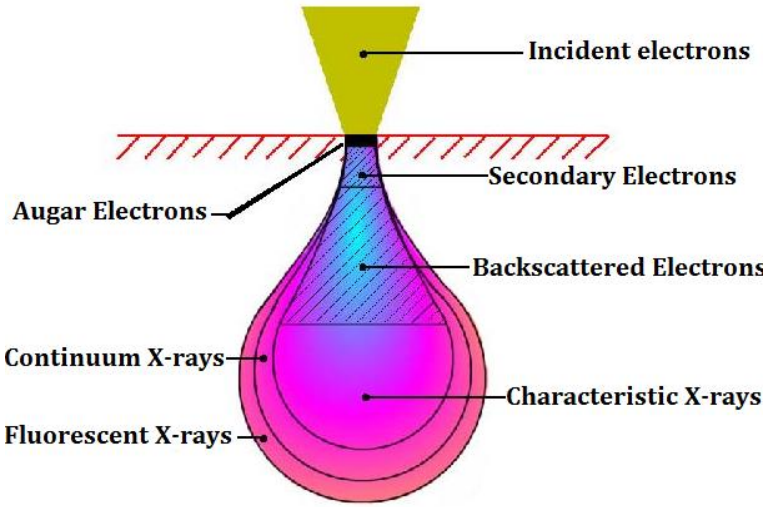

Figure 2.12 Interaction of electrons beam with specimen surface.

Electrons having energy comparable to the incident electrons and undergoing elastic collisions are called the backscattered electrons. Due to the inelastic collisions, the secondary electrons which are loosely bound get ejected. With this ejection, some vacancies are created. In order to fill the vacancies, electrons with higher energies de-excite to the lower energy states with the emission of some characteristic X-rays shown in Figure 2.13.The energy of the released beam is characteristic of a particular atoms. Thus, by measuring the amount of energy released, the atoms can be identified [26].

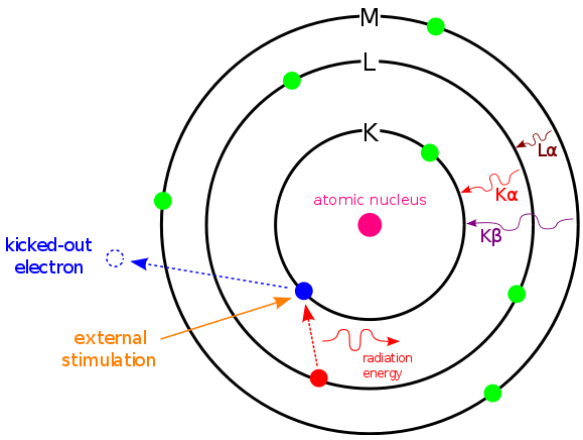

Figure 2.13 Principle of EDS.

2.2.4.3 Instrumentation and working

EDS is the integrated part of electron microscope. EDS instrumentation consists of X-ray detector, for cooling a liquid nitrogen dewar and software to collect and examine energy spectra. High energy electron beam is produced by the electron gun.

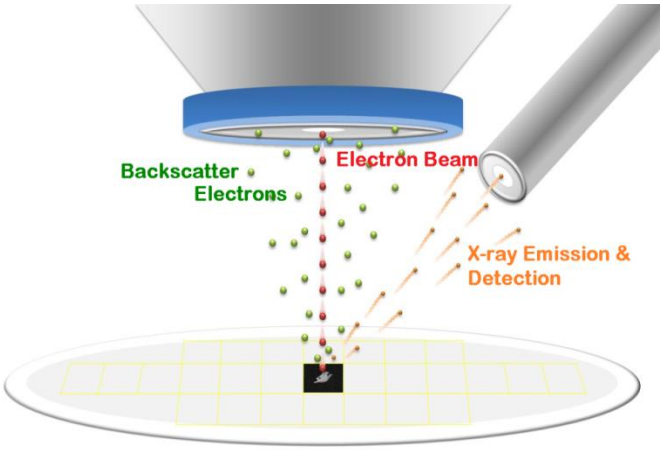

Figure 2.14 Schematic representation of EDS components [27].

The electron beam falls on the surface of the specimen and various interactions takes place. The X-rays emitted are absorbed by the detector (Si (Li) and convert them to the electrical pulses. The system software collects signal and analyze energy corresponding to the characteristic X-

rays of elements comprising the sample (Figure 2.14). The pictorial view of EDS attached to SEM is shown in Figure 2.15.

2.2.4.4 Sample preparation

In case of non-conducting samples a thin layer of gold with the help of sputter coating unit under the vacuum is applied on the surface of the sample so that it becomes conducting and then it is placed in the sample holder for analysis.

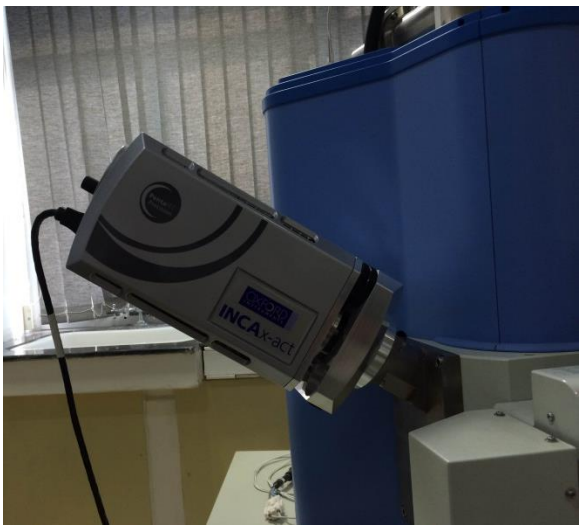

Figure 2.15 EDS instrument attached with SEM.

2.2.4.5 Applications of EDS

The applications of EDS include:

- Elemental analysis
- Qualitative and quantitative analysis of the samples
- Elemental mapping

In the present thesis, the presence of various elements has been confirmed by energy dispersive x-ray spectroscopy (EDS) of OXFORD analytical, attached with SEM.

2.2.5 Photoluminescence (PL) spectroscopy

2.2.5.1 Introduction

Photoluminescence is a non-destructive method to study the electronic structure of a material. During this process, the sample absorbs photons and then radiates them. Quantum mechanically, this happens as photo excitation allows the electrons of the sample to move into the permissible excited states. On de-excitation, energy released may be radiative or non-radiative. Photoluminescence is a contact less non-destructive method of to probe the electronic structure of a material [28]. With the help of this spectroscopy, one can measure the physical and chemical properties of the material and also detect the purity and the crystalline quality of the semiconductors.

2.2.5.2 Instrumentation and Working

Figure 2.16 shows the schematic diagram of a PL set-up, which is usually called as spectroflouorometer. It comprises of four main components: light source, sample, light filtering system, and a light detector. Generally, xenon lamp is used as a light source.

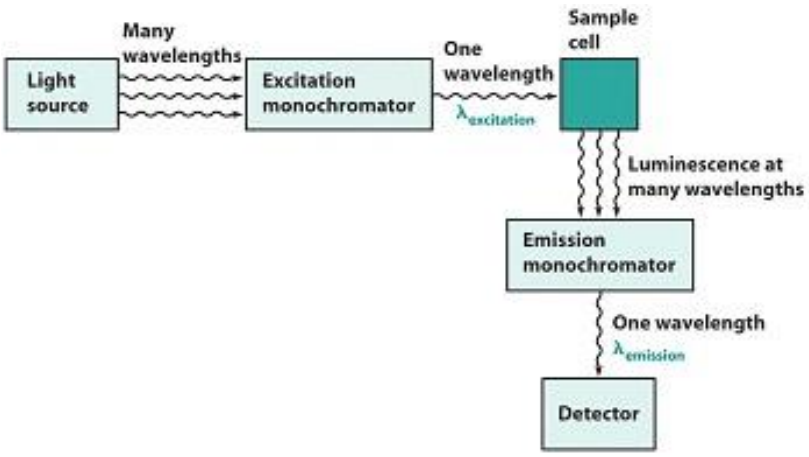

Figure 2.16 Experimental set-up of PL spectrophotometer.

PL spectroscopic technique, a laser light having energy greater than the optical band gap of the given sample, is directed towards the filter, which throws the selected wavelength light towards the cuvette that contains sample. The light emitted from the sample is diffracted by the diffraction grating in different directions depending upon their wavelengths. The detector measures signal intensity corresponding to each wavelength and the output device displays PL spectra of the sample under investigation. Pictorial view of Perkin Elmer LS55 spectrometer has been shown in Figure 2.17

Figure 2.17 Pictorial view of photoluminescence spectrometer.

2.2.5.3 Sample preparation

The powdered sample should be dispersed in suitable solvent, in which it dissolves completely. Moreover solvent should not react with the sample. Then keep the solution for ultra sonication for few hours.

2.2.5.4 Applications of PL spectroscopy

- Impurity levels and defect detection
- Determination of the Bandgap
- Recombination mechanism
- Material quality
- Emission and excitation spectra

In the present thesis, the PL spectra of the synthesized samples have been recorded using Perkin Elmer LS55 spectrometer.

2.2.6 Vibrating sample magnetometer (VSM)

2.2.6.1 Introduction

The VSM is used to examine the properties of magnetic materials. VSM is based on Faraday's law [29].

In VSM , a rod like sample holder is operated mechanically. The rod containing sample is situated between the two poles of the electromagnet and detection coils are mounted on to it. An induced voltage is produced in the detection coils due to the oscillatory motion of the magnetized sample. The induced voltage, proportional to magnetization, can be changed using dc magnetic field.

2.2.6.2 Instrumentation and working

Figure 2.18 shows the schematic representation of various components present in VSM. The sample is placed at centre of pair of pickup coils between the poles of an electromagnet. The sample is magnetized due to uniform magnetic field of electromagnet. The sample is set into vibrations along the vertical axis and the voltage is induced in the pickup coil, which is proportional to sample's magnetic moment. In the output we got magnetic moment (m) versus applied field (H). The magnetic field is produced by an electromagnet.

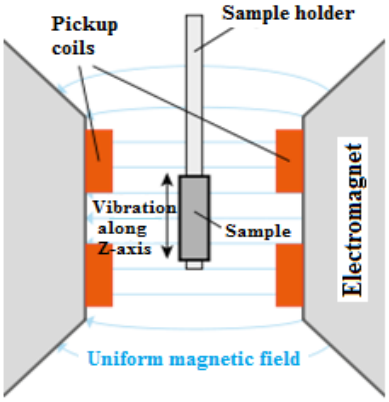

Figure 2.18 Schematic representation of VSM [30].

The voltage V through the sensing coils can be calculated as [31]:

$$V = m\,A\,F\,S$$

Where *m* stands for sample's magnetic moment, *A*, the vibration amplitude, *F* is frequency of vibration, and *S*, coil sensitivity. VSM can measure DC magnetic moment, which dependent on the magnetic field, temperature and time. It can do the susceptibility and magnetization studies. Pictorial view of VSM is shown in Figure 2.19.

Figure 2.19 Pictorial view of VSM [32].

2.2.6.3 Sample preparation

A few milligram of powder sample is required for analysis.

2.2.6.4 Applications of VSM

VSM is mainly used to know the magnetic properties of different materials such as powder, liquid and thin films. Diamagnetic, paramagnetic, ferromagnetic, ferrimagnetic, and antiferromagnetic properties of materials can be observed using this instrument.

In the present thesis, the magnetic measurements (M-H) have been performed by vibrating sample magnetometer (VSM) (Lake Shore).

References

[1] M. A. Shah, T. Ahmed, Principles of Nanoscience and Nanotechnology, Published by Alpha Science International Ltd, United Kingdom, 2010

[2] Phuruangrat A, Thongtem T, Thongtem S. Effects of ethylenediamine to water ratios on cadmium sulfide nanorods and nanoparticles produced by a solvothermal method. Materials Letters. 2009 Jul 15;63(17):1538-41.

[3] Lalayan AA. Formation of colloidal GaAs and CdS quantum dots by laser ablation in liquid media. Applied surface science. 2005 Jul 30;248(1):209-12.

[4] Zang J, Zhao G, Han G. Preparation of CdS nanoparticles by hydrothermal method in microemulsion. Frontiers of Chemistry in China. 2007 Mar 1;2(1):98-101.

[5] Marandi M, Taghavinia N, Mahdavi SM. A photochemical method for controlling the size of CdS nanoparticles. Nanotechnology. 2005 Jan 25;16(2):334.

[6] Tong H, Zhu YJ. Synthesis of CdS nanocrystals based on low-temperature thermolysis of one single-source organometallic precursor. Nanotechnology. 2006 Jan 16;17(3):845.

[7] Monte AF, Dantas NO, Morais PC, Rabelo D. Synthesis and characterisation of CdS nanoparticles in mesoporous copolymer template. Brazilian journal of physics. 2006 Jun;36(2A):427-9.

[8] Demazeau G. Solvothermal reactions: an original route for the synthesis of novel materials. Journal of Materials Science. 2008 Apr 1;43(7):2104-14.

[9] http://eng.thesaurus.rusnano.com/wiki/article729

[10] Pandey G, Dixit S. Growth mechanism and optical properties determination of CdS nanostructures. The Journal of Physical Chemistry C. 2011 Aug 22;115(36):17633-42.

[11] Deng ZX, Li L, Li Y. Novel inorganic-organic-layered structures: crystallographic understanding of both phase and morphology formations of one-dimensional CdE (E= S, Se, Te) nanorods in ethylenediamine. Inorganic chemistry. 2003 Apr 7;42(7):2331-41.

[12] Shanmugapriya T, Vinayakan R, Thomas KG, Ramamurthy P. Synthesis of CdS nanorods and nanospheres: shape tuning by the controlled addition of a sulfide precursor at room temperature. CrystEngComm. 2011;13(7):2340-5.

[13] http://www.smcr.fisica.unam.mx/8temasutiles/articulosutiles/Bas-XRD.pdf

[14]http://www.asdlib.org/onlineArticles/ecourseware/Bullen_XRD/LearningActivity_Diffraction BraggsLaw.pdf

[15] http://www.britannica.com/EBchecked/topic/76973/Bragg-law

[16] http://serc.carleton.edu/research_education/geochemsheets/techniques/XRD.html

[17] B.D. Cullity, S.R. Stock Elementary of X-ray Diffraction (third ed.)Prentice-Hall, Englewood Cliffs, NJ (2001)

[18] A. E. Owen, Fundamentals of UV-visible spectroscopy (1996).

[19] http://elibrary.bsu.az/azad/new/2476.pdf

[20] http://www.harpercollege.edu/tm-ps/chm/100/dgodambe/thedisk/labtech/spec20.html

[21]http://www.pharmatutor.org/pharma-analysis/analytical-aspects-of-uv-visible-spectroscopy/applications.html

[22] http://micron.ucr.edu/public/manuals/Tem-intro.pdf

[23] http://www.hk-phy.org/atomic_world/tem/tem02_e.html

[24] http://www.jnu.ac.in/AIRF/photogallery/tem.jpg

[25] http://micron.ucr.edu/public/manuals/EDS-intro.pdf

[26] http://serc.carleton.edu/research_education/geochemsheets/eds.html

[27] http://www.aspexcorp.com/solutions/omegamax/edxspectroscopy.aspx

[28] http://www.nrel.gov/pv/measurements/photoluminescence_spectroscopy.html

[29] Shanmugapriya T, Vinayakan R, Thomas KG, Ramamurthy P. Synthesis of CdS nanorods and nanospheres: shape tuning by the controlled addition of a sulfide precursor at room temperature. CrystEngComm. 2011;13(7):2340-5.

[30]http://upload.wikimedia.org/wikipedia/commons/f/f2/VSM_en.svg

[31]http://www.lakeshore.com/Documents/The%20Performance%20of%20the%20Model%207400%20VSM%20Sensitivity.pdf

[32] http://matxrz.net/uploads/3/3/1/7/3317090/7047690.gif

Chapter 3

Results & Discussions

Chapter 3

Results & Discussions

The present chapter deals with results obtained for Fe, Ni, Co and Gd-doped CdS nanostructures and their discussions. The various characterization techniques such as XRD, UV-visible, PL, TEM and VSM/SQUID have been employed in order to study their properties and to know the origin of magnetism in these doped nanostructures. The detail has been given as below:

3.1 Structural, optical and magnetic properties of Co-doped CdS nanorods

This section deals with the series of $Cd_{1-x}Co_xS$ (x = 0.00, 0.05, 0.10, 0.15) nanorods. The nanorods were synthesized by using solvothermal technique, as discussed in detail in chapter 2. The structural, optical and magnetic characteristics of undoped and Co-doped nanorods were examined. The obtained results are discussed below:

3.1.1 Morphological, structural and chemical compositional analyses

TEM images of undoped and 10% Co-doped CdS confirm nanorods morphology having average diameter 7-11 nm and 5-9 nm, respectively, as given in Figure 3.1 (a) and (b). Figure 3.1 (c) and (d) show high resolution TEM (HRTEM) images of 10% Co-doped CdS nanorods. No impurity or segregated secondary phase has been detected in HRTEM images; this confirms the high purity and defect-free nature of the synthesized nanorods. The lattice planes observed in HRTEM image (as shown in Figure 3.1 (d)) has been used to calculate the d-spacing values. The observed inter-planar spacing is about 0.335 nm, which is consistent with (002) plane of CdS hexagonal structure; this confirms that the growth of nanorods is along (002) plane. The sharp circular and

distinct rings have been observed in SAED pattern of 10% Co-doped CdS nanorods (inset Figure 3.1 (b)) displaying high crystallinity and polycrystalline nature of the synthesized nanorods.

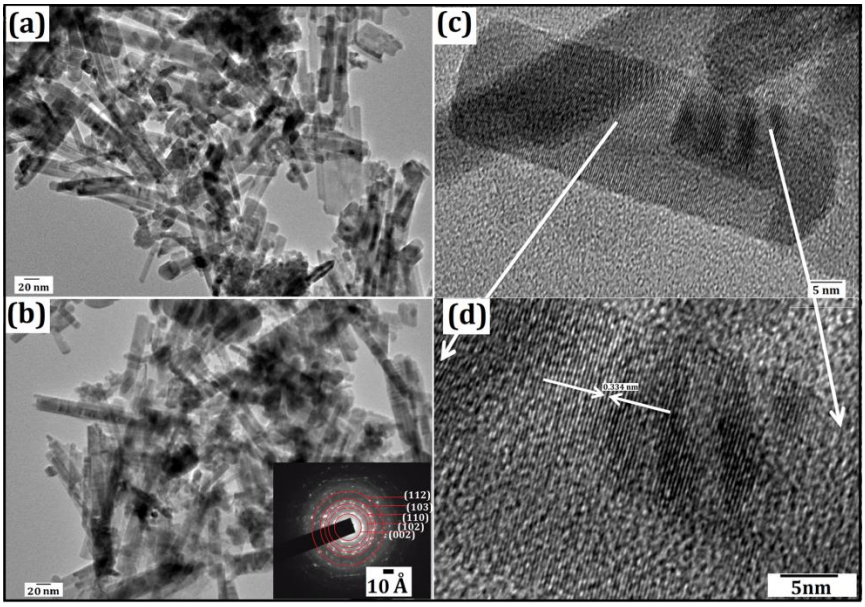

Figure 3.1 TEM micrographs of (a) undoped and (b) 10% Co-doped CdS nanorods (inset shows SAED patterns) (c) HRTEM of 10% CdS nanorods (d) enlarged part of HRTEM of 10% Co-doped CdS nanorods.

XRD patterns of the synthesized nanorods are shown in Figure 3.2. This validates the formation of single phase hexagonal wurtzite structure of CdS with $P6_3mc$ space group (JCPDS card no. 41-1049). It has been found that XRD peaks observed in undoped CdS nanorods around $2\theta \sim 58.28^{o}$, 69.36^{o} and 72.38^{o} corresponding to (202), (210) and (114) get suppressed upon Co doping and gets merged in case of Co-doped CdS nanorods. There is no peak related to any type of impurity; this depicts that Co ions gets substituted uniformly in CdS.

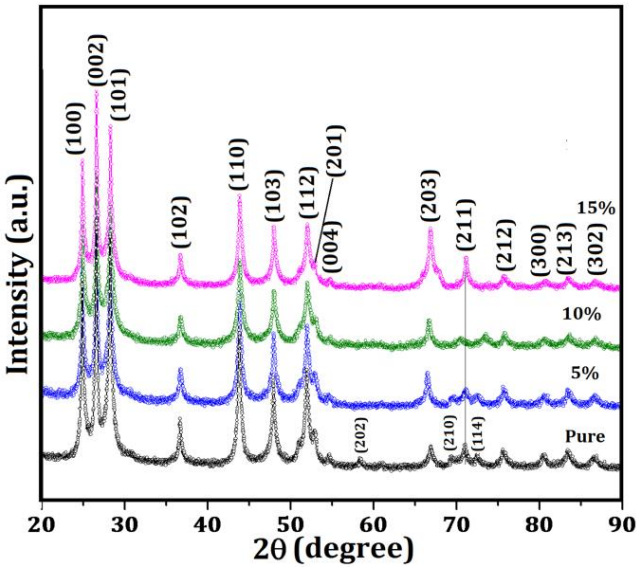

Figure 3.2 XRD patterns of undoped, 5%, 10% and 15% Co-doped CdS nanorods.

There is a clear shift in XRD patterns towards the higher 2θ in Co-doped nanorods as given in Figure 3.3, because of the smaller size Co^{2+} ions (82 pm) than Cd^{2+} ions (103pm). These results are well in agreement with literature [1-4].

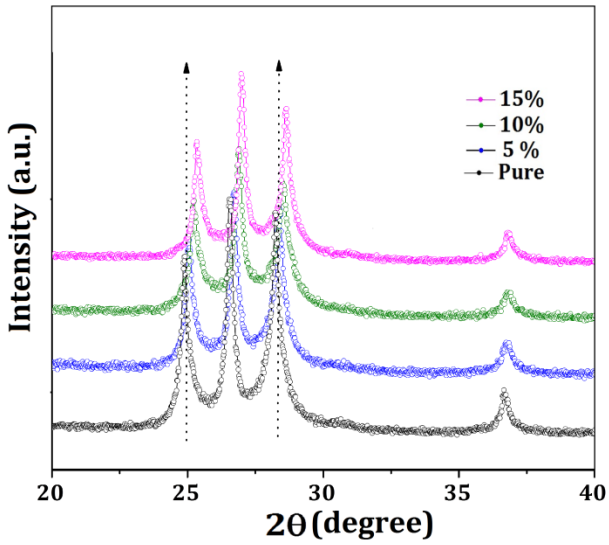

Figure 3.3 Magnified view XRD patterns of undoped, 5%, 10% and 15% Co-doped CdS nanorods around 2θ = 20 to 40° showing shifting of reflection peaks towards higher 2θ.

The XRD patterns (Figure 3.2) of Co-doped CdS nanorods possess high intense peaks than the undoped one; this reveals that the doping of Co in the CdS enhances the crystallinity of the synthesized nanorods. The low intensity of undoped CdS nanorods can be attributed to the low crystallinity and structural imperfections [4]. The broadening of XRD peaks has been observed due to smaller crystallite size of synthesized nanorods. It has been further noticed that broadening of XRD peaks increases upon Co-doping as is observed in the reflection peaks corresponding to (112) and (203) plane; this is precisely due to that the fact that in the synthesized nanorods, the number of planes available for x-ray diffraction, is too small [5]. The crystallite size (D) has been calculated using Williamson-Hall formula [4]:

$$\frac{\beta\, cos\theta}{\lambda} = \frac{1}{D} + \frac{\varepsilon\, sin\theta}{\lambda}$$

Where β is FWHM of the diffraction peak, λ is x-ray wavelength, θ is diffraction angle, ε – lattice strain. Further, the additional broadening in FWHM due to the instrument has been corrected, using a large-grain Si standard sample [5]:

$$\beta_{corrected} = (FWHM^2_{sample} - FWHM^2_{Si})^{1/2}$$

The calculated average crystallite sizes (Table 3.1) of the undoped, 5%, 10% and 15% Co-doped nanorods have been found to be, respectively, 3.05, 2.91, 2.80 and 2.78 nm. The doping of Co results in decreasing the average crystallite-size of the nanorods. These results are quite in agreement with TEM images. The lattice parameters *(a, c)* has been found using following relation [4]:

$$\frac{1}{d^2_{hkl}} = \frac{4}{3}\left[\frac{h^2 + hk + k^2}{a^2} + \frac{l^2}{c^2}\right]$$

Table 3.1 displays calculated lattice parameters of synthesized nanorods. The lattice parameters *a* and *c* have been found to decrease with Co doping, and, this leads to decrease in volume of unit

cell of CdS. Therefore, the substitution of Co at Cd site is resulting in lattice contraction and reduction in overall unit cell volume (Table 3.1). The observed lattice contraction upon the incorporation of smaller size Co atoms confirms its substitutional cationic sites occupancy in the CdS lattice. Table 3.1 shows the variation of lattice parameters and volume of unit cell with doping of Co in the CdS host. The ratio of lattice parameters *c/a* = 1.633, which is in good agreement for the hexagonal system [1-3].

Table 3.1 Lattice parameters, volume, crystallite size, absorption edge, band gap and saturation magnetization of undoped and Co-doped CdS nanorods.

Sample Description	a(Å)	b(Å)	Volume ($Å^3$)	Crystallite size (nm)	Absorption edge $\lambda_{1/2}$ (nm)	Band Gap (eV)	Magnetic Saturation (emu/g)
Undoped CdS	4.1150	6.7203	98.5476	3.05	520	2.46	0.034
5% Co CdS	4.1107	6.7129	98.2335	2.91	500	2.47	0.041
10% Co CdS	4.0820	6.6660	96.1899	2.80	480	2.58	0.070
15% Co CdS	4.0796	6.6260	95.5002	2.78	455	2.72	0.090

EDAX spectra of undoped and 10% Co-doped CdS nanorods are shown in Figure 3.4. No additional peak, related to any impurity or secondary phases related to cobalt or cadmium oxide or cobalt sulphide, have been detected in EDAX spectrum. This is depicting the phase undoped nature of synthesized nanorods. Further, it has been found that the elements, viz. Cd, S and Co are in their stoichiometric ratios.

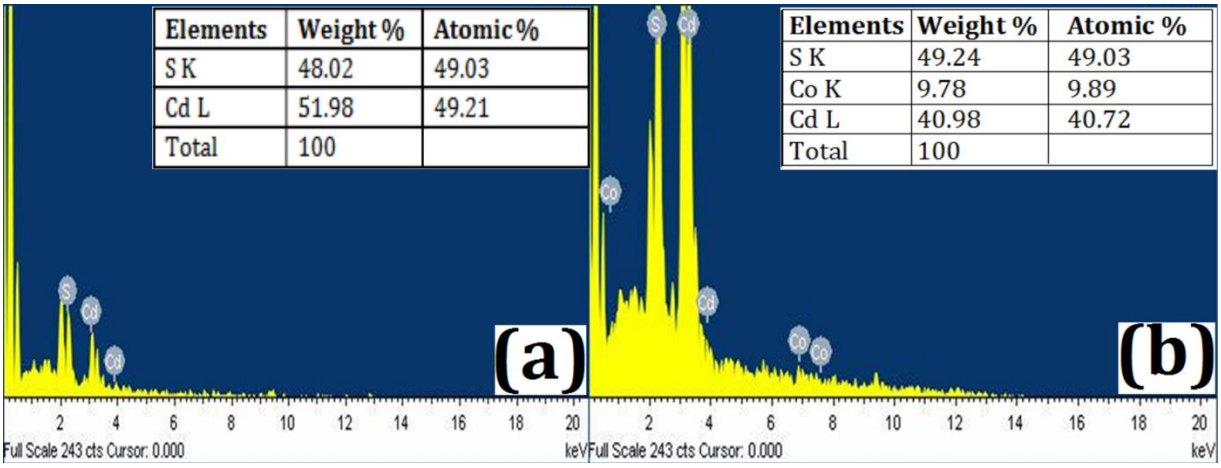

Figure 3.4 EDAX spectra of (a) Undoped and (b) 10% Co-doped CdS nanorods.

3.1.2 Optical analyses

3.1.2.1 UV-visible analysis

Figure 3.5 shows the UV-visible absorption spectra of the synthesized nanorods. The $\lambda_{1/2}$ method has been employed to calculate energy band gap [6]. In this method, the absorption band edge wavelength, called $\lambda_{1/2}$, has been calculated, which corresponds to 50% of the excitonic peak in the UV-visible absorption spectra [6]. Table 3.1 displays the calculated energy band gaps for the synthesized nanorods. The bandgap of undoped CdS nanorods, found to be 2.46 eV, is higher than bulk CdS, 2.4 eV; this is due to the Quantum confinement effect [7, 8].

Doping of the Co in CdS nanorods increases the band gap, and, consequently the absorption edge shifts towards the lower wavelength. The doping of Co in CdS results in smaller-size nanorods (Table 3.1), which decreases the crystallite size, and, thus, the band gap increases. Table 3.1 clearly reveals that undoped CdS nanorods have energy band gap, 2.46 eV. On increasing the dopant concentration to 15%, band gap increases to 2.72eV.

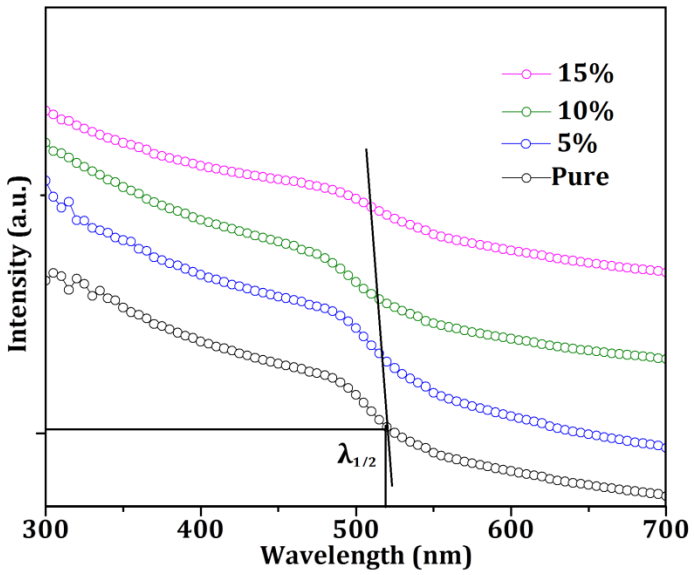

Figure 3.5 UV-visible absorption spectra of undoped, 5%, 10% and 15% Co-doped CdS nanorods.

The shift in the absorption edge has been observed to be towards the lower wavelength with increase in doping. The blue-shift is attributed to two reasons: First, due to the quantum confinement effect because of smaller size Co-doped CdS nanorods in comparison to the undoped CdS [7]; Figure 3.8 shows the energy band gap versus crystallite size variation. Second, due to the smaller size of Co ions that which results in reduction of lattice parameters and consequently unit cell volume. This distortion in the crystallographic structure, induces changes in electronic band structure of host CdS, and, thereby may be responsible for the higher energy band gap.

3.1.2.2 Photoluminescence spectra

This study is carried out to get information of electronic transitions pertaining to the dopants (or impurities, if any) and defects present in the synthesized nanorods. The substitution of Co in CdS results in introducing additional energy levels within its band gap, which alter the luminescence properties of doped-CdS nanorods. Figure 3.6 shows PL spectra of synthesized nanorods

obtained at excitation wavelength, 380 nm. The PL spectrum of synthesized nanorods is not complex; it represents the defect-free nature of the synthesized nanorods. In general, two types of emissions are possible in semiconductor nanostructures, viz., excitonic and trapped luminescence [8, 9]. The excitonic emission is sharp and occurs near the absorption edge of CdS, while the trapped emission is the broad and stokes-shifted. The main excitonic emission band at 529 nm, observed in the undoped and doped CdS nanorods [8], is the green emission in the synthesized nanorods ascribed to the surface donor-accepter pair recombination. The basic cause of these emissions is the d-d intra-ion transitions. This happens in two recombination processes occurring in the d-d intra-ion transitions, first the recombination of electrons and holes, secondly the recombination of free electrons and holes; this results in green emission [7, 8]. No shift in this emission band is noticed with the doping of Co.

A very weak peak originating at 512 nm in undoped CdS nanorods is due to the presence of the surface traps; however, upon doping of Co, shifting of this peak towards the higher wavelength, i.e., 514 nm, as well as enhancement in the intensity, has been observed [10]. The peak appearing at 487 nm is due to the host, i.e., CdS. The hump around 430 nm appeared in Co-doped CdS nanorods, is due to the blue emission and is absent in undoped CdS. Further, it has been found that intensity of hump increases with increase in the dopant concentration (Figure 3.6). This may be due the formation of deep Co d-derived states in the CdS bandgap as a result of hybridization of Co d-states with S p-states, and, may result in high density of states at the Fermi level; this de-stabilizes the paramagnetic ground state of Co. Introduction of spin polarization (dopant say Co) can stabilize it thereby separating the spin up and spin down electrons energetically; this is likely to be the reason of observed ferromagnetism [3].

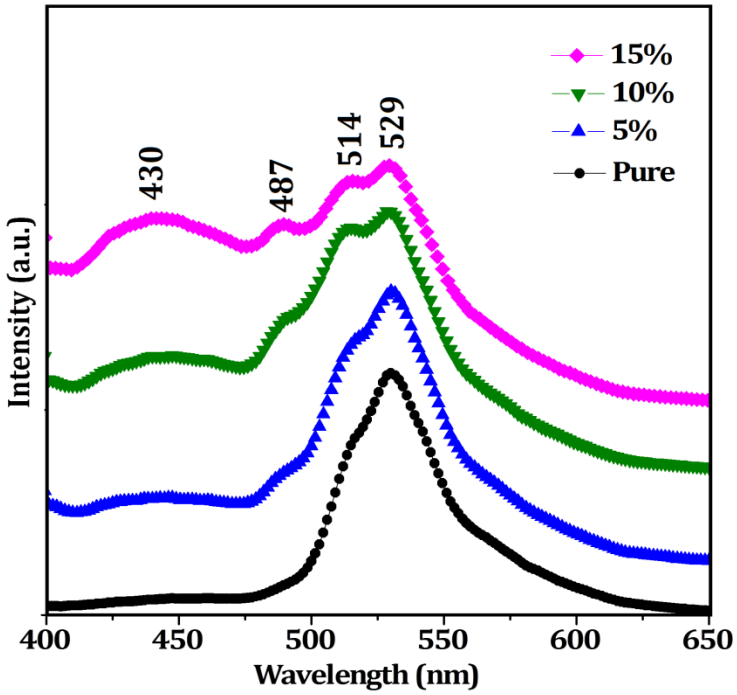

Figure 3.6 PL spectra of undoped, 5%, 10% and 15% Co-doped CdS nanorods.

With increase in the Co concentration, the increase in dipole-dipole interaction effects the defect related emission peaks. This results in high intense emission confirming the incorporation of Co in CdS.

3.1.3 Magnetic analysis

The magnetization versus applied magnetic field hysteresis (M-H) loops, as shown in Figure 3.7, reflect the ferromagnetic character of synthesized nanorods. The magnetic saturation has been found to be 0.034, 0.041, 0.070 and 0.090 emu/g for undoped, 5%, 10% and 15% Co-doped CdS nanorods, respectively. In the present report, we observe contradictory results as compared to the earlier reports [11-12], where they report that higher doping concentration of Co results in decrease in the saturation magnetization, which they attributed to the Cd or S vacancies or defects. The structural and optical studies confirm Co-incorporation in the CdS nanorods including their phase purity. Consequently, the observed ferromagnetic behaviour of synthesized

nanorods can mainly be due to Co-doping. The Co-doping may reduce the possibility of formation of Cd vacancies, if any [1]. As a result, it is speculated that the observed intrinsic ferromagnetism in the nanorods is related to the dopant-donor hybridization (p–d hybridization), and, ferromagnetic coupling of Co ions [13].

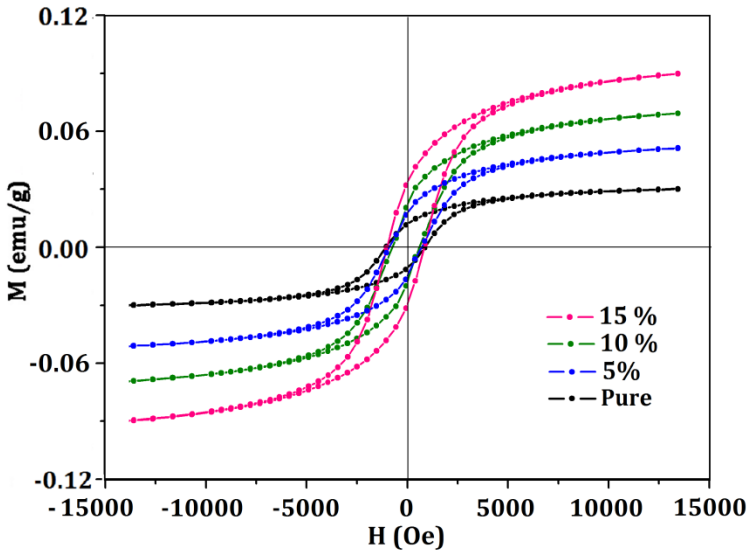

Figure 3.7 M-H hysteresis loops of undoped, 5%, 10% and 15% Co-doped CdS nanorods.

The variation of crystallite size, magnetic saturation and band gap of nanorods with doping of Co are shown in Figure 3.8.

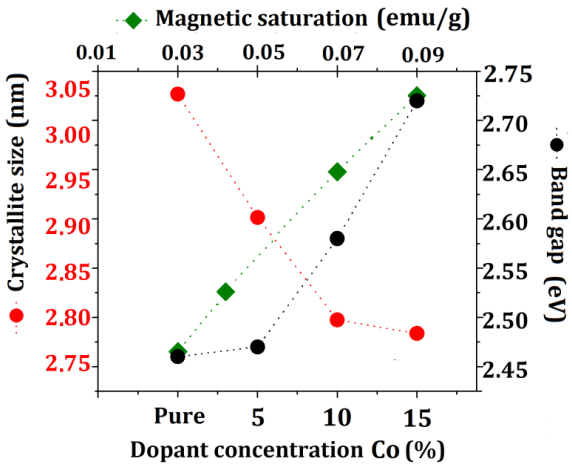

Figure 3.8 Variation of crystallite size, band gap and saturation magnetization with doping concentration of Co.

The lattice parameters have been found to reduce upon doping leading to contraction of unit cell volume (Table 3.1). Consequently, the crystal structure gets distorted resulting in the ferromagnetism. The magnetic saturation has been found to increase with Co-doping concentration (Table 3.1). The increase in saturation magnetization may be attributed to the increase in density of states of electrons near the Fermi level which induces ferromagnetic coupling between Co^{2+} ions. The PL spectra (Figure 3.6) confirm that the deep Co d-derived states in the band gap of CdS nanorods have been formed due to the hybridization of Co d-states with S p-states. This de-stabilizes the paramagnetic ground state of Co, and, thereby leads to ferromagnetism [14, 15].

There are numerous factors responsible for the ferromagnetism in dilute magnetic semiconductors such as carrier concentration interplay, magnetic impurity sites' randomness, and size-induced quantum confinement [16]. Defect formation energy at the surface of nanorods is higher than the bulk part because of the quantum-size effect; this leads to change in electronic structure of the nanomaterials [17]. The commonly observed surface defects in nanomaterials is, F-center due to sulfur vacancy with a trapped electron. These trapped electrons overlap with the

d-shells of doped Co atoms and thereby results in overlapped orbital states, of the order of Bohr radius and couple with the dopant (Co). The trapped electrons align so as to result in ferromagnetic coupling between the dopant atoms. The F-center (sulfur vacancy) mediated exchange mechanism may be responsible for the ferromagnetism in Co-doped CdS nanorods [17]. Figure 3.7 shows that undoped and Co-doped CdS nanorods possess small value of coercive and remnant field; this reveals their soft magnetic behavior. Ferromagnetic or antiferromagnetic interactions in Co-doped CdS nanorods depend on the distance between Co atoms, i.e., exchange anisotropy [5]. Dopant atoms (Co), at distances shorter than the others, may result in antiferromagnetic coupling; however, no such asymmetry is observed (Figure 3.7) in the hysteresis loops of the nanorods. The magnetic interactions in the synthesized nanorods are not antiferromagnetic but ferromagnetic; thus we can conclude that the indirect interactions among Co (II) centers lead to the observed ferromagnetism in the nanorods [18, 17, 19, 20]. Moreover, as reported by Sundaresan (2009), the ferromagnetism is universal phenomenon in CdS and is due to native surface defects [21].

3.2 Structural, optical and magnetic properties of Ni-doped CdS nanorods

This section deals with the series of $Cd_{1-x}Ni_xS$ (x = 0.00, 0.03, 0.05, 0.10) nanorods. The nanorods were synthesized by using solvothermal technique. The structural, optical and magnetic features of undoped and Ni-doped nanorods were studied. The obtained results are discussed below:

3.2.1 Structural and phase analyses

The XRD patterns of the undoped and Ni (3%,5% and 10 at wt.%) doped CdS nanorods are shown in Fig.3.9(a).Indexing of the peaks (100), (002), (101), (102), (110), (103), (112), (004), (202),(203), (210), (211), (114), (105) confirms hexagonal wurtzite structure of the nanorods according to the JCPDS card no.41-1049. No change in phase of the nanorods, on the addition of Ni, has been observed.Debye Scherrer formula is used to calculate the average crystallite size (D)[22]:

$$D = \frac{0.9\lambda}{\beta cos\theta}$$

where λ is the wavelength of Cu target (1.5418Å); θ, the glancing angle; and β, the full width at half maxima of the diffraction line.The crystallite size of undoped CdS has been found to be 23.79nm. On further increasing the dopant concentration upto 10%, the crystallite size reduces to 13.93nm.This decrement in crystallite size may be due smaller size of Ni atom as compared to that of Cd atom[23].These observations have been corroborated by TEM.The lattice parameters (a, c) were calculated using following relation [24]:

$$\frac{1}{d_{hkl}^2} = \frac{4}{3}\left[\frac{h^2 + hk + k^2}{a^2} + \frac{l^2}{c^2}\right]$$

The values of lattice parameters (Table.3.2) register decrease in case of the doped CdS nanorods. The zoomed view of the XRD spectra (Fig.3.9b) with peaks positioning at angles 26^{o} and 28^{o}, show a minor shift towards the higher angle in case of Ni-doped CdS nanorods.

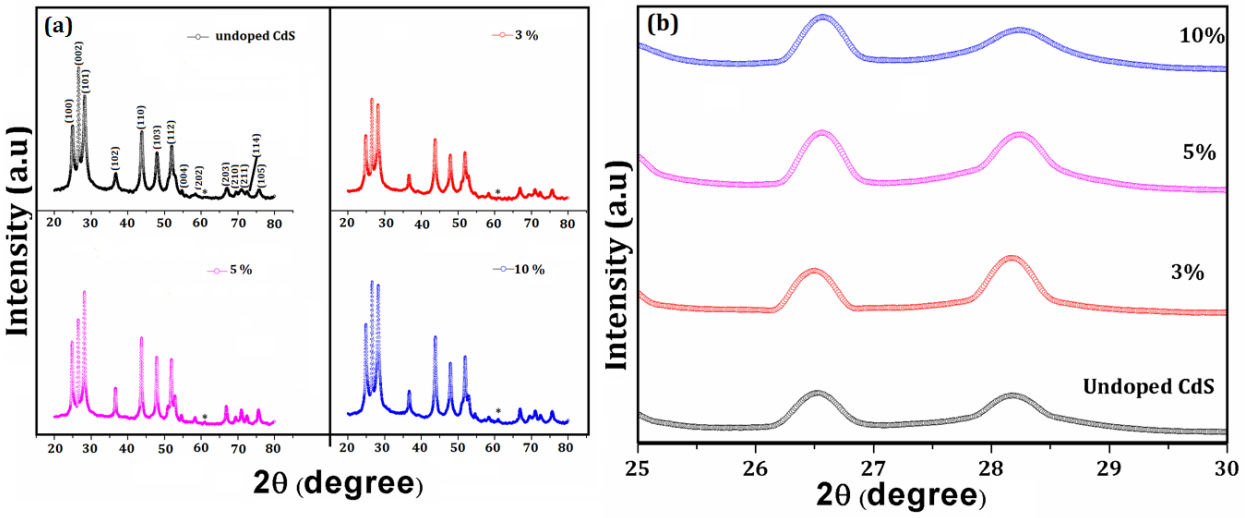

Figure 3.9 (a) XRD patterns of undoped and 3, 5, 10% Ni-doped CdS nanorods,(b)Magnified view XRD patterns from angle 25^{o} to 30^{o} showing shifting of peaks to the higher value of 2θ upon doping of Ni into the CdS lattice.

Figure 3.9(a) shows an additional peak in the doped samples, shown by astrisk(*), at an angle of 61^{o};this peak is missing in undoped CdS, however, appears on 3% Ni doping. Moreover, the intensity of this peak becomes high when the dopant concentration increases to 10%.This peak may be attributed to some impurity.The growth direction of the synthesized nanorods, i.e., a particular plane in which nanorods are grown, has been calculated using texture coefficient [25]:

$$Texture\ cofficient\ (hkl) = \frac{I\ (hkl)}{I'(hkl)}\left[\frac{1}{n}\sum I(hkl)/I'(hkl)\right]^{-1}$$

Where, I (hkl) is measured intensity in XRD patterns, I'(hkl) is the corresponding intensity of JCPDS data, and n, is number of peaks observed in the XRD patterns. The calculated texture coefficient has been found to be higher for (103) plane. This confirms the axis claiming growth of the synthesized nanorods is (103). HRTEM results also reveals that the synthesized nanorods grow along the (103) plane direction [24, 8, 26-28].

Table 3.2 Lattice parameters, Crystallite size and band gap values of undoped and Ni-doped CdS nanorods.

Sample Description	**a (Å)**	**c (Å)**	**Crystallite size (nm)**	**Bandgap(eV)**
Undoped CdS	4.1206	6.7290	23.79	2.47
3% Ni doped	4.11879	6.7262	20.56	2.51
5% Ni doped	4.1145	6.7141	16.24	2.54
10% Ni doped	4.1114	6.7026	13.93	2.55

3.2.2 Morphological analysis

The TEM, HRTEM and the SAED patterns of undoped and 10% Ni-doped CdS nanorods are shown in Figure 3.10 (a,b), which confirm their rod like morphology with length varying from 100 to 150 nm, and width, from 20 to 30 nm. HRTEM determines the d-spacing values.The observed interplanar spacing, incase of undoped CdS nanorods,has been found to be 0.187nm and,that for10% Ni-doped CdS nanorods, 0.189nm using JCPDS card no.41-1049;they are found to match with the plane [103] there by showing their growth along this plane.

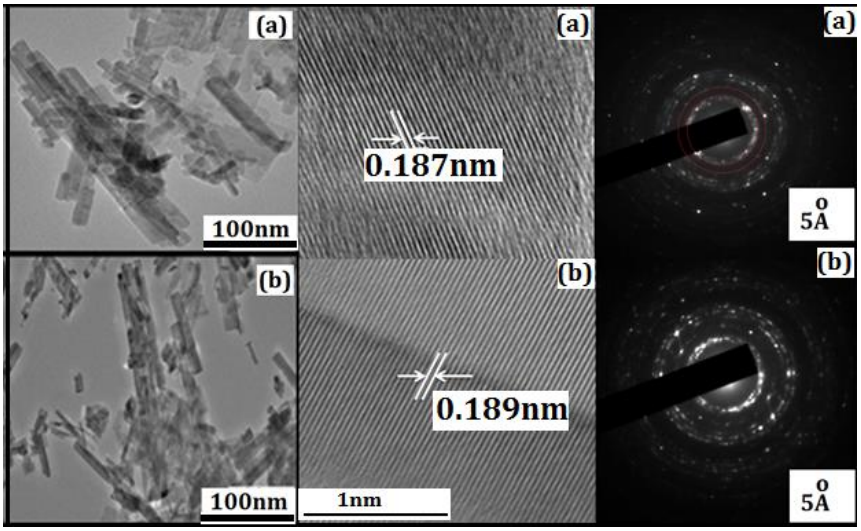

Figure 3.10 TEM, HRTEM and SAED pattern of (a)undoped and (b)10 % Ni doped CdS nanorods.

The complete circular rings have been formed in the SAED pattern, which confirm highly polycrystalline nature of the synthesised undoped and doped CdS nanorods.

3.2.3 Compositional Analysis

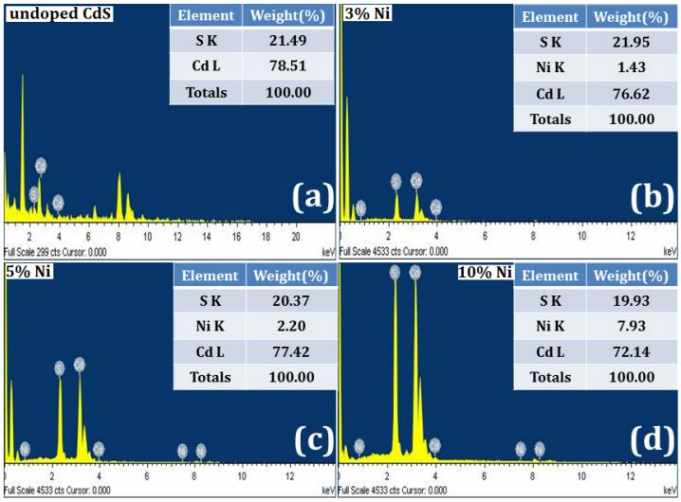

Figure 3.11 EDAX spectra of (a) Undoped CdS,(b) 3% Ni,(c)5% Ni ,(d) 10% Ni doped CdS nanorods.

EDAX analysis (Figure 3.11) has been performed; it confirms that the elements present in undoped and doped CdSare in stoichiometeric ratio without any impurity.

3.2.4 Optical analyses

3.2.4.1 UV- visible analysis

The absorption spectra of the CdS and Ni doped CdS nanorods are shown in Figure 3.12. The absorption spectra are used to calculate E_g of the synthesized nanoparticles, by applying Tauc's relation [29]:

$$(\alpha h\nu)^2 = A\left(h\nu - E_g\right)^n$$

Where, the constant A is function of the electronic transition probability;$h\nu$ *is* photon energy; h, Planck's constant. For direct allowed transitions, $n = 1/2$; for indirect allowed transitions,$n = 2$ for direct forbidden transitions, $n = 3/2$, and for indirect forbidden transitions,$n = 3$. The CdS nanoparticles giving direct transitions have $n = 1/2$.

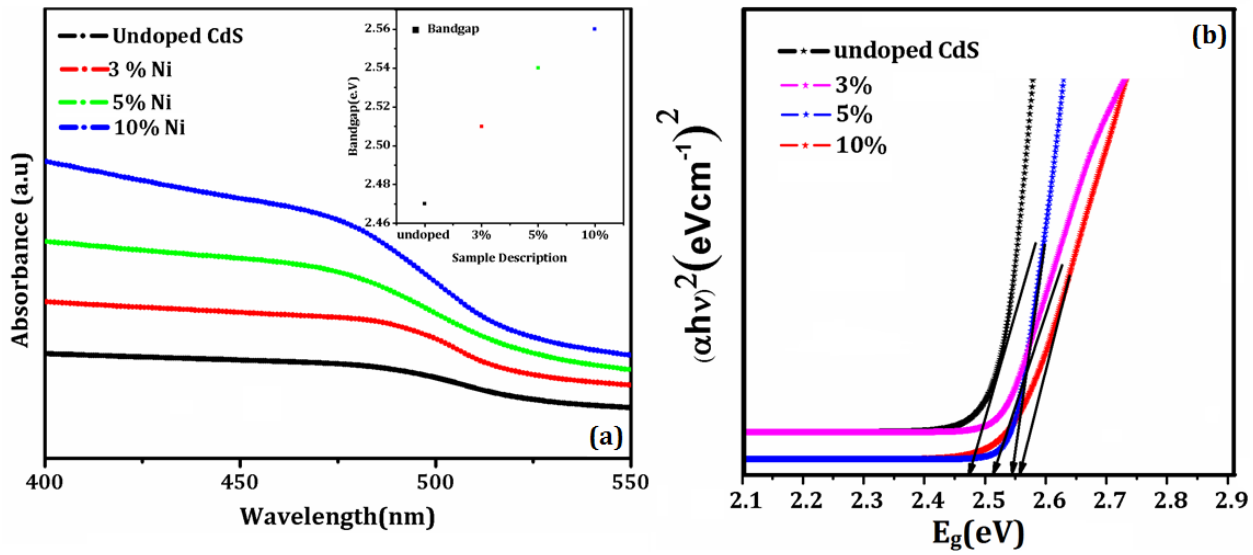

Figure 3.12 (a) UV-vis absorption spectra of Undoped,3%,5%,10% Ni-doped CdS nanorods, (b)Tauc's plot for the all the samples.

Figure 3.12(b) stands for variation of $(\alpha h\nu)^2$ - a function of energy of undoped and doped CdS nanorods. For undoped and doped CdS (with 10% doping), the band gaps have been found to be, respectively, 2.47 and 2.55 eV(inset of the Figure 3.12(a).The bandgap for undoped CdS is higher than bulk CdS due to quantum confinement [26].The doped CdS registers blue shift – as its XRD show decrease in crystallite size [26]. In addition to quantum confinement, smaller atomic radius of Ni atom is also responsible for increase in bandgap [30].

3.2.4.2 Photoliminescence spectra

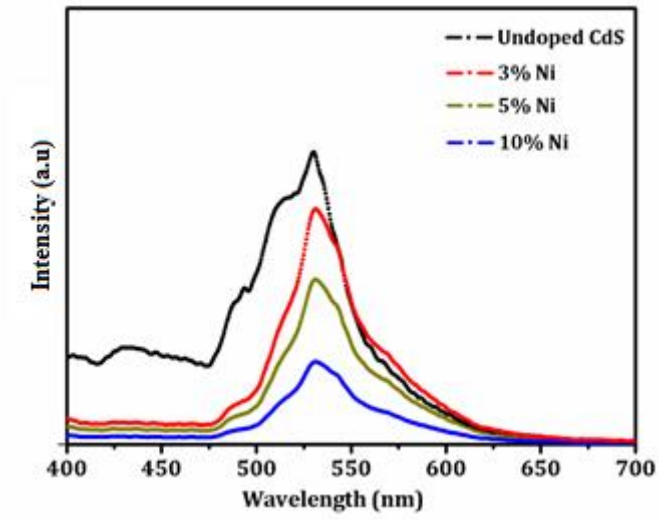

Figure 3.13 PL spectra of undoped ,3% 5%, 10% Ni doped CdS nanorods.

Photoluminescence spectra of undoped and Ni–doped CdS nanorods was done (Figure 3.13). The given spectra have been observed at excitation wavelength 380nm.The PL spectrum shows the defect free nature of the synthesized nanorods because of its non-complex nature. In case of undoped CdS nanorods, the small hump in this spectra at 429nm is due to blue emission [31]. The highest intensity peak at 530nm may be because of the near band edge transitions, which are due to electron hole recombinations [32].The basic reason for these emissions is the d-d intra-ion

transitions [33].There is no shift in this band emission with Ni-doping.Moreover, this peak is attributed to green emission.A weak peak, originating at 516nm, is due to the surface traps, which,upon doping, also get diminished.Another small emission band at shorter wavelength, 493nm, in undoped CdS nanorods,is due to the direct transition from conduction to valence band [34]. On increasing concentration of Ni metal, the luminesence intensity decreases due to the quenching effects [35].

3.2.5 Magnetic analysis

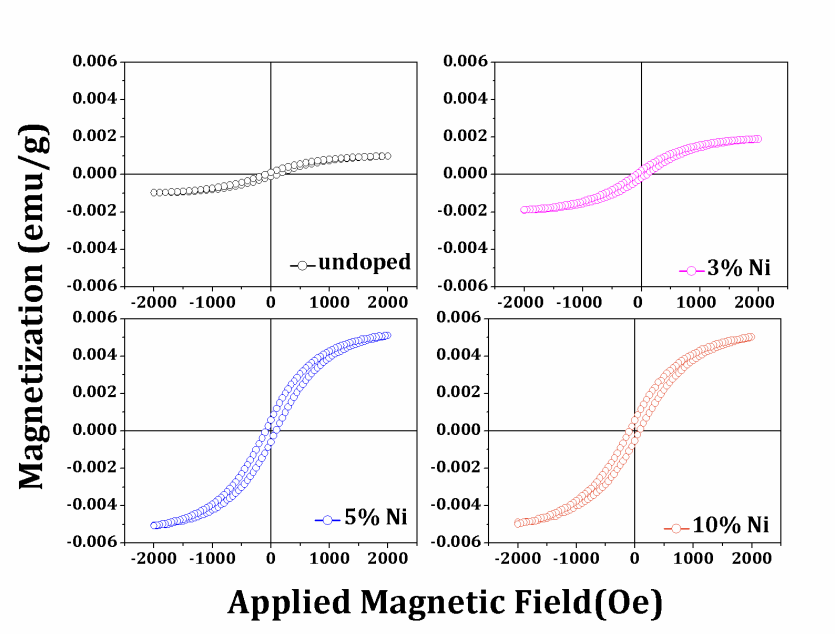

Figure 3.14 M-H hysteresis loops of undoped, 3%, 5% and 10% Ni-doped CdS nanorods.

Figure 3.14 confirms ferromagnetic nature of both the undoped and doped CdS nanorods. The magnetization values for undoped nanorods are found to be 0.0010emu/g and, those for 3% and 5% Ni-doped CdS nanorods, respectively, increase to 0.0018emu/g and 0.0054emu/g. However, on increasing concentration to 10%, the magnetization decreasesto0.0051emu/g. Origin of the magnetic behavior in some materials, with empty and full d or f shells, may be attributed to

various reasons, such as size effect, disorder, impurity [18].The restricted defect-states, due to addition of the dopant or any other vacancy playing vital role in constraining electron movement, induce collective ferromagnetism. From XRD, the crystallite size decreases from 23.79 to 13.93nm, which can be one of the reasons for observed ferromagnetic behavior being due to reduction in the size of the nanostructures – this further reduces the random motion of the electrons from one site to another, which, in turn, reduces kinetic energy of the electrons. Coulomb interactions and bandwidth ratio gets enhanced increasing magnetism [36]. There is no phase transformation occurrence but there is existence of certain disorders in the lattice, which may be attributed to some impurity; the extra peaks (with asterisk) in XRD confirm it. UV–Visible spectra confirm increment in the band gap, which may be attributed to the changes in the lattice structure due to the presence of some disorder – this further supports that appearance of ferromagnetism in the nanorods is due to quantum confinement and lattice disorders. The Direct exchange interactions are also responsible for the existence of ferromagnetic behavior in the nanostructures; according to which, the interatomic distance between the magnetic ions decides the magnetic nature of the material - if the distance is large, the ferromagnetic behavior would increase, and, if less, antiferromagnetic [19-20].Decrease in magnetization at higher concentration, in case of 10% Ni-doping, may be due to the occurrence of the super exchange interactions in between Ni ions [37].

3.3 Structural, optical and magnetic properties of Fe-doped CdS nanorods

This section deals with the series of $Cd_{1-x}Fe_xS$ (x = 0.00, 0.03, 0.05, 0.10, 0.15) nanorods. The nanorods were synthesized by solvothermal technique. The structural, optical and magnetic properties of undoped and Fe-doped nanorods were studied. The obtained results are discussed below:

3.3.1 Structural analyses

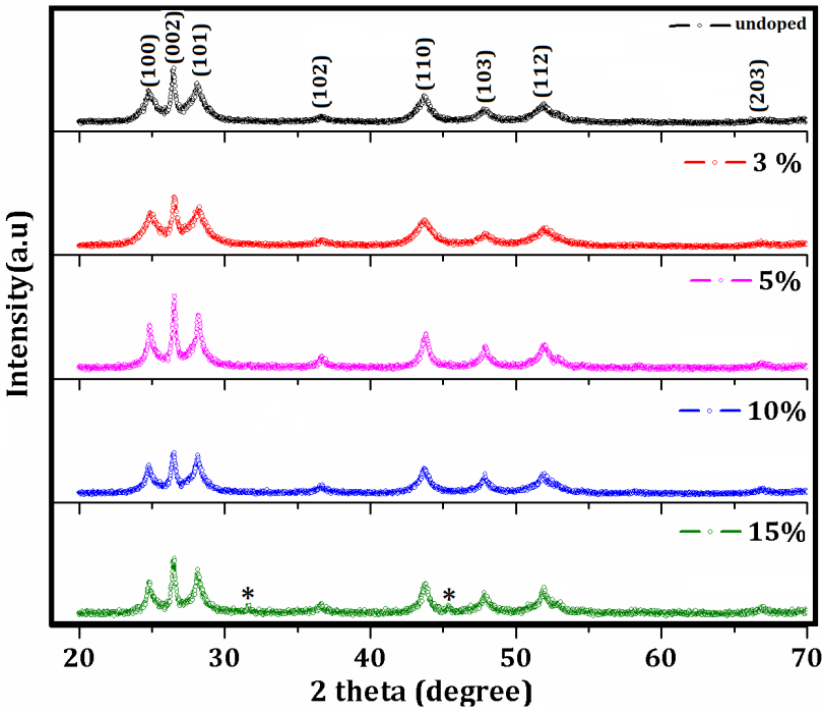

Figure 3.15 XRD patterns of undoped, 3%, 5%, 10% and 15% Fe-doped CdS nanorods.

XRD patterns of the synthesized nanorods are shown in Figure 3.15. The diffraction peaks positions are appropriately indexed as (100), (002), (101), (102), (110), (103), (112), (203) planes, which completely match with (JCPDS card no. 41-1049) revealing hexagonal wurtzite structure of both undoped and Fe-doped CdS nanorods. The crystallite size (D) has been calculated from the full-width at half maximum (FWHM), b, of a diffraction peak using Williamson-Hall formula [38]:

$$\frac{\beta\, cos\theta}{\lambda} = \frac{1}{D} + \frac{\varepsilon\, sin\theta}{\lambda}$$

Where, λ is wavelength of x-ray used, and, θ is the diffraction angle. The crystallite size for undoped, 3%, 5%, 10% and 15% Fe-CdS doped nanorods are found to be 7.243, 6.821, 6.495, 6.245 and 7.693 nm, respectively. From these calculations, it has been found that in case of undoped CdS, the crystallite size is larger ,but in case of doped CdS nanorods the crystallite size decreases ,which may be because of smaller ionic radii of Fe (64nm) than the ionic radii of Cd (103) [39]. The crystallite size has been found to decrease upto 10% doping, and, as on further, increasing the dopant concentration to 15%, the crystallite size increases, which may be due to the agglomeration of the synthesized nanostructures. The lattice parameters *(a, c)* have been calculated following relation [4]:

$$\frac{1}{d_{hkl}^2} = \frac{4}{3}\left[\frac{h^2 + hk + k^2}{a^2} + \frac{l^2}{c^2}\right]$$

Table 3.3 shows the lattice parameters of the nanorods. It has been found that the value of lattice parameters decreases in case of Fe-doped CdS nanorods upto 10% doping, as we increase the doping to 15% these lattice parameters start increasing, which are completely in agreement with the calculated crystallite size.

From Figure 3.15, it has also been found that there is no impurity peak till 10% doping concentration showing that Fe is completely substituted in the host lattice. But in case of 15% concentration, some of the impurity peaks have started originating, shown by asterisk (*); these may be due to the extra amount of the dopant or some of the Fe ions being segregating and occupying some other interstitial sites instead of replacing the host element, i.e., Cd ions.

Table 3.3 Lattice parameters, crystallite size, absorption edge wavelength and band gap of undoped and Fe-doped CdS nanorods.

Sample description	a(Å)	c(Å)	Crystallite Size (nm)	Wavelength (nm)	Bandgap(eV)
undoped CdS	4.1187	6.7264	7.243	480	2.58
3% Fe	4.1006	6.7068	6.821	478	2.59
5% Fe	4.1010	6.6969	6.495	473	2.62
10% Fe	4.1005	6.6864	6.245	483	2.56
15% Fe	4.1215	6.7185	7.693	485	2.55

3.3.2 Morphological analysis

TEM, HRTEM and SAED patterns of $Cd_{1-x}Fe_xS$ (x = 0, 0.1) are shown in Figure 3.16. The average size of synthesized nanorods have been found to be of 60 nm in length and 13nm in width for both the undoped and Fe-doped CdS nanorods, which are composed of several much smaller nanocrystallites, 6-7 nm, as calculated from the XRD. The d-spacing values are calculated by using the lattice planes observed in HRTEM image (Figure 3.16 (c, d)). The observed inter-planar spacing is about 1.3998 nm, which completely matches with (112) plane of CdS hexagonal structure; this depicts that the growth of nanorods is along the (112) plane. The corresponding SAED patterns (Figure 3.16 (e, f)) show sharp and circular rings showing the nanorods to be polycrystalline in nature. Absence of aggregation in HRTEM images confirms the phase purity and substitution of Fe CdS lattice.

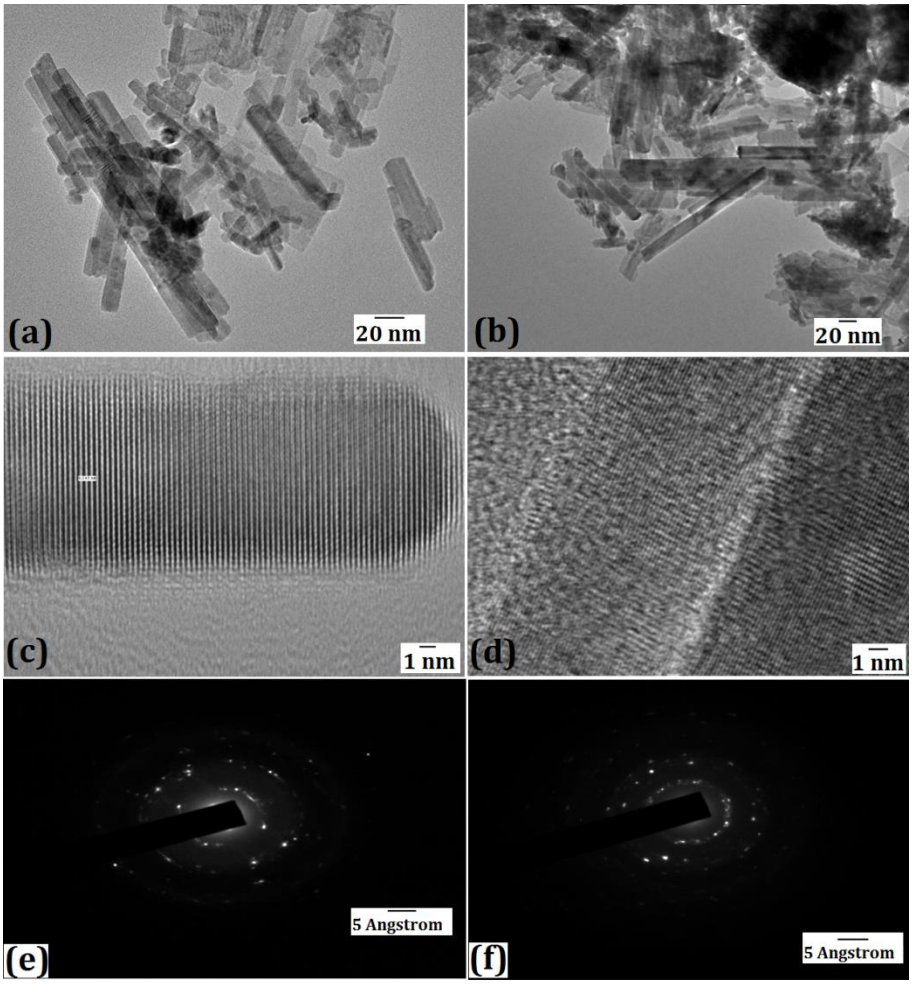

Figure 3.16 TEM micrographs of (a) Undoped and (b) 10% Fe-doped, HRTEM of (c) undoped and (d)10% Fe-doped, SAED pattern of (e) undoped and (f) 10% Fe-doped CdS nanorods.

3.3.3 Elemental analysis

Elemental analysis of the various constituent elements in case of undoped and Fe-doped CdS nanorods is given in Figure 3.17. It has been found that in case of undoped CdS nanorods, both cadmium and sulphide (atoms) are present in stoichiometeric ratio which clearly depicts from the weight pecent (inset Figure (a)). In case of Fe-doped CdS nanorods for various concentrations of the dopant, i.e., 3, 5, 10 and 15 (Figure (b to e), the calculated pecentage are found to be 3, 2.22, 6.63 and 13.30, respectively. These results confirm the doping of Fe into the host lattice.

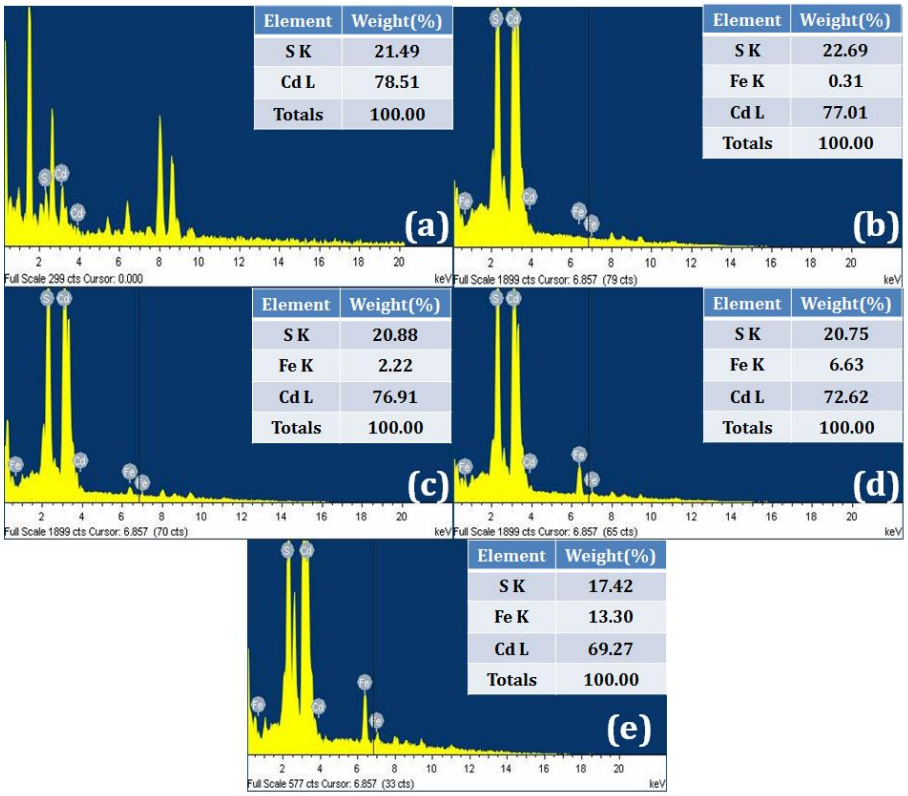

Figure 3.17 EDAX spectra of (a) undoped and (b) 3% (c) 5% (d) 10% (e)15% Fe-doped CdS nanorods.

3.3.4 Optical analyses

3.3.4.1UV-visible spectra

Figure 3.18 shows UV-visible absorption spectra of synthesized undoped and Fe doped CdS nanorods. Calculated bandgap for the given wavelength are shown in table (1) using the following expression:

$$E = \frac{hc}{\lambda_{max}}$$

where, E_g stands for bandgap energy, h for Planck's constant, c for velocity of light, and λ_{max} for maximum absorption by the CdS nanorods[6]. The absorption edge, pertaining to bandgap (2.58 eV), shifts to wavelength, 480 nm [39-41].

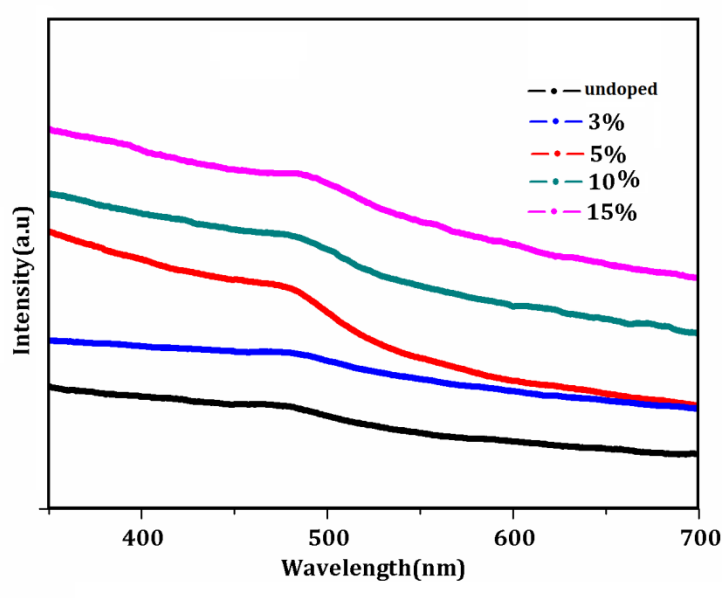

Figure 3.18 UV-visible absorption spectra of undoped, 3%, 5%, 10% and 15% Fe-doped CdS nanorods.

But there is no regular trend in the bandgap upto 5% of dopant concentration. A blue shift has been observed in the bandgap with increasing dopant concentration to 10% and, a red shift, for 15%. The absorption edge shift towards the higher wavelength side is an indication of the increase in particle size; this also corroborates with XRD. However, the decrease in the band gap value is precisely due to the introduction of new energy levels in the host lattice upon doping [42-43].

3.3.4.2 Photoluminescence spectra

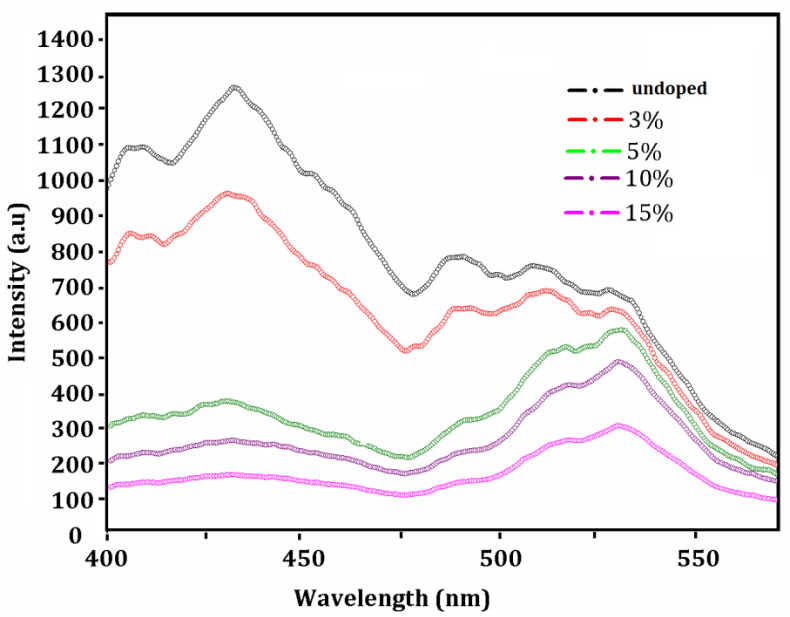

Figure 3.19 PL spectra of undoped,3%, 5%, 10% and 15% Fe-doped CdS nanorods.

Room temperature photoluminescence spectra of synthesized undoped and Fe-doped CdS nanorods obtained at excitation wavelength 380nm is shown in Figure 3.19. From the emission spectra, we find a hump at 408 nm and, a peak at 432 nm, which are due to blue emission. These are found to be prominent in case of undoped CdS nanorods and show decrease in intensity with increase in dopant concentration [39]. In case of doped samples, photo excited electrons are transferred to the Fe ion induced trap centers, which, in turn, result in quenching the luminescence [34, 44-46].

The peak originating at 488 nm is due to the host CdS. A weak peak originating at 509 nm, due to the presence of the surface traps, also registers decrease in its intensity upon increase in dopant concentration due to the formation of the non-radiative recombination centers [26]. Moreover, the another peak at 529 nm, precisely due to the green emission, may be attributed to the surface donor–accepter pair recombinations as well as d–d intra-ion transitions [8].

3.3.5 Magnetic analysis

Room temperature magnetic measurements of undoped and Fe-doped CdS nanorods are shown in Figure 3.20. It has been found that saturation magnetization values for undoped, 3%, 5%, 10% and 15% are 0.187, 0.300, 0.450, 0.675, and 0.600 emu g^{-1}, respectively. From the calculated magnetization values, it is concluded that synthesized undoped CdS nanorods are ferromagnetic in nature; however, the bulk CdS is diamagnetic in nature. On addition of Fe to the host lattice, an increase in magnetization values has been observed, which is in well agreement with earlier reports [47]. The reason for observed ferromagnetism is exchange interaction of magnetic dipoles between the nearest neighbours, which may be due to the dominant iron–iron super exchange interaction [44].

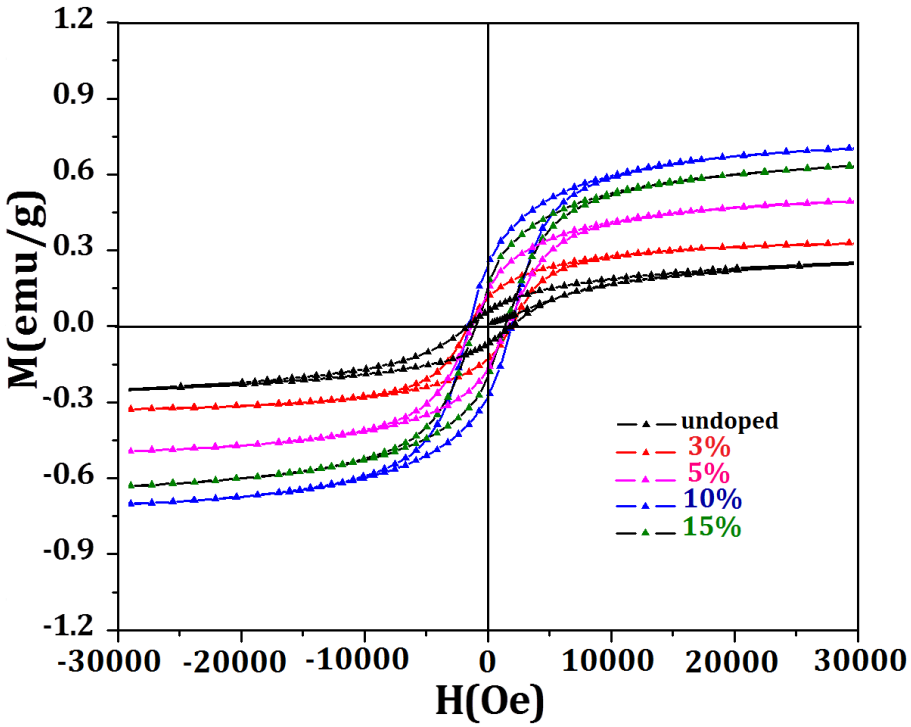

Figure 3.20 M-H hysteresis loops of undoped, 3%, 5%, 10% and 15% Fe-doped CdS nanorods.

The bound magnetic polaron model is also used to explain the ferromagnetism in DMS materials. According to this model polarons interact with the magnetic ions present at the interstitial sites, which give rise to indirect ferromagnetic interaction that align the magnetic polarons. So, the formation of bound magnetic polaron contributes to the ferromagnetism in metal doped DMS [36].The magnetization value for 15% Fe doping as compared to 10% has been found to decrease, which may attributed to increase in the crystallite size as calculated from the XRD values.

Similar observation has been reported by Sunil et al. [34] wherein the increase in dopant concentration has resulted in decreasing the magnetization values; this, in fact, is due to the presence of more grain boundaries at the higher dopant concentration. Some impurity peaks, originating at this higher concentration shown by (*), may also be responsible for this anomalous behaviour at 15% Fe concentration.

3.4 Structural, optical and magnetic properties of Gd-doped CdS nanorods

This section deals with $Cd_{1-x}Gd_xS$ (x = 0.00, 0.01, 0.03, 0.05, 0.10, 0.15) nanorods. The structural, optical and magnetic properties of undoped and Gd-doped nanorods, synthesized using solvothermal technique, were studied. The obtained results are discussed below:

3.4.1 Structural, morphological and compositional analyses

3.4.1.1 Structural analysis

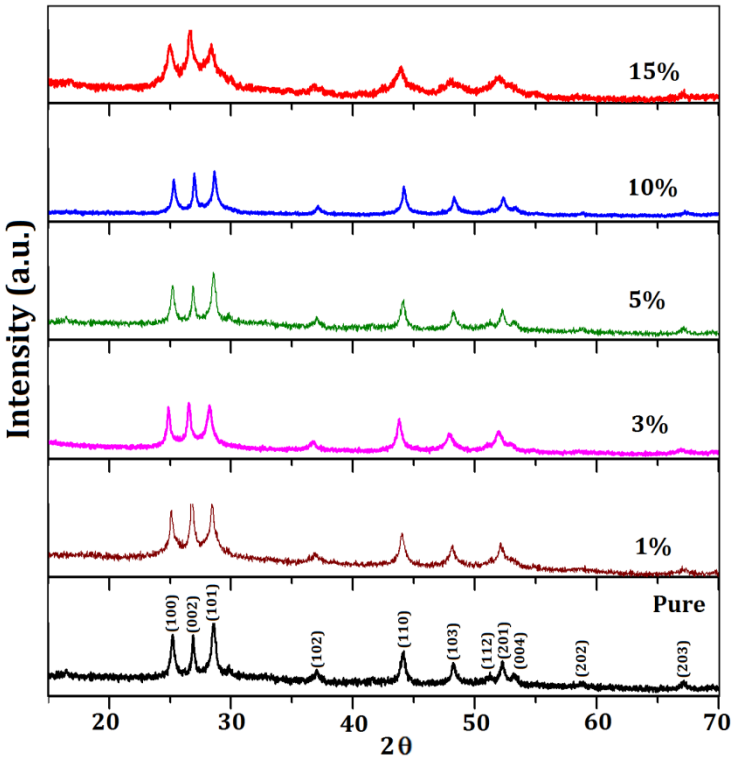

Figure 3.21 XRD patterns of undoped, 1%, 3%, 5%, 10% and 15% Gd-doped CdS nanorods.

Figure 3.21 shows XRD patterns of synthesized $Cd_{1-x}Gd_xS$ nanorods (x = 0.01, 0.03, 0.05, 0.10, 0.15), revealing their hexagonal wurtzite structure. There is no indication related to secondary phase or impurity in XRD patterns. The diffraction patterns, exhibiting broad peaks, show the nanorods being made of smaller crystallites. The lattice parameters *(a, c)* has been calculated (as shown in Table 1) using following relation [4]:

$$\frac{1}{d_{hkl}^2} = \frac{4}{3}\left[\frac{h^2 + hk + k^2}{a^2} + \frac{l^2}{c^2}\right]$$

Table 3.4 reveals Gd-doping results in the decrease of lattice parameters thereby indicating lattice contraction, because of less size of the Gd, as compared to Cd [22].

3.4.1.2 Morphological studies

Figure 3.22 reveals the TEM micrographs of undoped and 15 % Gd doped CdS nanorods .It confirms diameter of the nanorods, respectively, to be 14 and 26 nm.

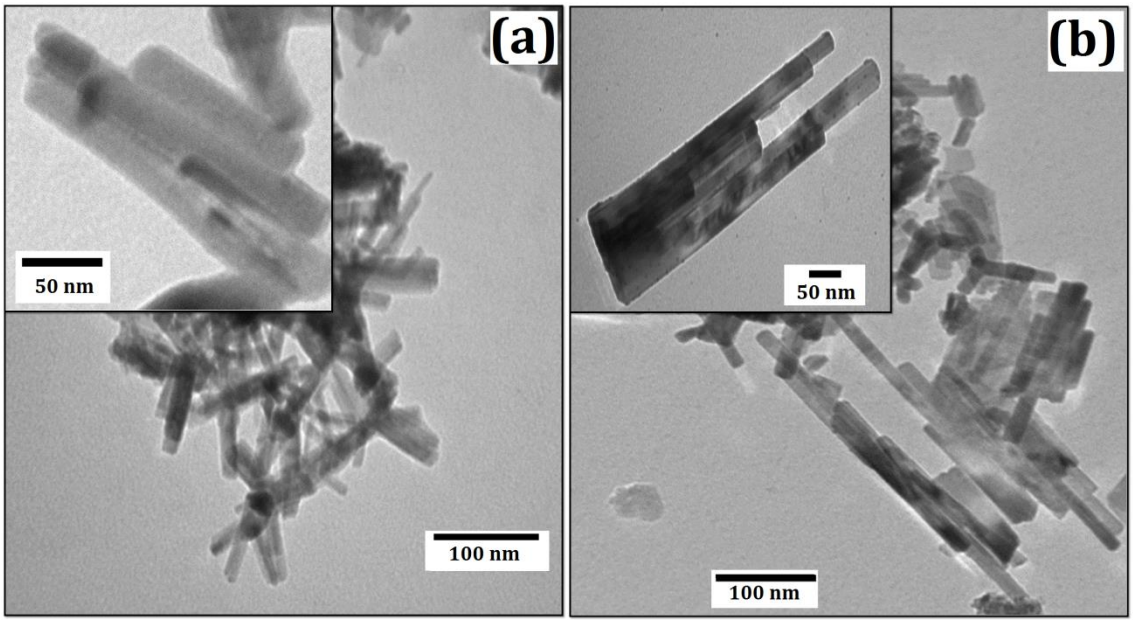

Figure 3.22 TEM images of (a) undoped and (b) 15% Gd-doped CdS nanorods.

3.4.1.3 Compositional analysis

Figure 3.23 represents the energy dispersive spectroscopy (EDS) spectra of the undoped and 10 % Gd-doped CdS nanorods. It has been found that the elements, Cd, S and Gd are there in stoichiometric ratio confirming the substitution of Gd in CdS lattice. Moreover, in the EDAX spectra, no impurity phase has been detected.

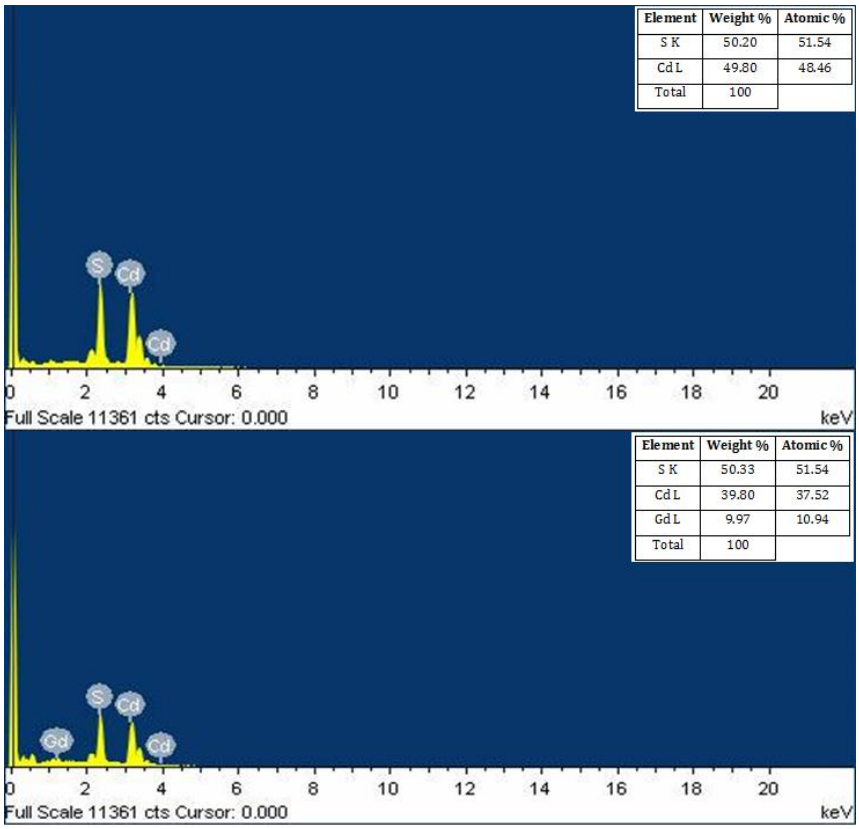

Figure 3.23 EDAX spectra of (a) undoped and (b) 10% Gd-doped CdS nanorods.

3.4 .2 Optical Studies

3.4.2.1 UV-visible spectra

UV-visible spectra of synthesized $Cd_{1-x}Gd_xS$ nanorods are shown in Figure 3.24. The energy band gap (E_g) has been calculated by employing '$\lambda_{1/2}$ method' [48]. Table 3.4 displays the calculated $\lambda_{1/2,}$ and corresponding E_g for the synthesized $Cd_{1-x}Gd_xS$ nanorods. A clear blue shift in band gap of the nanorods (absorption shifted to lower wavelength) with respect to the bulk counterpart CdS has been observed. This can be attributed to quantum confinement effect due to smaller crystallite size of the nanorods. The quantum confinement of electrons and holes in semiconducting nanorods results in increasing the effective band gap with decrease in size [8]. The variation of optical band gap with Gd-doping concentration is shown in Figure 3.25. It is depicting that the doping of Gd in CdS host leads to lattice contraction (as observed in XRD),

which further enhances the band gap upto 2.59 eV. This is well in agreement with XRD confirming distortion in lattice structures, which is responsible to cause changes in electronic band structure of CdS and, thereby is responsible for the increased energy band gap [7].

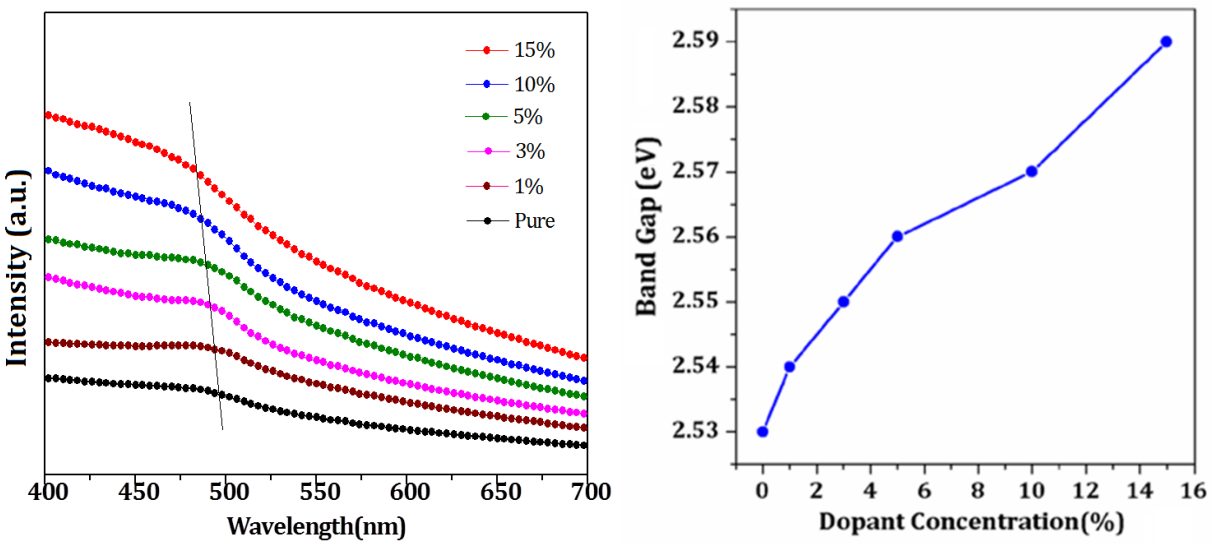

Figure 3.24 UV-vis spectra of Gd–doped CdS nanorods, (b) Variation of band gap with Gd-doping concentration.

3.4.2.2 Photoluminescence spectra

Figure 3.25 depicts the room-temperature photoluminescence spectra at the excitation wavelength of 380 nm. The undoped and doped CdS nanorods show their excitonic emission band at around 530 nm, and increase in the peak intensity with increase in dopant concentration [49]. These peaks are corresponding to the green emission and may be because of the surface donor-accepter pair recommendations as well as d-d intra-ion transitions. These arise due to two processes occurring in d-d intra-ion transitions: first, the recombination of the donor electrons with trapped holes in accepter level and, second, the recombination of free electros from conduction band with the captured holes in accepter level. Electrons and holes, after excitation, undergo non-radiative decay and, this gives rise to green emission [26]. The peak appears around 476 nm may be due to the Gd-doping in CdS, which shows that the Gd-doping introduces new

energy levels in the band gap; these are responsible for varying the luminescence properties of doped-CdS nanorods. The rare earth ions exhibit electron-electron and spin orbit interactions within 4f shell. These d-f transitions are strictly forbidden, as electric dipole transitions in case the rare earth ions occupy the inversion symmetry site in crystal lattice [49].

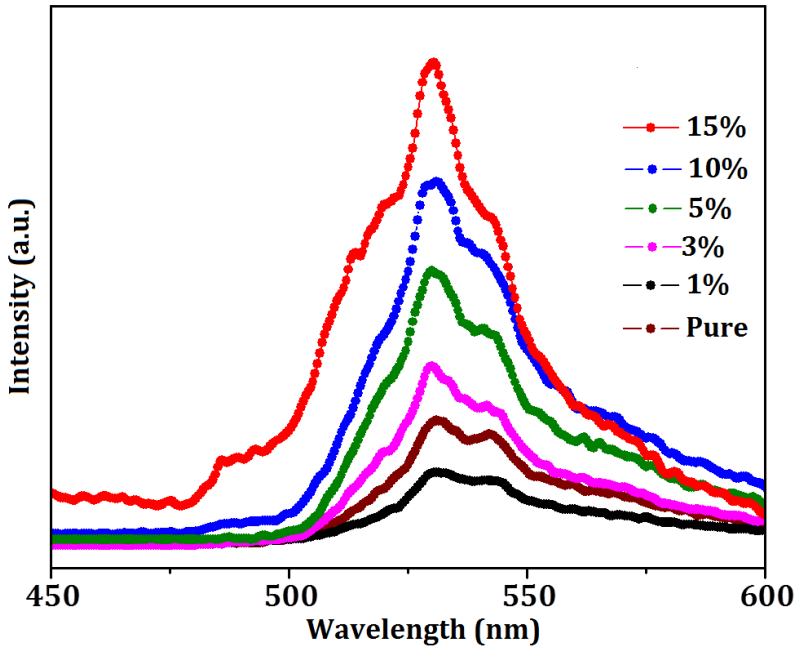

Figure 3.25 Photoluminescence spectra of undoped, 1%, 3%, 5%, 10% and 15% Gd-doped CdS nanorods.

3.4.3 Magnetic study

The magnetic properties of $Cd_{1-x}Gd_xS$ (x = 0.00, 0.01, 0.03, 0.05, 0.10 and 0.15) nanorods, shown in Figure 3.26, have been found to exhibit ferromagnetism. The magnetic saturation values has been found to be 0.0705, 0.1476, 0.2077, 0.2985 and 0.4223 emu/g for undoped, 3%, 5%,10% and 15% Gd-doped CdS nanorods, respectively (Table 3.4). Figure 3.26 (b) shows the increament in magnetization with Gd-doping. XRD and PL study confirm the phase undoped and defects free nanorods. This reveals the ferromagnetism in the nanorods to be mainly due to their nano size and doping. The electronic structure of CdS gets changed as we move from bulk to

nanoscale; this leads to the high defect formation energy that contributes to the ferromagnetism [26]. It has been known that there are numerous surface defects are presents nanomaterials. The electrons get trapped and overlap with the f-shells of doped Gd atoms thereby resulting in overlapped orbital states of the order of Bohr radius. These trapped electrons aligned their self in such a way that they lead to ferromagnetic coupling between the dopant atom [17]. For the material exhibiting ferromagnetism, there are two countable factors - presence of local magnetic moments and their ferromagnetic coupling and hybridization [50].

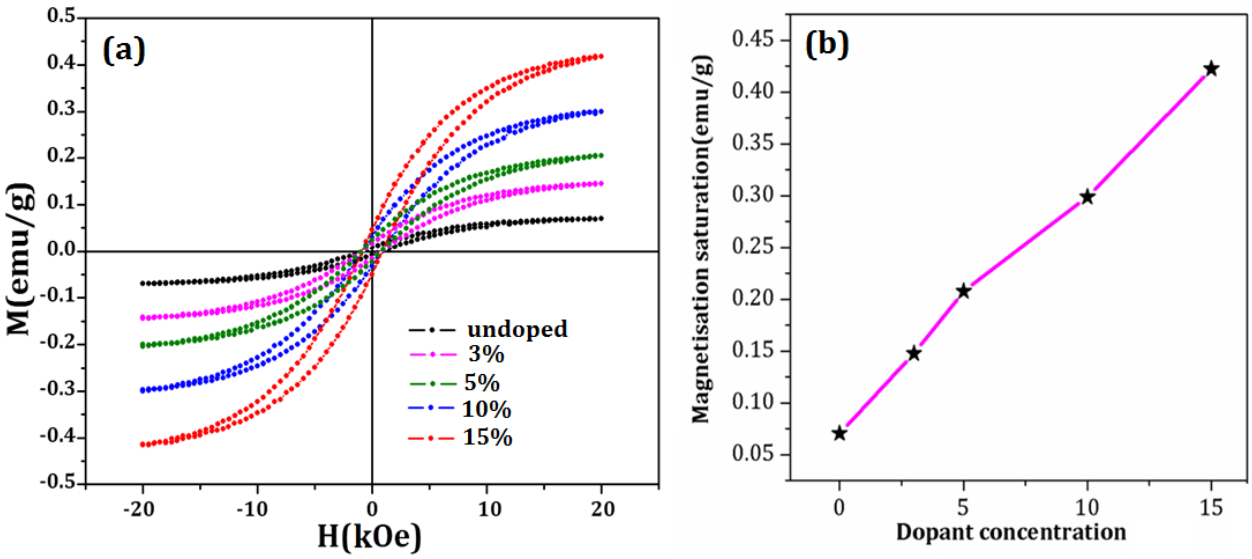

Figure 3.26 (a) M-H hysteresis loops of undoped, 3%, 5%, 10% and 15% Gd-doped CdS nanorods (b) Variation of magnetic saturation with doping concentration of Gd.

The doping of Gd has been found to reduce defects related to Cd or S thereby enhancing the magnetization. The hybridization between the charge carriers of Cd and Gd creates spin-split impurity band at the Fermi level of CdS; precisely, this may be reason for the observed ferromagnetism [2]. The ferromagnetism in doped CdS can also be attributed to the formation of small magnetic dipoles positioned at the surface of the nanorods. These magnetic dipoles interact

with their nearest neighbours within the nanorods, and the exchange energy in these magnetic dipoles resulting in alignment of dipoles in the same direction. As the surface to volume ratio for nanorods is very high, the number of magnetic dipoles, oriented in the same direction, is also high and, this lead to ferromagnetism.

3.5 Structural, optical and magnetic properties of Co-doped CdS nanoparticles

This section deals with the series of $Cd_{1-x}Co_xS$ (x = 0.00, 0.03, 0.05, 0.10) nanoparticles. The nanoparticles were synthesized by using hydrothermal technique as discussed in chapter 2. The magnetic, optical and structural properties of undoped and Co-doped nanoparticles were studied. The obtained results are discussed below:

3.5.1 Structural, morphological and compositional analyses

3.5.1.1 Structural analysis

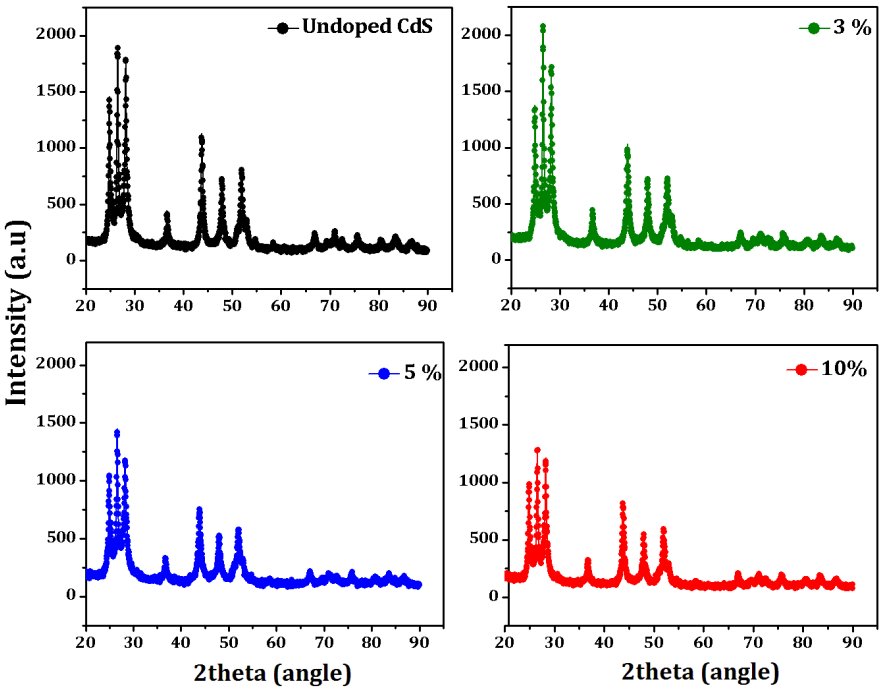

Figure 3.27 XRD patterns of undoped and Co-doped CdS nanoparticles.

Figure 3.45 shows the XRD spectra of the undoped CdS and Co-doped CdS nanoparticles; the peaks correspond to the wurtzite phase with hexagonal structure of CdS (JCPDS card no. 41-1049). There were no impurity peaks which depict the highly undoped nature of the synthesized nanoparticles. The decrease in lattice parameters (*a*, *c*) and crystallite size upon Co-doping (Table 3.4) can be attributed to the smaller radii of Co^{2+} (0.72 Å) ions in comparison to those of

Cd^{2+} (0.97 Å) ions. Moreover, the peak intensity reduces upon Co-doping due to the occurrence of the tensile strain that increases by replacement of the Cd by Co [51].

Table 3.4 Lattice parameters, crystallite size and bandgap of undoped and Co-doped CdS nanoparticles.

Sample Description	a(Å)	b(Å)	Crystallite size (nm)	Band Gap (eV)
Undoped CdS	4.1050	6.7213	32	2.9
3% Co CdS	4.1025	6.7148	29	2.9
5% Co CdS	4.0840	6.6852	27	3.1
10% Co CdS	4.0647	6.6348	23	3.2

3.5.1.2 Morphological and Compositional analysis

Figure 3.46 (a ,b, c) represents the TEM images of undoped, 5% and 10% Co-doped CdS nanoparticles, respectively. TEM confirms that the size of undoped and Co-doped CdS nanoparticles ranges between 35 and 25 nm. Figures 3.46 (d, e) show EDS spectra of undoped and 10% Co-doped nanoparticles, which confirm that all the required elements such as Co along with Cd and S are present in stoichiometric ratio. There were no extra peaks related to any impurity.

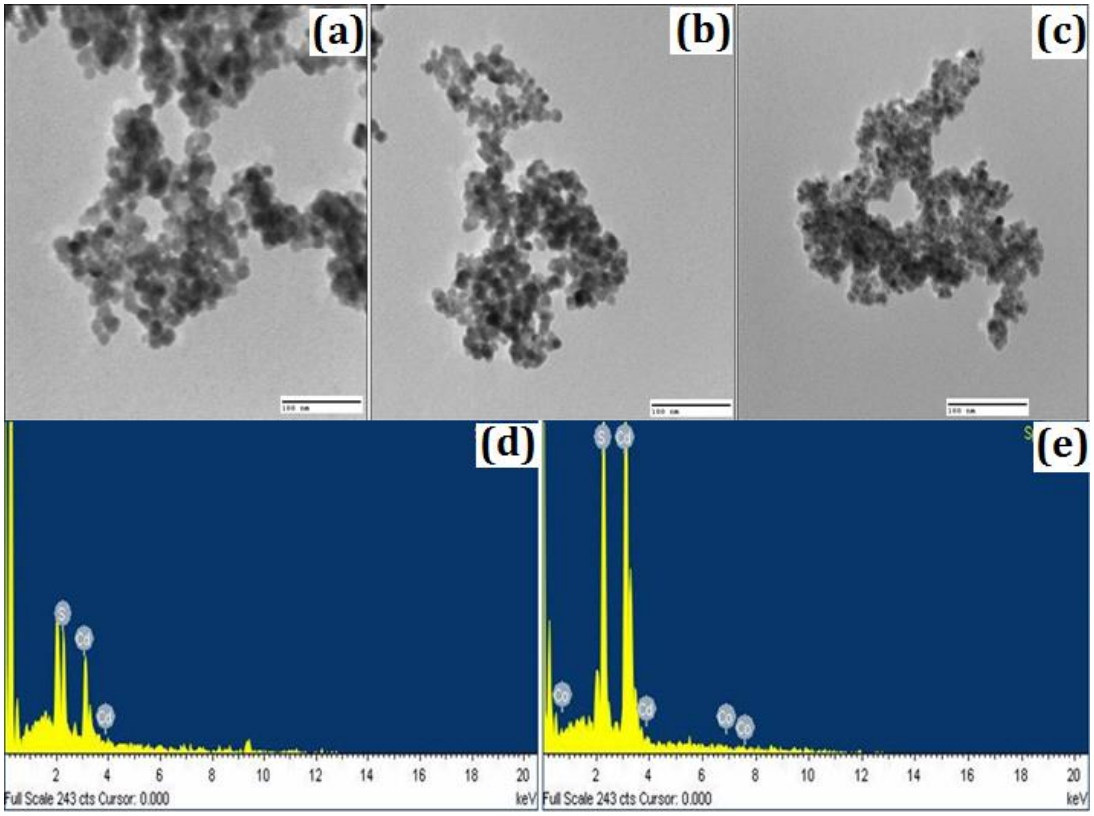

Figure 3.28 TEM images of (a) undoped (b) 5% and (c) 10% Co-doped CdS nanoparticles, (d) EDS images of undoped CdS (e) EDS of 5% Co-doped CdS nanoparticles.

3.5.2 Optical analyses

3.5.2.1 UV- vis analysis

The absorption spectra (Figure 3.47) of undoped and Co doped CdS nanoparticles is calculated using Tauc' relation [29]:

$$(\alpha h\nu)^2 = A\left(h\nu - E_g\right)^n$$

Where A is a constant – a function of probability of given electronic transitions; $h\nu$, the photon energy; h, Planck's constant. The bandgap (E_g) has been calculated by extrapolating line in the spectra and it was found to vary between 2.90 – 3.25 eV.

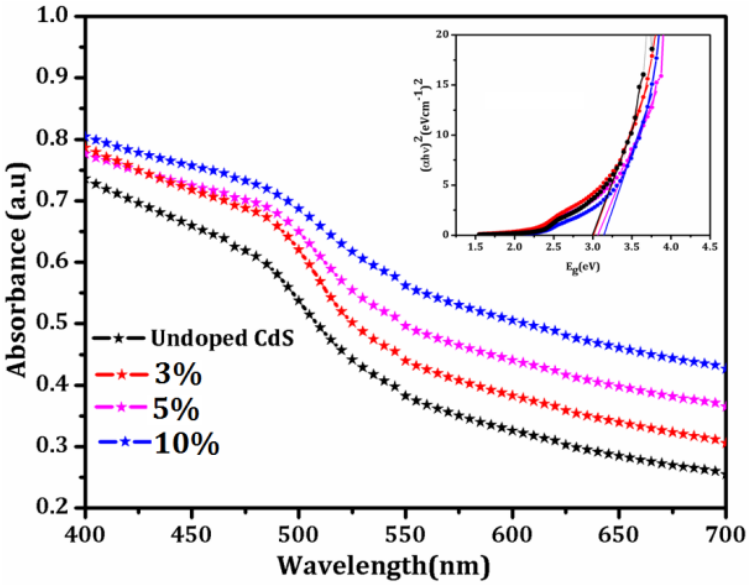

Figure 3.29 UV-visible absorption spectra of undoped and Co-doped CdS nanoparticles.

Similar observation has been found in one of the published articles [52]. The observed blue shift may be the cause of the reduction in the crystallite size due to quantum confinement effects upon Co-doping. The results are in well consistent with the XRD results as the crystallite size decreases upon doping [53].

3.5.2.2 Photoluminescence Spectra

The photoluminescence spectra of undoped and Co-doped CdS nanoparticles at excitation wavelength 380nm is shown in figure 3.48. In case of undoped CdS as well as Co-doped CdS nanoparticles the main excitonic peak occurs at 530 nm, which is due to electron-hole recombination giving rise to these green emissions. No shift in the peak has been observed. Upon increasing the limit of doping, the peak intensity was found to decrease, which may be due to the quenching effect by doped transition metal into the host lattice. The d-d electron interactions causes the green emissions. A small peak pertaining to undoped CdS, appears at 485 nm, and disappears, upon Co-doping [54].

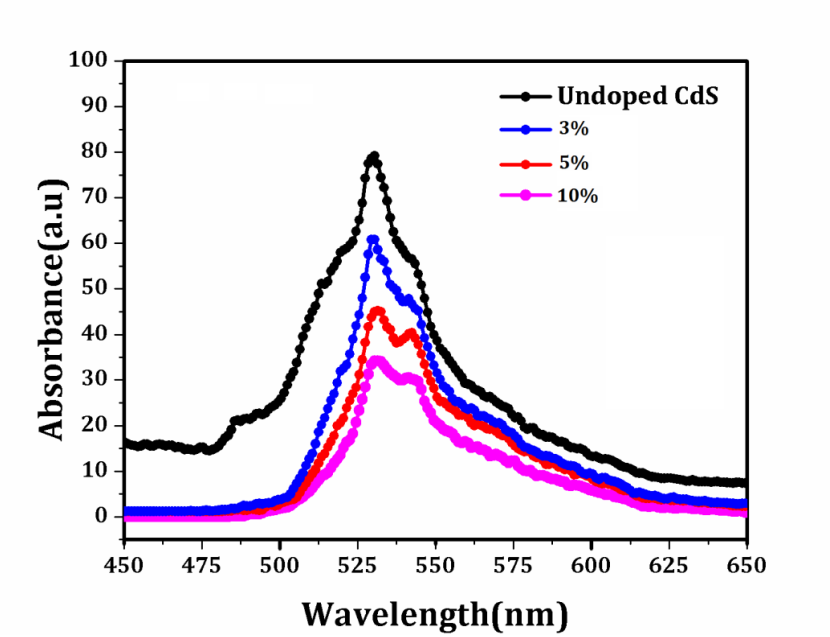

Figure 3.30 Photoluminescence spectra of undoped and Co-doped CdS nanoparticles.

3.5.3 Magnetic analysis

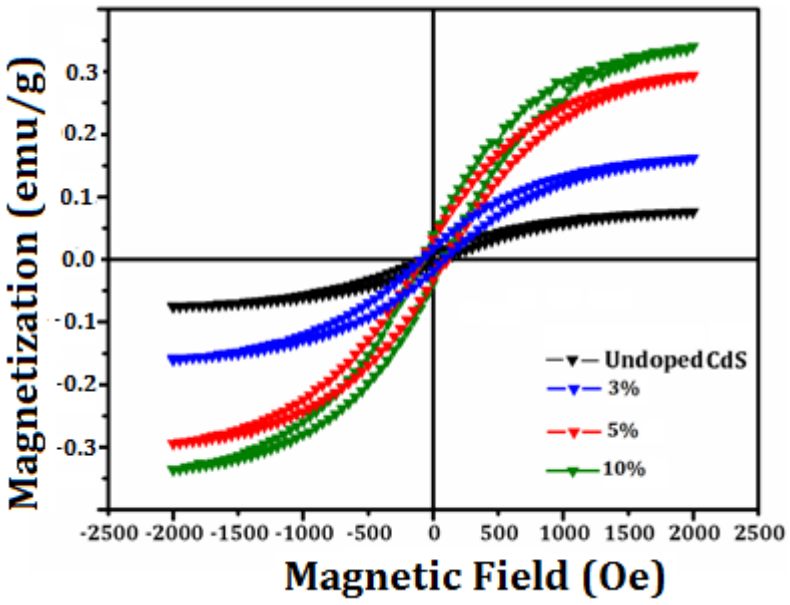

Figure 3.31 Magnetic curve of undoped and Co-doped CdS nanoparticles.

Figure 3.48 shows the magnetic curve of the undoped and Co-doped CdS nanoparticles. From the literature, it has been observed that the ferromagnetism in the undoped CdS nanoparticles is attributed to the presence of the Cd vacancy that changes the electronic configuration. The presence of any capping agent can also contribute to the ferromagnetic behavior. However, in our case, where no capping agent has been used, the origin of magnetism is possibly the result of carrier mediated exchange interactions [55]. The XRD analysis shows that the Co-doping results in ferromagnetism, which may be attributed to the intrinsic coupling between the doped Co ions, and not due to some secondary phase formation. The Co-doping, the concentration of bound magnetic polarons (F-centers) increases, which further rises the saturation magnetization as shown in Figure 3.48. Further, the ferromagnetism can also be said to be an intrinsic property of Co-doped CdS nanoparticles, which doesn't depend on the formation of secondary phase. The reports explore the theoretical explanation for the existence of the ferromagnetism in transition metal doped CdS nanostructures. Consequently, the ferromagnetism results, that decreases the formation energy of the Cd vacancy [51].

3.6 Structural, optical and magnetic properties of Ni - doped CdS nanoparticles

This section deals with the series of $Cd_{1-x}Ni_xS$ (x = 0.00, 0.03, 0.05, 0.10) nanoparticles synthesized by hydrothermal technique. The structural, optical and magnetic properties of undoped and Ni-doped nanoparticles were studied. The obtained results are discussed below:

3.6.1 Structural, morphological and compositional analyses

3.6.1.1 Structural analysis

X-ray pattern shows that for undoped and Ni-doped CdS nanoparicles (Figure 3.33), the peaks (110), (002), (101), (102), (110), (103), (112), (004), (201),(203), (211), (212), (300), (213), (302), appear, respectively, at 2θ = 24.88º, 26.57º, 28.23º, 36.60º, 43.93, 47.90º, 52.09º, 54.60º, 58.36º ,67.15º, 71.54º ,76.14º ,80.75º,83.47º, 86.60º. These peaks match with the JCPDS card no. 41-1049 revealing their hexagonal phase. No other impurity peaks were noticed – a test of high purity of the sample. The crystallite size of the nanoparticles has been calculated using the debye scherrer formula [4].

The calculated diameters of the particles are found to be 28, 27, 26, 22nm, respectively, for undoped CdS, 3%, 5% and 10% Ni-doped CdS nanoparticles. The crystallite size of the nanoparticles decreases upon Ni-doping due to the smaller ionic radius of Ni as compared to that of Cd [56]; similar results has been reported by Patel et .al [57] . The lattice parameters of Ni-doped CdS nanoparticles are a = 4.138Å and c = 6.7185Å, which are smaller than of CdS, i.e., a = 4.122 Å and c = 6.7267Å.

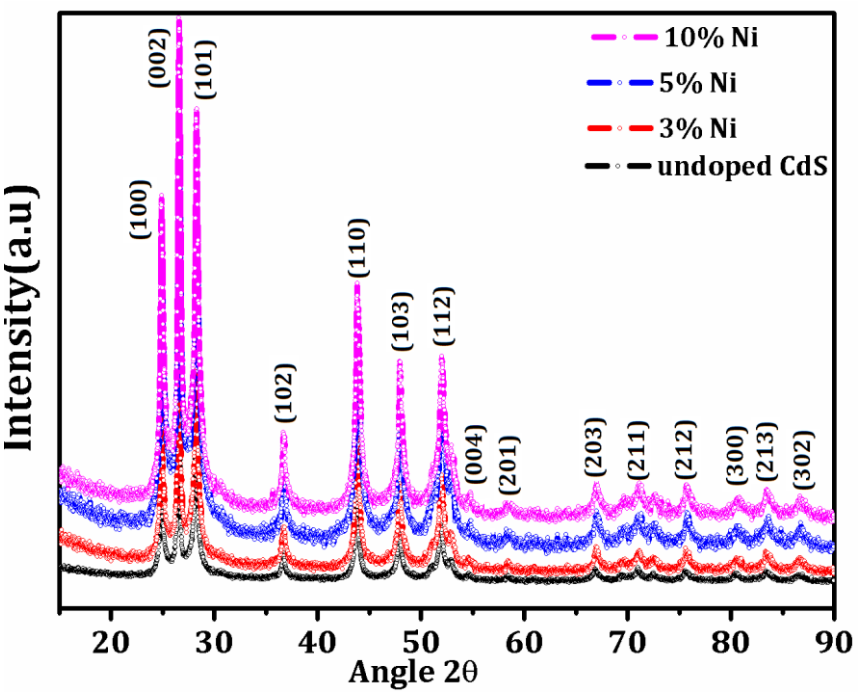

Figure 3.32 XRD patterns of $Cd_{1-x}Ni_xS$ ($0 \leq x \leq 0.1$) nanoparticles.

3.6.1.2 Morphological and Elemental analysis

TEM micrographs show nearly spherical morphology for both the undoped and 10% Ni-doped CdS nanoparticles (Figure 3.34 (a, b)) with the nanoparticles lying in the range of 28 nm - 22 nm. The size of the nanoparticles is similar as calculated from the XRD results. Figure 3.34(c) and 3.34(d) show, respectively, the EDAX spectrum of undoped and doped CdS nanoparticles, which confirm the presence of all the desired elements in appropriate amount, and rules out the possibility of any impurity element.

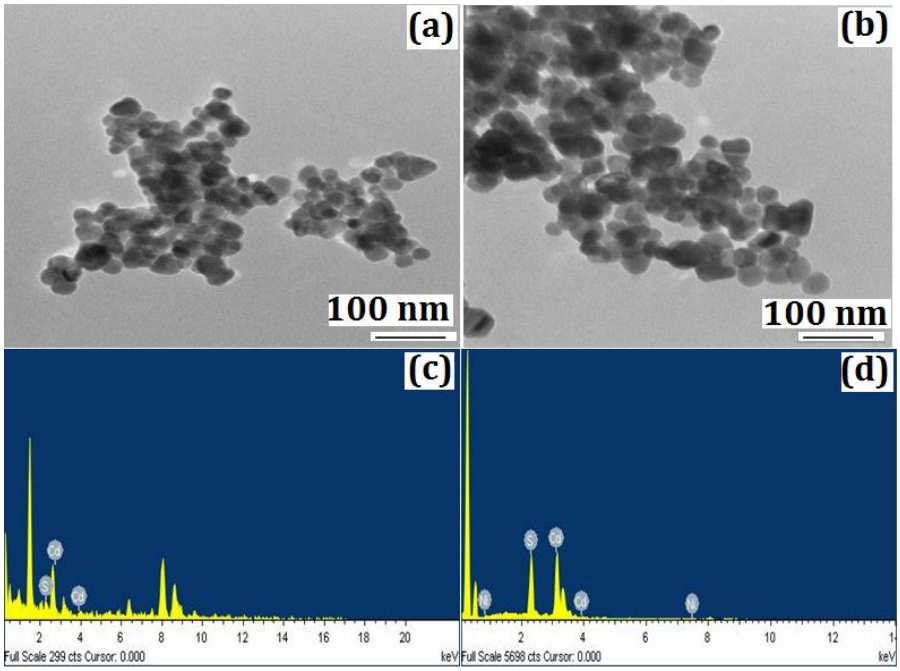

Figure 3.33 TEM micrographs of (a) Undoped (b) 3% and EDAX spectra of (c) Undoped (d) 10 % Ni-doped CdS nanoparticles.

3.6.2 Optical Studies

3.6.2.1 Photoluminescence Spectra

CdS nanoparticles have acceptors and donors, respectively, as Cd vacancies and interstitial sulphur and sulphur vacancies and interstitial cadmium [58]. The well-known green emission bands at 575 nm and at 525 nm are observed for all the as-synthesized samples. The enhancement in PL peaks at 575 and 525 nm are due to the presence of interstitial sulphur shown in Figure 3.35. Decrease in the emission intensity on Ni-doping is precisely due to quenching by Ni atoms [45, 59]. In case of undoped CdS nanoparticles, a small hump at 490nm is due to the electron- hole pairs recombination.

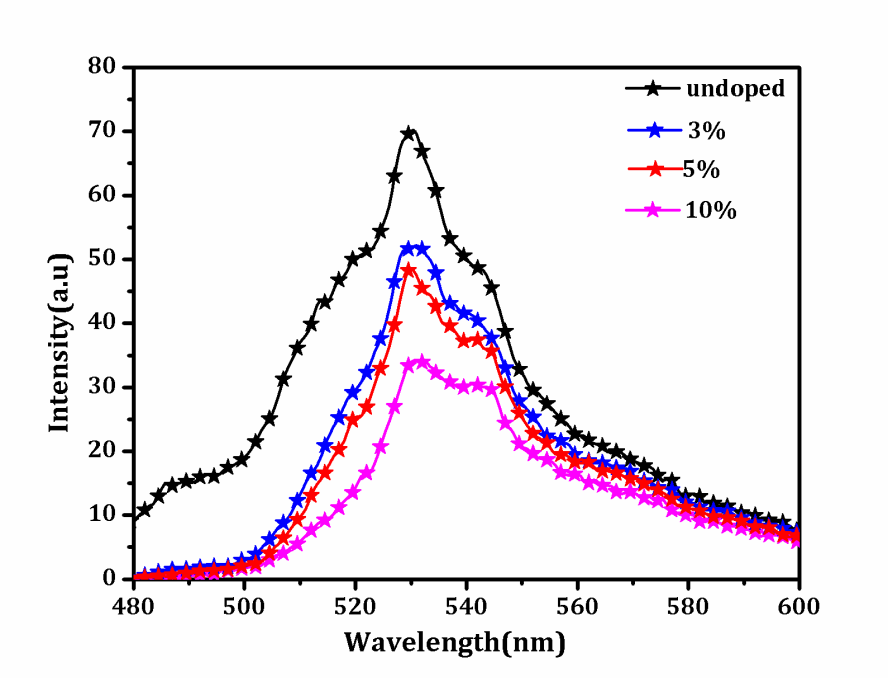

Figure 3.34 PL spectra of $Cd_{1-x}Ni_xS$ ($0 \leq x \leq 0.1$) nanoparticles at excitation wavelength of 480 nm.

3.6.2.2 UV-visible spectroscopy

The band-gap of the synthesized nanoparticles (Figure 3.36) has been found to be 2.46, 2.48, 2.52 and 2.55 eV for undoped CdS, 3%, 5% and 10% Ni-doped CdS nanoparticles, respectively. Bulk CdS is a direct bandgap (2.42eV) semiconductor, which show blue shift on being reduced to nanoscale; it is precisely due to quantum confinement resulting due to the localization of the electrons and hole [60, 26].

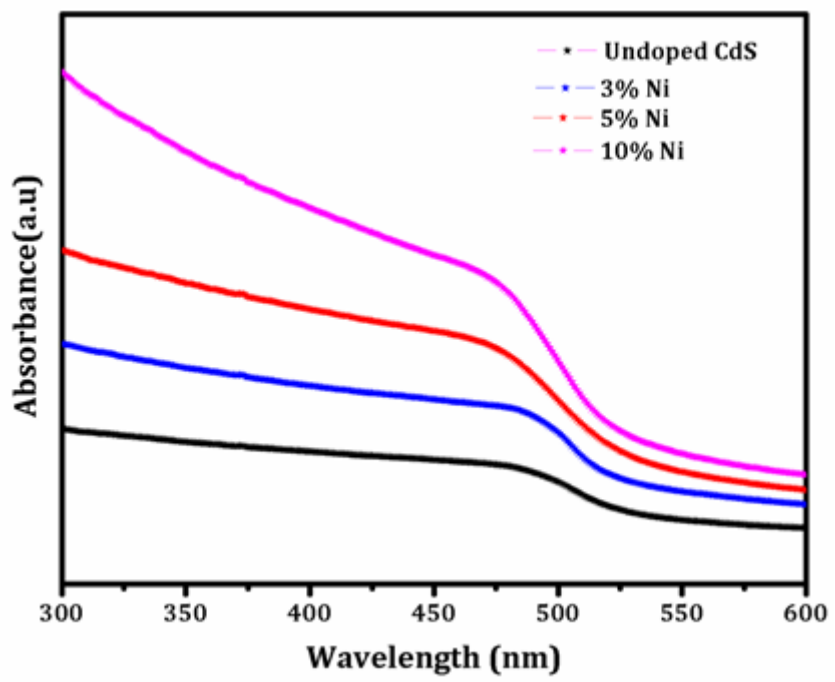

Figure 3.35 UV-visible spectra of $Cd_{1-x}Ni_xS$ ($0 \leq x \leq 0.1$) nanoparticles.

3.6.3 Magnetic analysis

The M-H curves (Figure 3.37), obtained at room temperature, reveal the ferromagnetic behavior of undoped CdS nanoparticles, which can be due to the vacancy or surface defects [36]. The curves indicate the magnetic saturation values at 0.039, 0.048, 0.2056 and 0.2807emu/g, respectively, for undoped CdS, 3%, 5% and 10% Ni-doped CdS nanoparticles. These curves also show increase in magnetization with increase in Ni content. The increased ferromagnetism in Ni-doped CdS nanoparticles may be due to the presence of some secondary phases. However, the XRD patterns do not reveal such phases. Thus, another reason for the magnetic behavior may be due to the (RKKY) or double exchange interactions [61, 26]. The ferromagnetism in Ni-doped CdS may be due to F-center (sulfur vacancy)-mediated exchange mechanism. Interatomic distance between the Ni-atoms may also be responsible for the magnetic character. The dopant

atoms of Ni, at shorter distances, may result in antiferromagnetic coupling. However, no symmetry has been observed in the hysteresis, which signifies the ferromagnetic interactions between the Ni atoms [62]

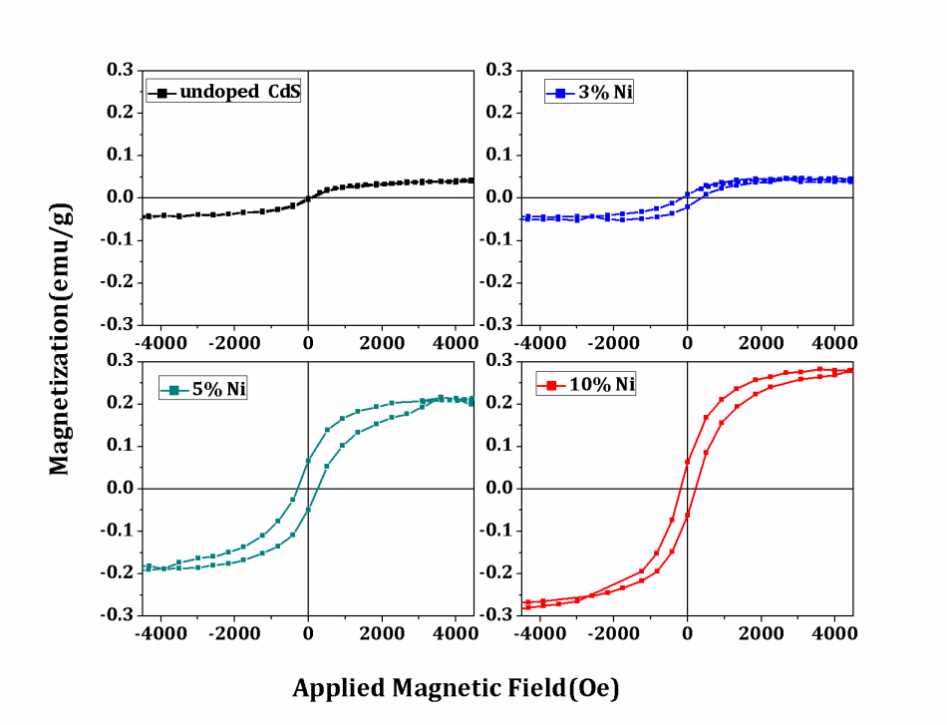

Figure 3.36 M–H curves of $Cd_{1-x}Ni_xS$ ($0 \leq x \leq 0.1$) nanoparticles.

3.7 Structural, optical and magnetic properties of Fe-doped CdS nanoparticles

The $Cd_{1-x}Fe_xS$ (x = 0.00, 0.03, 0.05, 0.10) nanoparticles were synthesized by hydrothermal technique. The optical, structural and magnetic properties of undoped and Fe-doped nanoparticles were studied. The obtained results are discussed below:

3.7.1 Structural, morphological and compositional analyses

3.7.1.1 Structural analysis

The phase and the crystallinity of the CdS nanoparticles, determined by XRD as shown in Figure 3.27, depicts the XRD pattern of undoped and Fe-doped CdS nanoparticles. All the diffraction peaks are well indexed according JCPDS card no.41-1049, which confirms the formation of the hexagonal wurtzite structure. Peak broadening depicts the crystalline nature of the synthesised nanoparticles. The highest intensity of the peak positioned at $\theta = 26.57^o$ suggest the growth of the nanoparticles along the plane [002]. No impurity peaks has been found in the XRD pattern. The crystallite size of the nanoparticles shown in Table 3.5 has been calculated using the debye scherrer formula [4].

The cystallite size values are found to be 39.88nm, 22.78nm, 13.29nm, 11.39nm for undoped CdS, 3%, 5%, 10% Fe-doped CdS nanoparticles, respectively. The decrease in the crystallite size could be attributed to the smaller ionic radii of Fe atom than the Cd atom. Similar observation has been found in the other reports. These results match with some of earlier reports [24,63]. The lattice parameters (a, c) have also been calculated, given in Table 3.27, using following relation:

$$\frac{1}{d_{hkl}^2} = \frac{4}{3}\left[\frac{h^2 + hk + k^2}{a^2} + \frac{l^2}{c^2}\right]$$

The calculated parameters confirmed the crystallite size decreases upon Fe-doping. The variation of the crystallite size upon doping has been shown in Figure 3.27(b).

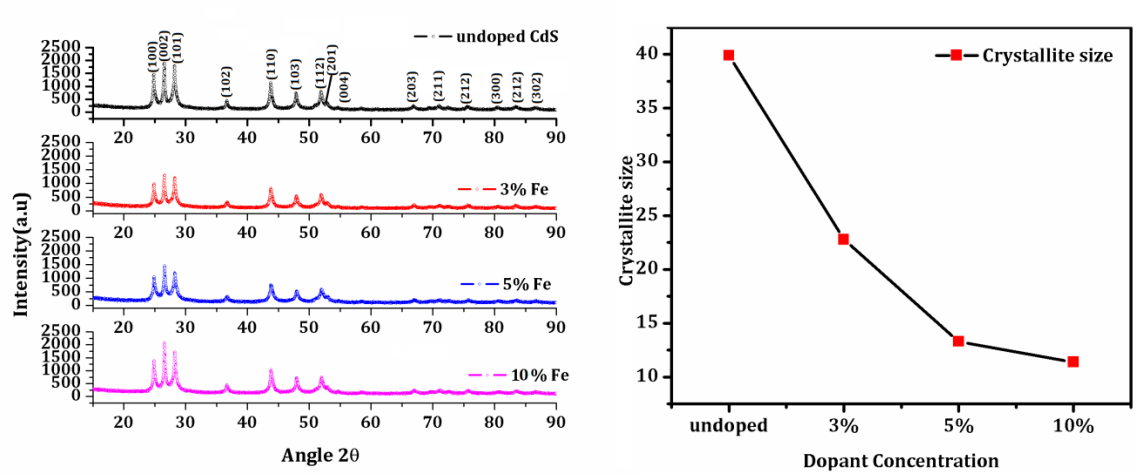

Figure 3.37 (a) XRD patterns of $Cd_{1-x}Fe_xS$ ($0 \leq x \leq 0.1$) nanoparticles, (b) variation of crystallite size with dopant concentration.

Table 3.5 Variation of crystallite size, band-gap on Fe-doped CdS nanoparticles.

Sample Description	Crystallite size(nm)	Wavelength(nm)	Bandgap(eV)
Undoped	39.88	498	2.48
3% Fe doped	22.78	492	2.52
5% Fe doped	13.29	486	2.55
10% Fe doped	11.39	479	2.58

3.7.1.2 Compositional Analysis

The electron dispersive spectroscopy (EDS) analysis has provided atomic composition of the constituent atoms and the foreign impurity atoms. From Figure 3.28, it has been found that Cd, S and Fe are present in appropriate amount. Figure 3.28 also shows increase in the intensity of Fe peak with increase in the dopant concentration. No other additional peaks have been observed in the EDS spectra.

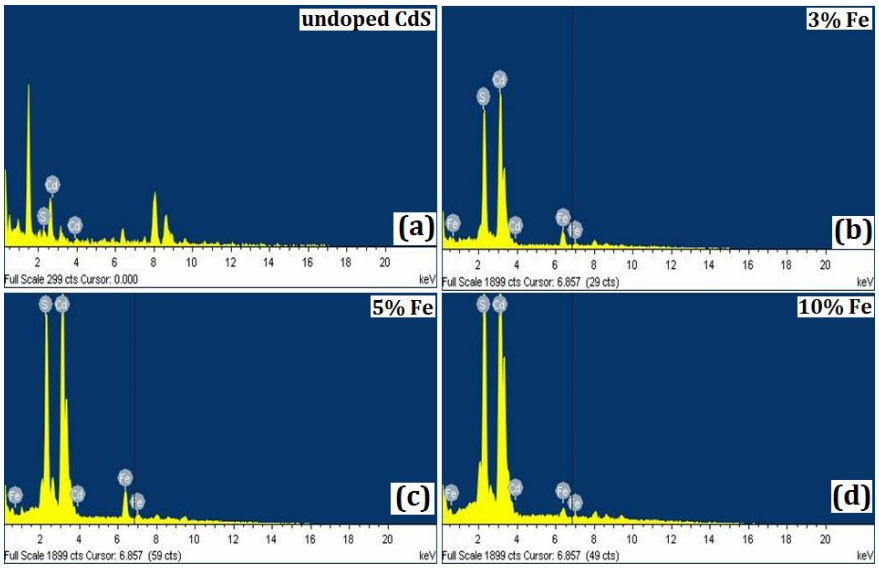

Figure 3.38 EDS spectra of (a) undoped, (b) 3%, (c) 5 %, (d) 10% Fe-doped CdS nanoparticles.

3.7.1.3 Morphological analysis

The TEM, HR-TEM, and SAED micrographs (Figure 3) of undoped and Fe-doped CdS nanoparticles reveal a spherical morphology having uniform particle size. Fe doping decreases the average size of undoped CdS nanoparticles from 25 to 18 nm. The Fe-doped CdS nanoparticles also suffer agglomeration. The d-spacing values are calculated by using the lattice planes observed in the HR-TEM image as shown in Figure 3e. The observed interplanar spacing is about 0.336 nm, which completely matches with the (002) plane of the CdS hexagonal structure; this depicts that the growth of nanoparticles is along the (002) plane. The corresponding SAED patterns in Figure 3d show sharp and circular rings indicating that the nanoparticles are of polycrystalline nature.

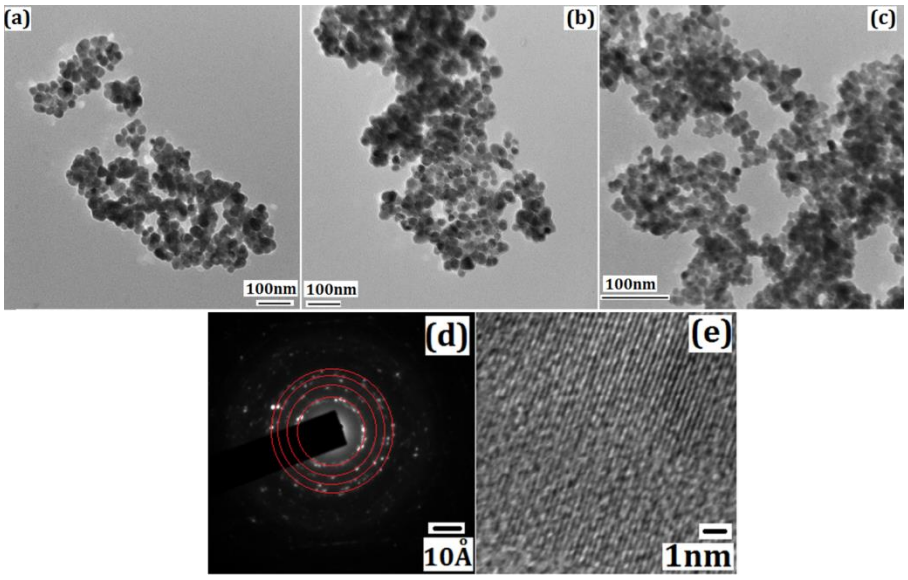

Figure 3.39 TEM micrographs of (a) undoped (b) 3% and (c) 10 % Fe-doped CdS nanoparticles (d) SAED pattern of 10 % Fe-doped CdS nanoparticles (e) HR-TEM of 10 % Fe-doped CdS nanoparticles.

3.7.2 Optical Studies

3.7.2.1 Photoluminescence Spectra

Figure 3.30 shows the PL spectra of the Fe-CdS nanoparticles at the excitation wavelength, 380 nm. It shows the most prominent peaks occur at 531nm and 542nm, which are attributed to the origin of the green emission occurring due to the d-d transitions [8]. There are two main factors, which are responsible for the occurrence of the green emission band. One, the recombination of free electrons with holes on an acceptor level, and, two, the recombination of the donor level electrons with acceptor level holes [64]. The small hump at 487nm is due to the CdS host lattice [24, 65]. Further, the peak position is not effected by doping; this is precisely due to the fact that the PL bands are not associated with Fe ions [63].

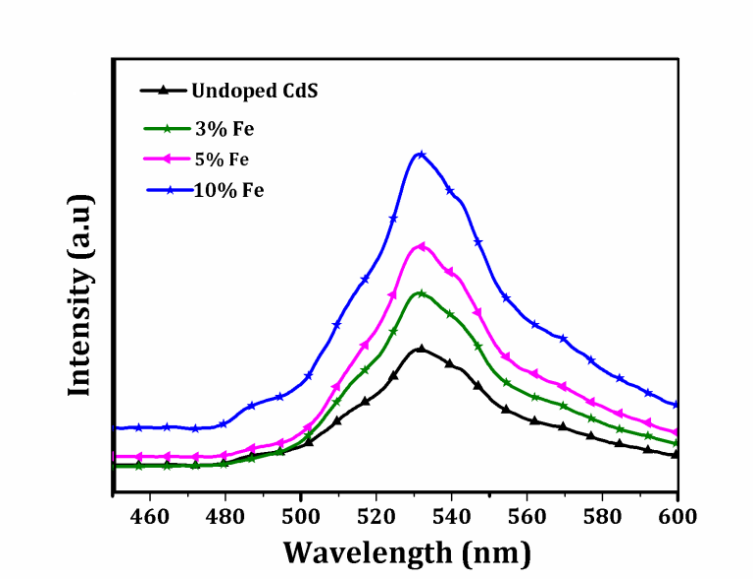

Figure 3.40 PL spectra of $Cd_{1-x}Fe_xS$ ($0 \leq x \leq 0.1$) nanoparticles at excitation wavelength of 480 nm.

3.7.2.2 UV-visible spectroscopy

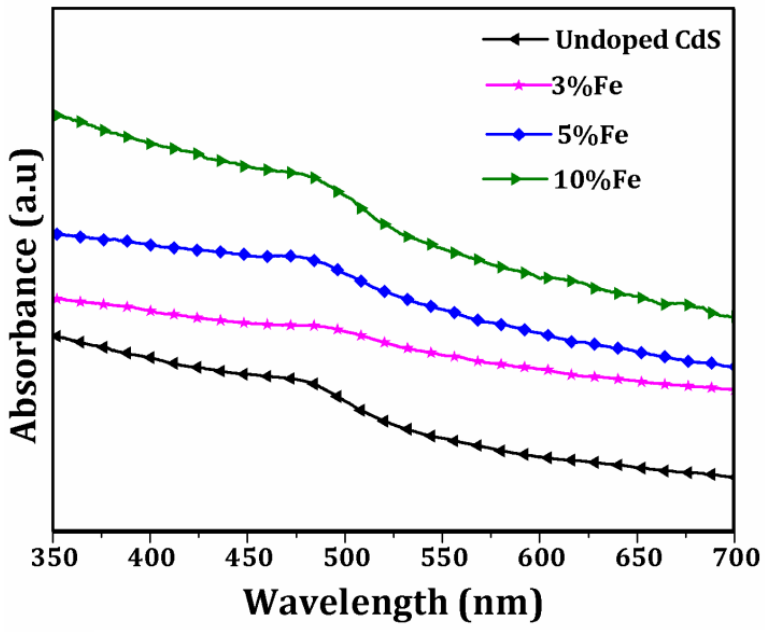

Figure 3.41 UV-visible spectra of $Cd_{1-x}Fe_xS$ ($0 \leq x \leq 0.1$) nanoparticles.

The calculated band gaps, given in Table 3.5, show a blue shift in the band gap (515 nm and 2.41 eV) [66], which increases with doping. The observed blue shift may be attributed to the decrease in the particle size, which is due to the smaller ionic radius of Fe as compared to that of Cd [67-69].

3.7.3 Magnetic Studies

Figure 3.32 shows the M-H hysteresis loops of undoped and Fe-doped CdS nanoparticles at room temperature. Hysteresis curves with magnetic saturation values 0.01, 0.02, 0.04, 0.07emu/g have been observed, respectively, for undoped, 3%, 5% and 10% doping. Fig.6b also shows the magnified view of the M-H hysteresis curves. The coericivity and remanent magnetization so found are shown in Table 3.6. Many factors are responsible for the origin of the magnetism. Among those, the presence of the magnetic dipoles on the nanoparticles' surface may be attributed to the occurrence of the ferromagnetic behavior of the Fe-doped CdS nanoparticles.

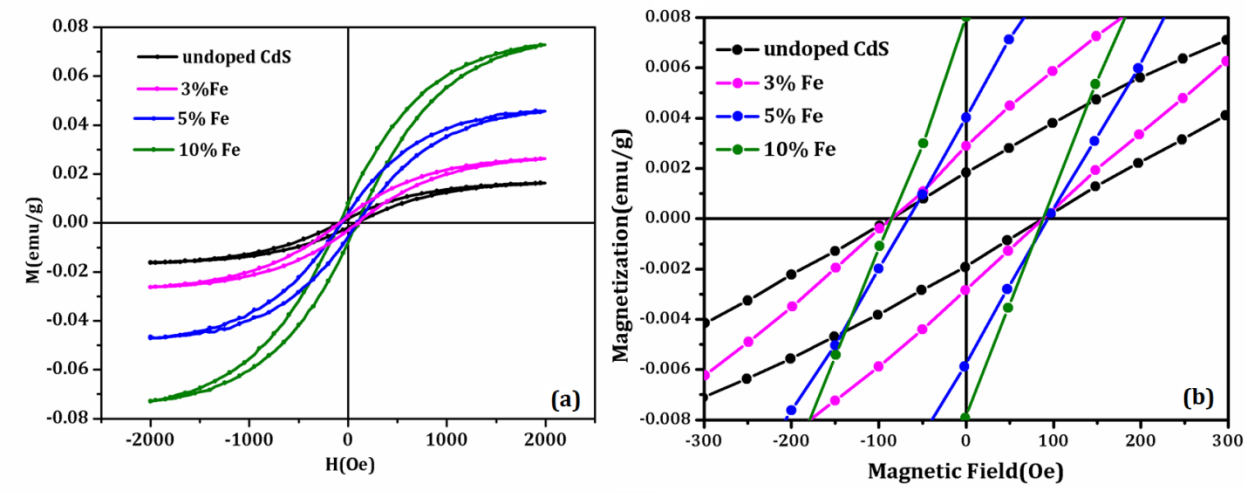

Figure 3.42 M–H curves of $Cd_{1-x}Fe_xS$ ($0 \leq x \leq 0.1$) nanoparticles, (b) Magnified view of M–H curve.

Table 3.6 Magnetic parameters of undoped, 3%, 5%, 10% Fe-doped CdS nanoparticles

Sample Description	Saturation magnetization (emu/g)	Remanent magnetization (emu/g)	Coercive field (Oe)
Undoped	0.015	0.0018	87.14
3% Fe doped	0.027	0.0026	86.52
5% Fe doped	0.048	0.0040	79.85
10% Fe doped	0.071	0.0079	86.78

Magnetic dipoles interact with the nearest neighbours and orient themselves in the same direction due to more magnetic dipoles being at the surface of the nanoparticles; this immensely influences the magnetic character of the Fe-doped CdS nanoparticles [70]. The Fe doping has been found to enhance the magnetic behavior, which agrees well with our earlier report [24]. The origin of ferromagnetism in dilute magnetic semiconductors is possibly due to the presence of various defects or vacancies, which increase with the dopant concentration [71].The reason for increase in the ferromagnetic behavior is the formation of bound magnetic polarons originating because of the charge imbalance between the ions of Fe and Cd. Further, the formation of bound magnetic polarons enhances the saturation magnetization [47, 36, 72]

3.8 Structural, optical and magnetic properties of Gd-doped CdS nanoparticles

This section deals with the series of $Cd_{1-x}Gd_xS$ (x = 0.00, 0.03, 0.05, 0.10) nanoparticles synthesized by using hydrothermal technique. The structural, optical and magnetic properties of undoped and Gd-doped nanoparticles were studied. The obtained results are discussed below:

3.8.1 Structural, morphological and compositional analyses

3.8.1.1 Structural analysis

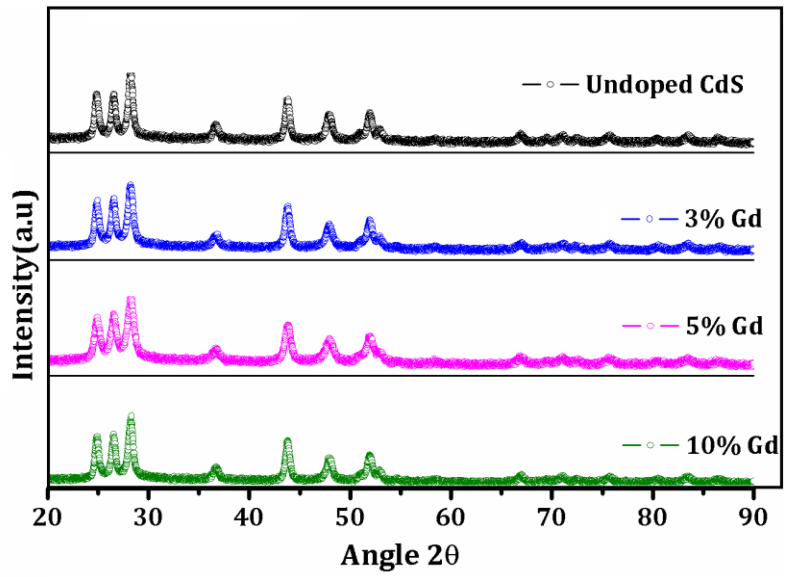

Figure 3.43 XRD patterns of $Cd_{1-x}Gd_xS$ ($0 \leq x \leq 0.1$) nanoparticles.

The XRD pattern of undoped and Gd-doped CdS nanoparticles, shown in Figure 3.38 showing that nanoparticles exhibits hexagonal structure that completely matches with JCPDS card number 41-1049. There is no secondary phase formation in Gd-doped samples showing the incorporation of Gd into CdS lattice [73]. The crystallite size of undoped CdS upon Gd-doping at 3%, 5%,10%, decreases from 25 nm, respectively, to 22nm, 20nm, 19nm. The reduction in the size of the nanoparticles may be due to the smaller size of Gd ions as compared to the Cd ions and moreover the strain induced in lattice system due Gd doping [74].

3.8.1.2 Morphological and Elemental analysis

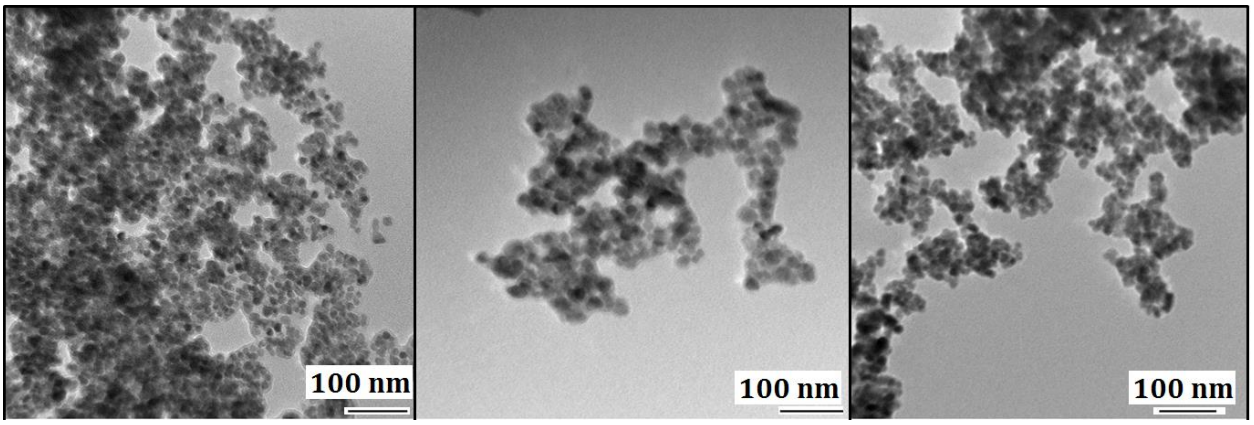

Figure 3.44 TEM micrographs of (a) undoped (b) 5% Gd and (c) 10% Gd doped CdS nanoparticles.

The TEM images of undoped, 5% and 10% Gd-doped CdS nanoparticles confirm them to be, respectively, of 25, 22, 20 nm in diameter.

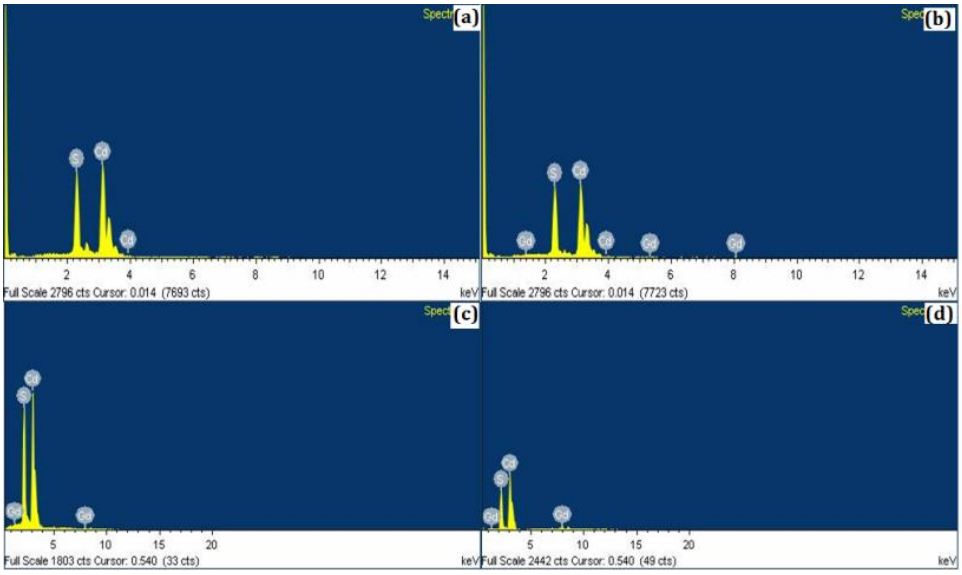

Figure 3.45 EDAX spectra of (a) undoped, (b) 3% Gd, (c) 5%, (d) 10% Gd-doped CdS nanoparticles.

Figure 3.40 (a), (b), (c) and (d) show the EDAX of undoped, 3%, 5% and 10% Gd-doped CdS nanoparticles, which confirm the presence of Cd, S and Gd without any other contamination. All elements are found to be in their stoichiometric ratio. No supplementary peaks associated with the impurity, have been observed in the spectra, which confirms their purity.

3.8.2 Optical Studies

3.8.2.1 UV-visible spectroscopy

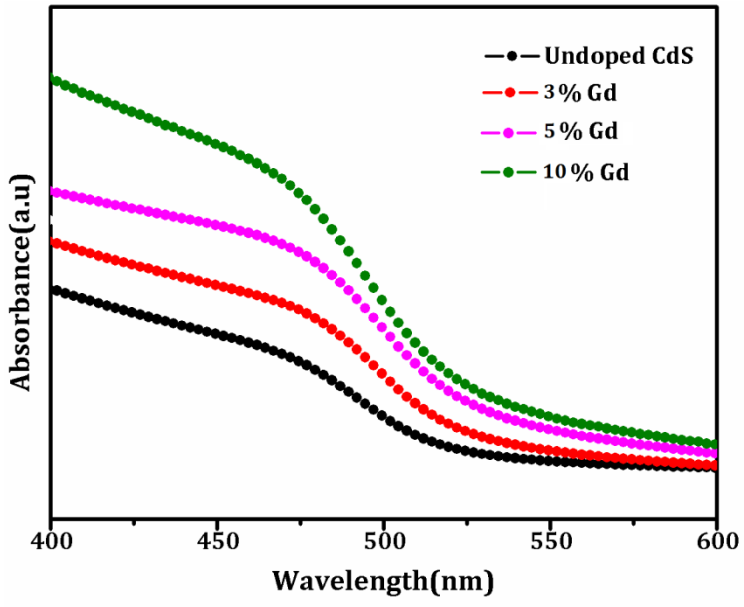

Figure 3.46 UV-visible absorption spectra of undoped and Gd-doped CdS nanoparticles.

UV-visible spectra of undoped and doped nanoparticles is shown in figure 3.46; their band gap (E_g) has been calculated (Table) by using following relation:

$$E_g = \frac{hc}{\lambda_{max}}$$

Where h is Planck's constant; c, the velocity of light and λ_{max}, the maximum absorption of CdS nanoparticles. Doping of the Gd in CdS nanoparticles increases the band gap, and, consequently the absorption edge shifts towards the lower wavelength [75]. The doping of Gd in CdS results in

smaller-size nanoparticles, which decreases the crystallite size, and, thus, the band gap increases due to the smaller ionic radii of Gd as compared to those of Cd [60, 76-77].

Table 3.7 Bandgap values of undoped and Gd-doped CdS nanoparticles.

Sample Description	Band gap(eV)
Undoped	2.43
3% Gd	2.49
5% Gd	2.56
10% Gd	2.60

3.8.2.2 Photoluminescence Spectra

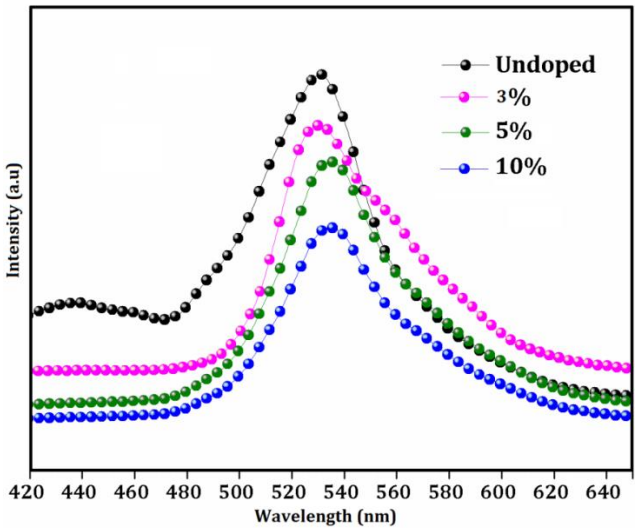

Figure 3.47 PL spectra of $Cd_{1-x}Gd_xS$ ($0 \leq x \leq 0.1$) nanoparticle.

Figure 3.38 shows the photoluminescence spectra of the undoped and Gd-doped CdS nanoparticles at excitation wavelength of 380nm; a small hump at 430 nm has been found in undoped CdS nanoparticles, which may be due to the blue emissions, however, with doping, the

intensity of doped nanoparticles registers decrease. Another major peak observed in undoped and Gd-doped CdS nanoparticles is at 530 nm. This peak is attributed to the green emission. In case of 5% Gd-doped CdS nanoparticles the green emission peak slightly shifted to the higher wavelength.

3.8.3 Magnetic studies

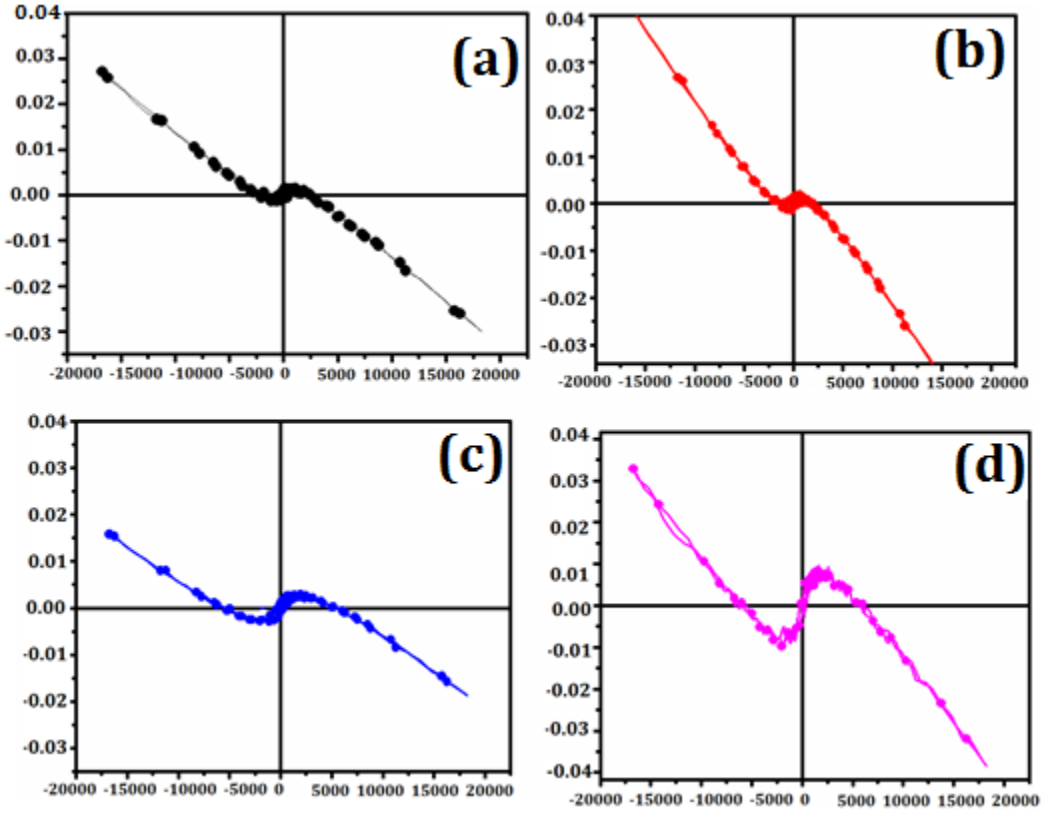

Figure 3.48 M–H curves of $Cd_{1-x}Gd_xS$ ($0 \leq x \leq 0.1$) nanoparticles.

The magnetic properties of undoped and Gd-doped CdS nanoparticles were investigated using VSM at room temperature, which revealed the magnetic saturation to be 0.0705, 0.002, 0.0029, 0.004 and 0.009 emu/g, respectively, for undoped, 3, 5 and 10% doped nanoparticles. In fact, the precise reason of ferromagnetism at room temperature in II-VI materials is yet to be ascertained; there are several possibilities, such as the presence of defects, quantum confinement and capping

agent. The charge imbalance between Gd and Cd ions can also give rise to several defects, which leads to the formation of bound magnetic polarons (F-centers). With Gd concentration, the bound magnetic polarons (F-centers) increase thereby increasing the saturation magnetization. The another major cause for the existence of the ferromagnetism is the large surface area of nanoparticles; this promotes interaction of large number of magnetic dipoles .The first principle calculations also suggest that the doping of Gd ions into host lattice may result in ferromagnetism. Therefore, the room-temperature ferromagnetism, due to Gd doping in CdS nanoparticles, is intrinsic in nature, and, can be a source of future spintronic applications [78-80].

References

[1] Hu T, Zhang M, Wang S, Shi Q, Cui G, Sun S. CdS: Co diluted magnetic semiconductor nanocrystals: synthesis and ferromagnetism study. CrystEngComm. 2011; 13(19):5646-9.

[2] Saravanan L, Pandurangan A, Jayavel R. Synthesis of cobalt-doped cadmium sulphide nanocrystals and their optical and magnetic properties. Journal of Nanoparticle Research. 2011 Apr 1; 13(4):1621-8.

[3] Bogle KA, Ghosh S, Dhole SD, Bhoraskar VN, Fu LF, Chi MF, Browning ND, Kundaliya D, Das GP, Ogale SB. Co: CdS Diluted Magnetic Semiconductor Nanoparticles: Radiation Synthesis, Dopant− Defect Complex Formation, and Unexpected Magnetism. Chemistry of Materials. 2007 Dec 19; 20(2):440-6.

[4] Cullity, B. D., and S. R. Stock. "Elementary of X-ray Diffraction." Englewood Cliffs, 3rd (2001).

[5] Sharma P, Lotey GS, Singh S, Verma NK. Solution-combustion: the versatile route to synthesize silver nanoparticles. Journal of nanoparticle research. 2011 Jun 1; 13(6):2553-61.

[6] Gegova R, Iordanova R, Bachvarova-Nedelcheva A, Dimitriev Y. Synthesis, Structure And Optical Properties Of TiO_2/TeO_2/MnOm (M= Zn, B) Gels: A Comparison. Journal of Chemical Technology and Metallurgy. 2015 Jul 1; 50(4):449-58.

[7] Murray C, Norris DJ, Bawendi MG. Synthesis and characterization of nearly monodisperse CdE (E= sulfur, selenium, tellurium) semiconductor nanocrystallites. Journal of the American Chemical Society. 1993 Sep; 115(19):8706-15.

[8] Kumar S, Jindal Z, Kumari N, Verma NK. Solvothermally synthesized europium-doped CdS nanorods: applications as phosphors. Journal of Nanoparticle Research. 2011 Oct 1;13(10):5465-71.

[9] Wang Y, Meng G, Zhang L, Liang C, Zhang J. Catalytic growth of large-scale single-crystal CdS nanowires by physical evaporation and their photoluminescence. Chemistry of materials. 2002 Apr 15; 14(4):1773-7.

[10] Yadav RS, Mishra P, Mishra R, Kumar M, Pandey AC. Growth mechanism and optical property of CdS nanoparticles synthesized using amino-acid histidine as chelating agent under sonochemical process. Ultrasonics sonochemistry. 2010 Jan 31; 17(1):116-22.

[11] Wolf SA, Awschalom DD, Buhrman RA, Daughton JM, Von Molnar S, Roukes ML, Chtchelkanova AY, Treger DM. Spintronics: a spin-based electronics vision for the future. Science. 2001 Nov 16; 294(5546):1488-95.

[12] Dietl T. A ten-year perspective on dilute magnetic semiconductors and oxides. Nature materials. 2010 Dec 1;9(12):965-74.

[13] Srivastava P, Kumar P, Singh K. Room temperature ferromagnetism in magic-sized Cr-doped CdS diluted magnetic semiconducting quantum dots. Journal of Nanoparticle Research. 2011 Oct 1;13(10):5077-85.

[14] Liu XC, Shi EW, Chen ZZ, Zhang HW, Xiao B, Song LX. High-temperature ferromagnetism in (Co, Al)-codoped ZnO powders. Applied physics letters. 2006 Jun 19;88(25):252503.

[15] Chakraborti D, Ramachandran S, Trichy G, Narayan J, Prater JT. Magnetic, electrical, and microstructural characterization of ZnO thin films codoped with Co and Cu. Journal of Applied Physics. 2007 Mar 1;101(5):053918.

[16] Bhide VG, Salkalachen S, Rastog AC, Rao CN, Hegde MS. Depth profile composition studies of thin film CdS: Cu2S solar cells using XPS and AES. Journal of Physics D: Applied Physics. 1981 Sep 14;14(9):1647.

[17] Kumar S, Kumar S, Jain S, Verma NK. Magnetic and structural characterization of transition metal co-doped CdS nanoparticles. Applied Nanoscience. 2012 Jun 1;2(2):127-31.

[18] Dietl T, Ohno H, Matsukura F, Cibert J, Ferrand D. Zener model description of ferromagnetism in zinc-blende magnetic semiconductors. Science. 2000 Feb 11;287(5455):1019-22.

[19] Meiklejohn WH, Bean CP. New magnetic anisotropy. Physical Review. 1957 Feb 1;105(3):904.

[20] Coey JM, Venkatesan M, Fitzgerald CB. Donor impurity band exchange in dilute ferromagnetic oxides. Nature materials. 2005 Feb 1;4(2):173-9.

[21] Sundaresan A, Rao CN. Ferromagnetism as a universal feature of inorganic nanoparticles. Nano Today. 2009 Feb 28;4(1):96-106.

[22] Baiju KV, Shukla S, Sandhya KS, James J, Warrier KG. Photocatalytic activity of sol-gel-derived nanocrystalline titania. The Journal of Physical Chemistry C. 2007 May 31;111(21):7612-22.

[23] Luo M, Liu Y, Hu J, Liu H, Li J. One-pot synthesis of CdS and Ni-doped CdS hollow spheres with enhanced photocatalytic activity and durability. ACS applied materials & interfaces. 2012 Mar 12;4(3):1813-21.

[24] Kaur K, Lotey GS, Verma NK. Optical and magnetic properties of Fe-doped CdS dilute magnetic semiconducting nanorods. Journal of Materials Science: Materials in Electronics. 2014 Jun 1;25(6):2605-10.

[25] Kaur K, Lotey GS, Verma NK. Structural, magnetic, dielectric and magnetodielectric properties of Gd-doped CdS nanorods. Materials Science in Semiconductor Processing. 2014 Mar 31;19:6-10.

[26] Kaur K, Lotey GS, Verma NK. Structural, optical and magnetic properties of cobalt-doped CdS dilute magnetic semiconducting nanorods. Materials Chemistry and Physics. 2013 Dec 16;143(1):41-6.

[27] Zhang P, Gao L. Synthesis and characterization of CdS nanorods via hydrothermal microemulsion. Langmuir. 2003 Jan 7;19(1):208-10.

[28] Jindal Z, Verma NK. Structural and optical properties of CdS nanorods and CdS/ZnS nanoslabs. Physica E: Low-dimensional Systems and Nanostructures. 2011 Feb 28;43(4):1021-5.

[29] Kumar GA, Thomas V, Jose G, Unnikrishnan NV, Nampoori VP. Optical properties of porphyrins in borate glassy matrix. Materials chemistry and physics. 2002 Jan 15;73(2):206-11.

[30] Firdous A, Singh D, Ahmad MM. Electrical and optical studies of pure and Ni-doped CdS quantum dots. Applied Nanoscience. 2013 Feb 1;3(1):13-8.

[31] Zhai X, Xia Y, Sun D, Xu J. Cd2+ Counterion-Assisted Synthesis of Uniform CdS Nanospheres Capped with the Anionic Surfactant Sodium dodecylsulfate. Journal of Dispersion Science and Technology. 2014 Jan 2;35(1):76-83.

[32] Jindal Z, Verma NK. Effect of Mn doping on solvothermal synthesis of CdS nanowires. Materials Sciences and Applications. 2010 Oct 29;1(04):210.

[33] Kaur K, Lotey GS, Verma NK. Ferromagnetism in Gd-doped CdS dilute magnetic semiconducting nanorods. Journal of Materials Science: Materials in Electronics. 2014 Jan 1;25(1):311-6.

[34] Kumar S, Verma NK. Effect of Ni-doping on optical and magnetic properties of solvothermally synthesized ZnS wurtzite nanorods. Journal of Materials Science: Materials in Electronics. 2014 Feb 1;25(2):785-90.

[35] Dev P, Xue Y, Zhang P. Defect-induced intrinsic magnetism in wide-gap III nitrides. Physical review letters. 2008 Mar 19;100(11):117204.

[36] Singh R. Unexpected magnetism in nanomaterials. Journal of Magnetism and Magnetic Materials. 2013 Nov 30;346:58-73.

[37] Schwartz DA, Norberg NS, Nguyen QP, Parker JM, Gamelin DR. Magnetic quantum dots: synthesis, spectroscopy, and magnetism of Co2+-and Ni2+-doped ZnO nanocrystals. Journal of the American Chemical Society. 2003 Oct 29;125(43):13205-18.

[38] Lotey GS, Jindal Z, Singhi V, Verma NK. Structural and photoluminescence properties of Eu-doped ZnS nanoparticles. Materials Science in Semiconductor Processing. 2013 Dec 31;16(6):2044-50.

[39] Sekhar H, Rao DN. Spectroscopic studies on Fe 3+ doped CdS nanopowders prepared by simple coprecipitation method. Journal of Alloys and Compounds. 2012 Mar 15;517:103-10.

[40] Bangal M, Ashtaputre S, Marathe S, Ethiraj A, Hebalkar N, Gosavi SW, Urban J, Kulkarni SK. Semiconductor nanoparticles. Hyperfine interactions. 2005 Jan 1;160(1-4):81-94.

[41] Sambandam B, Michael RJ, Rajendran N, Arumugam S, Manoharan PT. Manganous ion dictated morphology change and ferromagnetism in CdS nanocrystals. Journal of Nanoparticle Research. 2012 Sep 1;14(9):1-5.

[42] Jindal Z, Verma NK. Photoluminescent properties of ZnS: Mn nanoparticles with in-built surfactant. Journal of materials science. 2008 Oct 1;43(19):6539-45.

[43] Elilarassi R, Chandrasekaran G. Influence of Co-doping on the structural, optical and magnetic properties of ZnO nanoparticles synthesized using auto-combustion method. Journal of Materials Science: Materials in Electronics. 2013 Jan 1;24(1):96-105.

[44] Limaye MV, Singh SB, Das R, Poddar P, Kulkarni SK. Room temperature ferromagnetism in undoped and Fe doped ZnO nanorods: microwave-assisted synthesis. Journal of Solid State Chemistry. 2011 Feb 28;184(2):391-400.

[45] Borse PH, Deshmukh N, Shinde RF, Date SK, Kulkarni SK. Luminescence quenching in ZnS nanoparticles due to Fe and Ni doping. Journal of materials science. 1999 Dec 1;34(24):6087-93.

[46] Salimian S, Shayesteh SF. Structural, optical and magnetic properties of Mn-doped CdS diluted magnetic semiconductor nanoparticles. Journal of superconductivity and novel magnetism. 2012 Aug 1;25(6):2009-14.

[47] Murali G, Reddy DA, PoornaPrakash B, Vijayalakshmi RP, Reddy BK, Venugopal R. Room temperature magnetism of Fe doped CdS nanocrystals. Physica B: Condensed Matter. 2012 Jun 15;407(12):2084-8.

[48] G.S. Lotey, N.K. Verma, J. Nanopart. Res. 13, 5397 (2011)

[49] Qu SC, Zhou WH, Liu FQ, Chen NF, Wang ZG, Pan HY, Yu DP. Photoluminescence properties of Eu3+-doped ZnS nanocrystals prepared in a water/methanol solution. Applied physics letters. 2002 May 13;80(19):3605-7.

[50] Delikanli S, He S, Qin Y, Zhang P, Zeng H, Zhang H, Swihart M. Room temperature ferromagnetism in Mn-doped CdS nanorods. Applied Physics Letters. 2008 Sep 29;93(13):132501.

[51] Zhao J, Li X, Li Z. Synthesis of Co-doped CdS nanocrystals by direct thermolysis of cadmium and cobalt thiolate clusters. Journal of Nanomaterials. 2015 Jan 1;16(1):191.

[52] Heiba ZK, Mohamed MB, Imam NG. Biphasic quantum dots of cubic and hexagonal Mn doped CdS; necessity of Rietveld analysis. Journal of Alloys and Compounds. 2015 Jan 5;618:280-6.

[53] Heiba ZK, Mohamed MB, Imam NG. Structural tuning of CdS nanoparticles with nucleation temperature and its reflection on the optical properties. Journal of Molecular Structure. 2015 Aug 15;1094:91-7.

[54] J. Hasanzadeh, S. F. Shayesteh, Optica Applicata. XLI, (2011) 921.

[55] Coey JM, Venkatesan M, Fitzgerald CB. Donor impurity band exchange in dilute ferromagnetic oxides. Nature materials. 2005 Feb 1;4(2):173-9.

[56] Kaur K, Verma NK. Ferromagnetic behavior of $Cd_{1-x}Ni_xS$ nanorods: a novel study. Journal of Materials Science: Materials in Electronics. 2015 Nov 1;26(11):8285-91.

[57] Patel NH, Deshpande MP, Chaki SH. Study on structural, magnetic properties of undoped and Ni doped CdS nanoparticles. Materials Science in Semiconductor Processing. 2015 Mar 31;31:272-80.

[58] Singh V, Sharma PK, Chauhan P. Synthesis of CdS nanoparticles with enhanced optical properties. Materials Characterization. 2011 Jan 31;62(1):43-52.

[59] Yadav K, Dwivedi Y, Jaggi N. Structural and optical properties of Ni doped ZnSe nanoparticles. Journal of Luminescence. 2015 Feb 28;158:181-7.

[60] Banerjee R, Jayakrishnan R, Ayyub P. Effect of the size-induced structural transformation on the band gap in CdS nanoparticles. Journal of Physics: Condensed Matter. 2000 Dec 18;12(50):10647.

[61] Al-Hussam AM, Jassim SA. Synthesis, structure, and optical properties of CdS thin films nanoparticles prepared by chemical bath technique. Journal of the Association of Arab Universities for Basic and Applied Sciences. 2012 Apr 30;11(1):27-31.

[62] Benstaali W, Bentata S, Bentounes HA, Abbad A, Bouadjemi B. Influence of Ni–Ni separation on the optoelectronic and magnetic properties of Ni-doped cubic cadmium sulphide. Materials Science in Semiconductor Processing. 2014 Jan 31;17:53-8.

[63] Singh J, Verma NK. Synthesis and characterization of fe-doped CdSe nanoparticles as dilute magnetic semiconductor. Journal of superconductivity and novel magnetism. 2012 Oct 1;25(7):2425-30.

[64] Singh V, Chauhan P. Structural and optical characterization of CdS nanoparticles prepared by chemical precipitation method. Journal of Physics and Chemistry of Solids. 2009 Jul 31;70(7):1074-9.

[65] Kaur, K., Lotey, G.S., Verma, N.K., Mater, J.: Sci: Mater. Electron. 25, 311 (2014)

[66] Berger, L.I., SemiconductorMaterials, C.R.C.: Press, Boca Raton. FL (1997)

[67] Wang Y, Ramanathan S, Fan Q, Yun F, Morkoc H, Bandyopadhyay S. Electric field modulation of infrared absorption at room temperature in electrochemically self assembled quantum dots. Journal of nanoscience and nanotechnology. 2006 Jul 1;6(7):2077-80.

[68] Malik MA, O'Brien P, Revaprasadu N. Synthesis of TOPO-capped Mn-doped ZnS and CdS quantum dots. Journal of Materials Chemistry. 2001;11(9):2382-6.

[69] Kotkata MF, Masoud AE, Mohamed MB, Mahmoud EA. Synthesis and structural characterization of CdS nanoparticles. Physica E: Low-dimensional Systems and Nanostructures. 2009 Aug 31;41(8):1457-65.

[70] Sharma PK, Dutta RK, Pandey AC, Layek S, Verma HC. Effect of iron doping concentration on magnetic properties of ZnO nanoparticles. Journal of Magnetism and Magnetic Materials. 2009 Sep 30;321(17):2587-91.

[71] Madhu C, Sundaresan A, Rao CN. Room-temperature ferromagnetism in undoped GaN and CdS semiconductor nanoparticles. Physical Review B. 2008 May 29;77(20):201306.

[72] Sambasivam S, Joseph DP, Reddy DR, Reddy BK, Jayasankar CK. Synthesis and characterization of thiophenol passivated Fe-doped ZnS nanoparticles. Materials Science and Engineering: B. 2008 May 15;150(2):125-9.

[73] Gupta A, Sil A, Verma NK. Preparation, characterization and ionic conductivity studies of ZrO2 dispersed mixed halide matrix (KCl) 0.9–(NaCl) 0.1. Journal of Physics and Chemistry of Solids. 2009 Feb 28;70(2):340-3.

[74] Pandey G, Dixit S, Shrivastava AK. Effect of Gd 3+ doping and reaction temperature on structural and optical properties of CdS nanoparticles. Materials Science and Engineering: B. 2015 Oct 31;200:59-66.

[75] Zhang ZH, Chin WS, Vittal JJ. Water-soluble CdS quantum dots prepared from a refluxing single precursor in aqueous solution. The Journal of Physical Chemistry B. 2004 Dec 2;108(48):18569-74.

[76] Unni C, Philip D, Gopchandran KG. Studies on optical absorption and photoluminescence of thioglycerol-stabilized CdS quantum dots. Spectrochimica Acta Part A: Molecular and Biomolecular Spectroscopy. 2008 Dec 15;71(4):1402-7.

[77] Dongre JK, Nogriya V, Ramrakhiani M. Structural, optical and photoelectrochemical characterization of CdS nanowire synthesized by chemical bath deposition and wet chemical etching. Applied Surface Science. 2009 Apr 1;255(12):6115-20.

[78] Shi H, Zhang P, Li SS, Xia JB. Magnetic coupling properties of rare-earth metals (Gd, Nd) doped ZnO: First-principles calculations. Journal of Applied Physics. 2009 Jul 15;106(2):023910.

[79] Ma X. The magnetic properties of Gd doped ZnO nanowires. Thin Solid Films. 2012 Jun 30;520(17):5752-5.

[80] Akyol M, Kılıç Çetin S, Ekicibil A. Microstructural and magnetic properties of Ax: $Zn_{1-x}O$ (A= Mn, Gd and Mn/Gd) nanocrystals. Philosophical Magazine. 2016 Jan 2;96(1):31-44.

Chapter 4

Conclusions

Chapter 4

Conclusions

This chapter concludes the present thesis work. The summary of key results has been given, along with an insight into the future scope of the present research work.

4.1 Conclusions

In the present thesis, transition metals and rare earth metals (Co, Ni, Fe and Gd)-CdS nanostructures have been studied in detail. The work was divided into two parts:

(a) Co, Ni, Fe and Gd-doped CdS nanorods

(b) Co, Ni, Fe and Gd-doped CdSe nanoparticles

The main outcome of the research work is given below:

4.1.1 Co-doped CdS nanorods

- Dilute magnetic semiconducting nanorods: undoped and Co-doped CdS of size 7-11 nm were synthesized using solvothermal technique.
- The sharp circular and distinct rings, observed in SAED pattern of 10% Co-doped CdS nanorods, show the high crystallinity and polycrystalline nature of the synthesized nanorods.

- HRTEM depicts the inter-planar spacing is about 0.335 nm, which is consistent with (002) plane of CdS hexagonal structure, which confirms growth of nanorods along (002) plane.
- XRD confirmed synthesized CdS nanorods possess hexagonal wurtzite structure with $P6_3mc$ space group.
- UV-visible absorption spectra reveal the band gap 2.46 - 2.72 eV.
- Photoluminescence spectra show defects free nature of nanorods. The broad hump around 430 nm is caused due to the blue emission in the spectra.
- The magnetic saturation have been found, respectively, due to 0.034, 0.041, 0.070 and 0.090 emu g^{-1} for undoped, 5%, 10% and 15% Co-doped CdS nanorods.
- The reason for the ferromagnetism in nanorods may be due to F-center (sulfur vacancy) mediated exchange mechanism.The magnetic interactions in the synthesized nanorods are not antiferromagnetic but, ferromagnetic.
- The increase in saturation magnetization may be attributed to the increase in density of states of electrons near the Fermi level which induces ferromagnetic coupling between the Co^{2+} ions.

4.1.2 Ni-doped CdS nanorods

- Undoped and Ni-doped CdS ($Cd_{1-x}Ni_xS$; x = 0.00, 0.03, 0.05, 0.10) nanorods were synthesized using solvothermal technique.
- XRD confirmed the hexagonal wurtzite structure (JCPDS card no. 41-1049) of undoped and Ni-doped CdS nanorods.

- The crystallite size of undoped CdS has been found to be 23.79 nm, whereas upon 10% Ni-doping, it decreased to 13.9 nm. This decrement in crystallite size may be due smaller size of Ni atom as compared to that of Cd atom.
- EDAX confirmed that the elements found in undoped and doped CdS are in stoichiometric ratio without any impurity
- For undoped and doped CdS (with 10 % doping), the band gaps have been found to be, respectively, 2.47 and 2.55 eV. The bandgap for undoped CdS is higher than bulk CdS;
- The PL spectrum shows the defect free nature of the synthesized nanorods. This spectrum reveals the occurrence of green emission at 530 nm, which is due to d–d interatomic transitions.
- On increasing concentration of Ni metal, the luminescence intensity decreases due to the quenching effects by Ni.
- The TEM, HRTEM and the SAED images of undoped and 10 % Ni-doped CdS nanorods confirmed their rod like morphology with length varying from 100 to 150 nm, and width, from 20 to 30 nm.
- HRTEM determines the d-spacing values. The observed interplanar spacing, in case of undoped CdS nanorods, has been found to be 0.187 nm and, that for 10 % Ni-doped CdS nanorods, 0.189 nm using JCPDS card no. 41-1049; they are found to match with the plane [103] thereby showing their growth along this plane.
- VSM depicted ferromagnetic behavior of the nanorods. The magnetization values for undoped nanorods are found to be 0.0010emu/g and, those for 3% and 5 % Ni-doped CdS nanorods, respectively, increase to 0.0018 and 0.0054 emu/g. On further increasing concentration to 10 %, the magnetization decreased to 0.0051emu/g.

4.1.3 Fe-doped CdS nanorods

- Solvothermal technique has been used for the synthesis of Fe-doped CdS nanorods ($Cd_{1-x}Fe_xS$) with (x = 0.0, 0.03, 0.05, 0.01, 0.15).
- The diffraction peaks completely match with JCPDS card no. 41-1049 revealing hexagonal wurtzite structure of both undoped and Fe-doped CdS nanorods.
- The average size of synthesized nanorods has been found to be of 60 nm in length and 13 nm in width. SAED patterns, shows sharp and circular rings indicating that the nanorods are of polycrystalline nature.
- The absorption edge in the UV-Visible spectra got shifted to wavelength 480 nm, which corresponds to the bandgap of 2.58 eV - higher in comparison to that of bulk CdS, and is responsible for the observed blue shift upon increasing dopant concentration to 10 %, and, a red shift, when increased to 15 %.
- PL confirmed the luminescence quenching in the doped samples as compared to the undoped CdS.
- The saturation magnetization has been found to be 0.187, 0.300, 0.450, 0.675, and 0.600 emu g^{-1}, respectively, for undoped, 3, 5, 10 and 15 % doped nanorods, precisely due to the fact that the observed ferromagnetism is a result of exchange interaction of magnetic dipoles between the nearest neighbours - attributable to the dominant iron–iron super exchange interactions. The magnetization value for 15 % doping was found to decrease as compared to that of 10 %.

4.1.4 Gd-doped CdS nanorods

- Gd-doped CdS nanorods were synthesized by solvothermal technique.

- TEM images of undoped and 15 % Gd doped CdS nanorods depict their diameter to be 14 and 26 nm, respectively.
- It has been found that the elements Cd, S and Gd are there in stoichiometric ratio.
- The blue shift of synthesized nanoparticles vis a vis the bulk CdS has been observed.
- In PL spectra, the excitonic emission band around 530 nm has been found in case of undoped and doped CdS nanorods, and the peak intensity increasing at higher dopant concentration.
- The magnetic saturation has been found to be 0.0705, 0.1476, 0.2077, 0.2985 and 0.4223 emu/g for undoped, 3, 5, 10 and15 % Gd-doped CdS nanorods, respectively. It has been found that doping of Gd may reduce defects related to Cd or S thereby increasing the magnetization.

Table 4.1 Comparison of various parameters observed for common doping concentration of Co, Ni, Fe and Gd into CdS nanorods

Dopant → / **Properties ↓**	**Co-doped CdS nanorods**			**Ni-doped CdS nanorods**			**Fe-doped CdS nanorods**			**Gd-doped CdS nanorods**		
	0%	**5%**	**10%**	**0%**	**5%**	**10%**	**0%**	**5%**	**10%**	**0%**	**5%**	**10%**
Structure and Phase	Hexagonal structure and wurtzite phase			Hexagonal structure and wurtzite phase			Hexagonal structure and wurtzite phase			Hexagonal structure and wurtzite phase		
Average particle size (nm)	Length 100-140 nm and diameter 7-11 nm			Length 100-150 nm and diameter 20-30 nm			Length 100-60 nm and diameter 20-18 nm			Length 100-80 and diameter 14-26 nm		
E_g *(eV)*	2.46	2.47	2.58	2.47	2.54	2.55	2.58	2.62	2.56	2.53	2.56	2.59
Magnetic behavior	Ferro-magnetic	Ferro-magnetic	Ferro-magnetic	Ferro-magnetic	Ferro-magnetic	Ferro-magnetic	Ferro-magnetic	Ferro-magnetic	Ferro-magnetic	Ferro-magnetic	Ferro-magnetic	Ferro-magnetic
M_s *(emu/g)*	0.034	0.041	0.070	0.001	0.005	0.005	0.187	0.450	0.600	0.0705	0.2077	0.4223

4.1.5 Co-doped CdS nanoparticles

- $Cd_{1-x}Co_xS$ (x = 0.00, 0.03, 0.05, 0.10) nanoparticles were synthesized by using hydrothermal technique.
- XRD confirmed that there were no impurity peaks which depict the highly undoped nature of the synthesized nanoparticles. Lattice parameters (a, c) and crystallite size decreases upon Co-doping due to smaller ionic radii of Co than Cd.
- TEM images of undoped, 5% and 10% Co-doped CdS nanoparticles respectively. TEM confirmed the size of undoped and Co-doped CdS nanoparticles being in the range of 35-25 nm.
- The bandgap calculated using Tauc' relation has been observed to lie between 2.90 – 3.25 eV.
- In PL spectra, no peak shift has been observed. Upon increasing the limit of doping, the peak intensity decreases that may be due to the quenching effect by doped transition metal into the host lattice.
- The origin of magnetism in doped CdS nanoparticles is possibly due to the interactions between delocalized carriers of the host material i.e CdS and d spins of the Co ions.

4.1.6 Ni-doped CdS nanoparticles

- $Cd_{1-x}Ni_xS$ (x = 0.00, 0.03, 0.05, 0.10) nanoparticles were synthesized using hydrothermal technique.
- The diameters of the particles are found to be 28, 27, 26, 22nm, respectively, for undoped CdS, 3%, 5% and 10% Ni-doped CdS nanoparticles.

- The lattice parameters of Ni-doped CdS nanoparticles, a = 4.138Å and c = 6.7185Å, smaller than those of CdS, a = 4.122 Å and c = 6.7267Å.
- TEM confirmed that the size of the synthesized nanoparticles lies in the range of 28nm-22nm.
- EDAX spectrum of doped and undoped CdS nanoparticles confirmed the presence of all the required elements in appropriate amount.
- PL spectra of undoped and Ni-doped CdS nanoparticles shows that the major excitonic peak occurs at 575 nm and at 525 nm those are due to the green emission. A small hump at 490nm is observed in undoped CdS nanoparticles.
- The band-gap values (E_g) of the synthesized nanoparticles are 2.46, 2.48, 2.52 and 2.55 eV for undoped CdS, 3%, 5% and 10% Ni-doped CdS nanoparticles respectively.
- The decrement in the crystallite size of the nanoparticles is due to the quantum confinement, which results because of the localization of the electrons and hole in the semiconductors.
- The magnetic saturation values 0.039, 0.048, 0.2056 and 0.2807 emu/g are, respectively, for undoped CdS, 3%, 5% and 10% Ni-doped CdS nanoparticles. F-center -mediated exchange mechanism responsible for the ferromagnetism.

4.1.7 Fe-doped CdS nanoparticles

- The present study deals with the investigation of the optical and magnetic properties of synthesized undoped and Fe-doped CdS nanoparticles.
- The syntheses of nanoparticles were carried out using hydrothermal technique.

- XRD confirmed that synthesized nanoparticles have wurtzite phase with hexagonal structure.
- The size of nanoparticles has been found to be 39.88nm, 22.78nm, 13.29nm, 11.39nm, respectively, for undoped CdS, 3%, 5%, 10% Fe-doped CdS.
- The blue shift may be due to reduction in the size of the particles upon Fe-doping due to the lesser ionic radius of Fe than Cd.
- Magnetic study confirmed that the undoped as well as Fe-doped CdS nanoparticles exhibit ferromagnetism at room temperature. Hysteresis curves with magnetic saturation values 0.01, 0.02, 0.04, 0.07emu/g have been observed, respectively, for undoped, 3%, 5% and 10% doping. The presence of the magnetic dipoles on the surface of the nanoparticles may be attributed to the presence of the ferromagnetic behavior of the Fe-doped CdS nanoparticles. Magnetic dipoles interact with the nearest neighbors and orient themselves in the same direction; this is why the number of magnetic dipoles is more at the surface of the nanoparticles. This greatly influences the magnetic character of the Fe-doped CdS nanoparticles.

4.1.8 Gd-doped CdS nanoparticles

- The successful syntheses of undoped and Gd-doped CdS nanoparticles have been carried out using hydrothermal method.
- XRD reveals the formation of wurtzite structure of the undoped and Gd-doped CdS nanoparticles, without any secondary phase.
- The crystallite size of undoped CdS has been found to be 25nm, further for 3%, 5%,10% Gd doping crystallite size decreases to 22nm, 20nm, 19nm respectively.
- No supplementary peaks, associated with the impurity, were observed in EDAX spectra.

- The doping of Gd in CdS results in smaller-size nanoparticles, which decreases the crystallite size, and, thus, the band gap increases because of shorter ionic radii of Gd than that of Cd.
- The room temperature magnetic properties of undoped and Gd-doped CdS nanoparticles were investigated using VSM; the magnetic saturation has been found to be 0.0705, 0.0025, 0.0029, 0.004 and 0.009 emu/g for undoped, 3, 5 and 10% Gd-doped CdS nanoparticles, respectively. The charge imbalance between Gd and Cd ions can give rise to more number of defects, which leads to formation of bound magnetic polarons (F-centers).With increase in Gd concentration, bound magnetic polarons (F-centers) increase, subsequently increasing the magnetization values.

Table 4.2 Comparison of various parameters observed for common doping concentration of Co, Ni, and Fe and Gd into CdS nanoparticles

Dopant → / **Properties ↓**	**Co-doped CdS nanoparticles**			**Ni-doped CdS nanoparticles**			**Fe-doped CdS nanoparticles**			**Gd-doped CdS nanoparticles**		
	0%	**5%**	**10%**	**0%**	**5%**	**10%**	**0%**	**5%**	**10%**	**0%**	**5%**	**10%**
Structure and Phase	Hexagonal structure and wurtzite phase			Hexagonal structure and wurtzite phase			Hexagonal structure and wurtzite phase			Hexagonal structure and wurtzite phase		
Average particle size (nm)	32	27	23	28	26	22	39	13	11	24	22	20
E_g *(eV)*	2.9	3.1	3.2	2.46	2.52	2.55	2.48	2.55	2.58	2.43	2.56	2.60
Magnetic behavior	Ferro-magnetic	Ferro-magnetic	Ferro-magnetic	Ferro-magnetic	Ferro-magnetic	Ferro-magnetic	Ferro-magnetic	Ferro-magnetic	Ferro-magnetic	Ferro-magnetic	Ferro-magnetic	Ferro-magnetic
M_s *(emu/g)*	0.05	0.27	0.34	0.039	0.2056	0.2807	0.01	0.04	0.07	0.0025	0.004	0.009

4.2 Future scope of research

- The study can be extended to the co-doping of transition and rare earth doped CdS nanostructures (nanotubes, nanowires, nanocubes etc.).
- The other sophisticated instruments could be used for characterization in order to fully explore the origin of magnetism such as x- ray photon spectroscopy (XPS), magnetic circular dichroism (MCD), x-ray absorption spectroscopy (XAS).
- Electrical properties of the metal doped CdS nanostructures can also be done.
- Magnetic studies can be extended by analysis at various low as well as high temperatures.